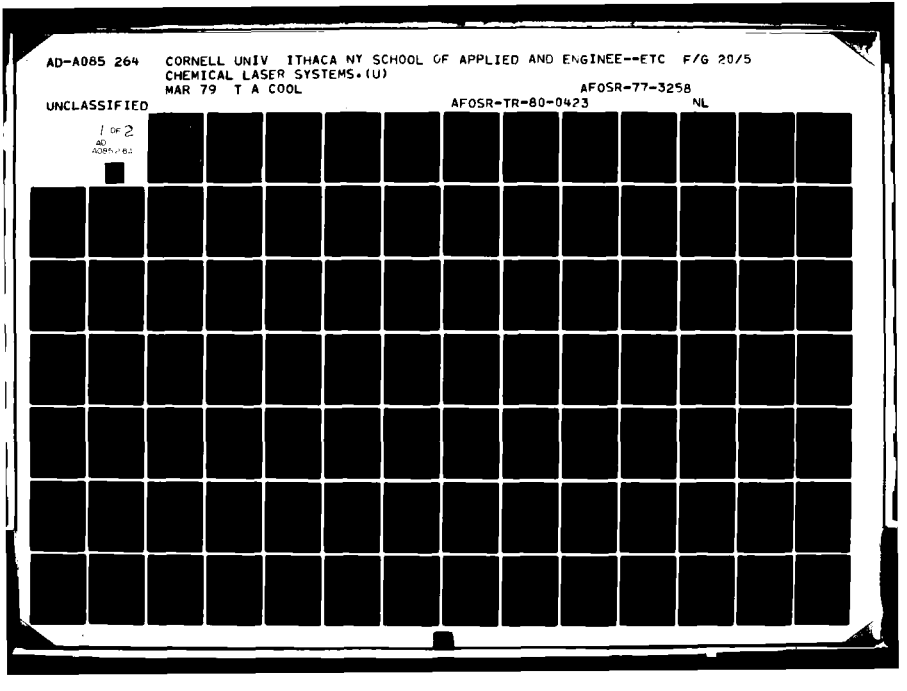
AD-A085 264 CORNELL UNIV ITHACA NY SCHOOL OF APPLIED AND ENGINEE--ETC F/G 20/5
CHEMICAL LASER SYSTEMS.(U)
MAR 79 T A COOL
AFOSR-77-3258
UNCLASSIFIED
AFOSR-TR-80-0423
NL
1 OF 2
AD
A085264

CHEMICAL LASER SYSTEMS

FINAL SCIENTIFIC REPORT ON

Air Force Office of Scientific Research

Grant AFOSR 77-3258

For the period: 1 April 1977 - 31 March 1979

Submitted by: Dr. Terrill A. Cool
Professor of Applied and Engineering Physics
Cornell University
Ithaca, New York 14853

Submitted to: Dr. Russell Armstrong
Chemical Sciences Division
Air Force Office of Scientific Research

UNCLASSIFIED

SECURITY CLASSIFICATION OF THIS PAGE (When Data Entered)

REPORT DOCUMENTATION PAGE

READ INSTRUCTIONS BEFORE COMPLETING FORM

1. REPORT NUMBER: AFOSR-TR-80-0423	2. GOVT ACCESSION NO.: AD-A085 264
3. RECIPIENT'S CATALOG NUMBER	
4. TITLE (and Subtitle): CHEMICAL LASER SYSTEMS	5. TYPE OF REPORT & PERIOD COVERED: 1 Apr 77 - 31 Mar 79 Final Report
	6. PERFORMING ORG. REPORT NUMBER
7. AUTHOR(s): Dr. Terrill A. Cool	8. CONTRACT OR GRANT NUMBER(s): AFOSR-77-3258
9. PERFORMING ORGANIZATION NAME AND ADDRESS: Cornell University, Applied and Engineering Physics, Ithaca, New York 14853	10. PROGRAM ELEMENT, PROJECT, TASK AREA & WORK UNIT NUMBERS: 61102F, 2303/B1
11. CONTROLLING OFFICE NAME AND ADDRESS: AF Office of Scientific Research/NC, Bldg. 410, Bolling AFB, DC 20332	12. REPORT DATE: 31 Mar 79
	13. NUMBER OF PAGES: 104
14. MONITORING AGENCY NAME & ADDRESS (if different from Controlling Office): Final rpt. 1 Apr 77 - 31 Mar 79	15. SECURITY CLASS. (of this report): Unclassified
	15a. DECLASSIFICATION/DOWNGRADING SCHEDULE

16. DISTRIBUTION STATEMENT (of this Report)

Approved for public release; distribution unlimited.

17. DISTRIBUTION STATEMENT (of the abstract entered in Block 20, if different from Report)

18. SUPPLEMENTARY NOTES

19. KEY WORDS (Continue on reverse side if necessary and identify by block number)

Electronic Transition Chemical Lasers
Chemiluminescence
Yttrium Halides
Scandium Halides
Radiative Lifetime Measurements
Laser-Induced Fluorescence
Spectroscopic Constants
Radiative Lifetimes
Photon Yield
PH3/N2O Reactions

20. ABSTRACT (Continue on reverse side if necessary and identify by block number)

The major effort undertaken was a thorough spectroscopic study of the products of reactions of yttrium and scandium atoms with halogen molecules. These studies have shown that chemiluminescence for these reaction systems does not originate from electronically excited monohalide molecules as suggested by previous investigators, but instead arises from electronically excited metal dihalide molecules, MX2*. Excitation spectra from the monohalides of yttrim and scandium were recorded with the laser-induced fluorescence method. Spectroscopic constants and radiative lifetimes were determined for several

DD FORM 1 JAN 73 1473

UNCLASSIFIED

407 111

previously unobserved electronic states. An evaluation of the chemiluminescence from chemical reactions initiated in PH3/N2O mixtures was performed.

I. SUMMARY OF COMPLETED RESEARCH

Two different types of chemically reactive systems of potential interest for the development of electronic transition chemical lasers were studied in detail under this Grant.

Chemiluminescence from Yttrium and Scandium Halides

The major effort undertaken was a thorough spectroscopic study of the products of reactions of yttrium and scandium atoms with halogen molecules. These studies have shown that chemiluminescence for these reaction systems does not originate from electronically excited monohalide molecules as suggested by previous investigators, but instead arises from electronically excited metal dihalide molecules, MX_2^*. Production of the metal dihalides appears to require the formation of vibrationally excited metal monohalides, $MX^\dagger$, in a precursor reaction. Radiative lifetime measurements were made for the chemiluminescent MX_2^* bands and kinetic studies of the M/X_2 reaction systems were performed with emphasis on the $Y/C\ell_2$ system.

Excitation spectra from the monohalides of yttrium and scandium were recorded with the laser-induced fluorescence method. Spectroscopic constants and radiative lifetimes were determined for several previously unobserved electronic states. Computer generated spectral simulations were used for the determination of the spectroscopic constants and Franck-Condon factors associated with the fluorescence band systems. A detailed discussion of the studies of the Y/F_2, $Y/C\ell_2$, Y/Br_2, Y/I_2, Sc/F_2, $Sc/C\ell_2$, Sc/Br_2, and Sc/I_2 systems appear in Sections II and III of this report.

Chemiluminescence from PH_3/N_2O Mixtures

An evaluation of the chemiluminescence from chemical reactions initiated in PH_3/N_2O mixtures was performed. It was established that continuum radiation emitted over the wavelength range from 320 to 1600 nm was likely to originate from electronically excited $(PO)_2^*$ exciplex molecules formed from chemically produced metastable $PO(^4\Pi)$ molecules. Photon yield measurements for the chemiluminescence showed that the photon yield for the 320-900 nm range varied linearly with reagent pressure. The photon yield at 660 Torr was 0.02%, a value probably too low to be of chemical interest. Intracavity absorption/gain measurements performed with a tunable dye laser revealed that the majority of the visible emission is a true continuum indicative of transitions to an unbound lower state. No detectable absorption or amplification associated with the continuum emission was observed. An evaluation of the sensitivity of the intracavity absorption technique permitted an estimate of the maximum possible density of absorbers of no more than $10^{13}/cm^3$. The gain, if present, was too low to support laser oscillations.

A detailed summary of the studies of chemiluminescence from the PH_3/N_2O reaction system is presented in Section IV of this report.

II.*

SPECTROSCOPIC STUDIES OF THE PRODUCTS OF REACTIONS OF YTTRIUM AND SCANDIUM ATOMS WITH HALOGEN MOLECULES. I. THE ORIGIN OF CHEMILUMINESCENCE

Howard C. Brayman, David R. Fischell and Terrill A. Cool

School of Applied and Engineering Physics
Cornell University
Ithaca, New York 14853

*This section constitutes a paper submitted to the Journal of Chemical Physics.

SPECTROSCOPIC STUDIES OF THE PRODUCTS OF REACTIONS OF YTTRIUM AND SCANDIUM ATOMS WITH HALOGEN MOLECULES. I. THE ORIGIN OF CHEMILUMINESCENCE*

Howard C. Brayman, David R. Fischell and Terrill A. Cool

School of Applied and Engineering Physics
Cornell University
Ithaca, New York 14853

ABSTRACT

Observations of laser induced fluorescence from the products of the reactions of yttrium and scandium atoms with halogen molecules have shown that chemiluminescence does not originate from electronically excited metal monohalide molecules as previously suggested, but instead arises from electronically excited dihalide molecules, MX_2^*. Production of the metal dihalides appears to require the formation of vibrationally excited metal monohalides, $MX^{\ddagger}$, in a precursor reaction. Radiative lifetime measurements for chemiluminescent bands are presented.

*Supported by the Air Force Office of Scientific Research under Grant AFOSR 77-3258.

I. INTRODUCTION

Recent studies have been reported of the chemiluminescence produced in reactions between yttrium and scandium atoms and halogen molecules.[1] In contrast to the chemiluminescences observed from other metal atom-oxidizer combinations which originate from band systems with wavelengths ranging extensively throughout the visible spectrum,[2] the chemiluminescences associated with these reactions are selectively confined to relatively narrow (100-200 Å) wavelength intervals in the blue spectral region.[1] In the Sc/F_2 and $Y/C\ell_2$ systems the photon yield associated with this selective emission feature was reported to be relatively high, exceeding a few percent of the total reaction probability.[1] The origin of these chemiluminescences has been ascribed to electronic transitions in electronically excited yttrium or scandium monohalide molecules, MX*, formed in the reactions[1]

$$M + X_2 \rightarrow MX^* + X \qquad (1)$$

where M = Sc or Y, and X = F, Cℓ, or Br, although the observed selective chemiluminescent features do not correspond to any presently known band systems in these molecules. Indeed the absence of emission from the several known band systems in these molecules, energetically accessible via reactions (1), is in remarkable contrast to prior expectations of the chemiluminescence associated with a statistical distribution of energy among the product states of reactions (1).

In the studies reported here it has been found that the chemiluminescences do not originate from yttrium or scandium monohalides formed from reactions (1), but instead arise from electronically excited dihalide molecules MX_2^* formed in a subsequent chemical reaction. A likely candidate for this

reaction is

$$MX^{\dagger} + X_2 \rightarrow MX_2^* + X, \qquad (2)$$

where $MX^{\dagger}$ denotes vibrationally hot molecules formed in the reaction between M and X_2.

Laser induced fluorescence (LIF) methods have been used here for measurements of the radiative lifetimes associated with the chemiluminescent electronic band systems in YCl_2, YBr_2, YClBr, and YI_2 molecules. LIF techniques have also been employed to obtain excitation spectra and radiative lifetimes for several new band systems in the yttrium and scandium monohalides. Spectroscopic constants and Franck-Condon factors are summarized for the observed band systems in the following paper,[3] hereafter referred to as II.

II. EXPERIMENTAL APPARATUS

The experimental apparatus was designed to provide a convenient means for the vaporization of yttrium or scandium and a reaction zone for the observations of chemiluminescence and laser induced fluorescence from products of reactions between yttrium or scandium and halogen molecules (F_2, Cl_2, Br_2, I_2). Detailed descriptions of apparatus and techniques appear in refs. 4 and 5. An effusive flow of yttrium or scandium vapor was provided by the oven system shown in Fig. 1. A commercially available electrically heated graphite oven, Astro Industries, model 1000-2560-PP, was modified to accomplish the experimental objectives. A major change was the installation of an oven liner to separate the interior hot zone from the surrounding graphite heat shields and heating elements. This cylindrical liner was made of either pure tantalum, or a 90% tantalum/10% tungsten alloy of 1.5 mm thickness. The liner served to protect the graphite oven components from the effects of the yttrium, scandium and halogen gases. The liner also

provided for the containment of the effusive flow of either yttrium or scandium from a ca. 2250°K tantalum crucible without contamination from degassing of the graphite oven components. This inner liner was connected directly to the reaction chamber as illustrated in Fig. 1. The liner had an inside diameter of 3.8 cm and a length of 28 cm. A background pressure of less than 10^{-5} Torr at operating temperature was readily achieved within the reaction chamber and oven liner. The surrounding graphite oven was purged with helium and maintained at a pressure of about 0.10 Torr by means of a separate oven pumping system. Measurements of the pressure within the reaction chamber were made with an ionization gauge (for pressures below 10^{-3} Torr), or a thermocouple gauge (for pressures above 10^{-3} Torr). Temperature estimates of the tantalum liner were made with an optical pyrometer sighted through the oven view port shown in Fig. 1. Typically the oven was run at about 2000°K for scandium and 2250°K for yttrium. These temperatures provided vapor pressures of about 0.7 Torr within the tantalum crucible.[6]

The reaction chamber was a water cooled stainless steel tube, 14 cm long with a 12 cm inside diameter. The chamber was fitted with four view ports. Two ports provided access for the optical axis of a dye laser used to excite LIF; a third port at right angles to these was used for viewing fluorescence and chemiluminescence; the fourth port was used for occasional monitoring of the reaction flame intensity and provided access for injection of the halogen gases into the reaction zone. Collimating tubes of 18 cm length with internal apertures were installed on both laser ports to minimize laser scattering. Additional measures to reduce scattered light included the use of an internally threaded beam stop on the laser

exit port and use of a stainless steel cone to define the optical cone for collection of the LIF. All view ports were purged with small flows of helium to prevent fogging by condensed particles. The optical layout is shown schematically in Fig. 2.

Three types of injectors were used for introduction of the halogen gases to the reaction chamber. The first of these, used primarily for preliminary studies of the Y + $C\ell_2$ reaction system, consisted of a single water-cooled copper tube of 0.023 cm i.d. The tube was pointed downstream with its exit 0.28 cm below the optical axis. A better injector which gave a more uniform density of halogen gas in the reaction chamber consisted of ten 0.04 cm diameter holes, equally spaced around the inner circumference of a ring flange of 7.5 cm i.d. located at the bottom of the reaction chamber, 3 cm below the optical axis. For studies of the reactions with iodine a third injector was built because the water cooling of the first two types caused clogging to occur. It consisted of a single uncooled stainless steel tube pointed downstream with its exit 0.7 cm below the optical axis. The iodine reservoir was maintained at 100°C to provide an iodine vapor pressure of 65 Torr. The iodine metering valve and connecting lines were heated to prevent condensation.

The flow pumping system for the reaction chamber consisted of a 425 ℓ/min roughing pump, a 10 cm oil diffusion pump and a liquid-nitrogen-cooled activated charcoal cryotrap.[7]

Laser excited fluorescence was viewed at right angles to the laser beam as indicated in Fig. 2. The conical light baffle, collimating apertures, and beam stop were effective in eliminating nearly all of the scattered laser light and background oven radiation from the field of view

of the fluorescence detecting RCA 7265 photomultiplier. The fluorescence PMT signal was preamplified by a Tektronix 7A16A 225 MHz amplifier. The signal was then fed to a Biomation 8100 transient digitizer. The digitized output was sent to a Decgraphic GT-40 minicomputer for further processing. A second PMT, exposed to a portion of the dye laser beam, served as a trigger source for the transient recorder and occasionally as a monitor of the dye laser amplitude to provide normalization of the fluorescence intensity. With the use of thirteen different dyes, laser induced fluorescence could be excited over the wavelength interval from 3600-6500 Å. Fluorescence excitation spectra obtained by continuous scans of the dye laser wavelength had a spectral resolution of 0.05-0.10 nm.

The N_2 laser and dye laser were of our own construction. The N_2 laser delivered 1-1.5 mJ pulses of 8 nsec duration at a repetition rate of 15 Hz. The dye laser followed the standard Hansch design[8] and consisted of the dye cell, a 20X expanding telescope, blazed grating and output coupler. Scanning of the grating was accomplished by mounting the grating and dye laser on the base of a surplus scanning monochromator. The output of the dye laser could be set to any desired wavelength to within ±0.05 nm. Typical dye laser output energies were 10^{-4}J.

A. Laser induced fluorescence detection

A schematic diagram of the apparatus used for the LIF experiments is shown in Fig. 2. Two types of signal processing were employed. Measurements of radiative lifetimes were performed by tuning the dye laser to a fixed wavelength corresponding to a given rare-earth halide transition of interest. The GT-40 minicomputer performed signal averaging over a time interval selected to include about four decay time constants. The

averaging was done over as many laser pulses as was necessary to achieve a sufficiently high signal-to-noise ratio for accurate lifetime determinations.

A different method of signal averaging was used when the dye laser was continuously scanned to produce laser excitation spectra. After each laser pulse the digitized fluorescence signal was integrated over a selected time interval (typically 100-150 nsec) to give a total fluorescence signal. Each succeeding result was added to the previous signal until a set number of pulses (generally 45) had occurred. The final summed signal was then stored as part of a data array, and the process was initiated again. With a typical laser scan rate of 5 Å/min and a repetition rate of 15 Hz, each summed data point represented 0.25 Å; thus there would be 180 laser pulses per angstrom of dye laser scan. The final data array could contain up to 1024 such data points corresponding to a laser scanning interval of 256 Å. The completed digitized scans were stored on floppy discs for further normalization to correct for the wavelength dependence of the dye laser output, for the wavelength-dependent response of the fluorescence detection system, and, in some cases, to subtract out residual scattered laser light appearing with the signal. These data then provided the input for graphical video displays and hard copies obtained with a data plotter. The software developed for the GT-40 minicomputer permitted pulse-by-pulse normalization of the fluorescence intensity by the laser output intensity as the laser was scanned. In practice this proved to be unnecessary and offered no advantage over the usual method employed which was to normalize the fluorescence output of a given run by the separately recorded wavelength-dependent laser output for that run.

B. Chemiluminescence recording

The apparatus of Fig. 3 was used for observations of chemiluminescence from the reaction zone. A lens with an f/5 entrance cone was used to focus chemiluminescence on the entrance slit of a 0.3 meter McPherson model 218 monochromator. The output of an RCA 7265 PMT mounted on the monochromator exit slit was fed to a PAR model 126 lock-in amplifier with a model 116 differential preamplifier. The chemiluminescence was chopped at 1.2 kHz; a miniature light bulb and photodiode built into the chopper housing provided a reference signal for the lock-in amplifier. The monochromator entrance slits were typically set at 250 μm, and a grating blazed at 3000 Å with 1200 lines/mm was employed. Scan speeds of 20 to 50 Å/min were used. Chemiluminescence spectra were usually taken with use of 1:30 halogen-helium gas mixtures which gave very steady and reproducible flame intensities.

The chemiluminescence data presented in Section III are uncorrected for phototube response.

C. Reagents

Yttrium (99.9% pure) and scandium (99% pure) metals were obtained from Alfa Ventron. The metals were obtained in ingot form with samples ranging from 10 to 50 g in weight. The larger ingots were cut down to 13 g in size in an argon-filled glove box. The scandium was shipped in mineral oil which was removed prior to cutting by cleaning with trichloroethylene and acetone. Care was taken at all stages of handling and oven loading to prevent exposure of the samples to the atmosphere. The sources and stated purities of the halogen gases used were: Cl_2, Matheson Co., 99.965%; F_2 (5% mixture in helium), Air Products, 98%; Br_2, E.M. Laboratories, 99.999%; I_2, Fisher Scientific, 99.995%.

III. EXPERIMENTAL RESULTS

A. Chemiluminescence for yttrium-halogen reaction systems

The strong chemiluminescence from the Y + $C\ell_2$ flame reported by Gole and co-workers[1] was easily observable in the apparatus of Figs. 1 and 3. Proper adjustment of the $C\ell_2$ flow rate led to a blue flame, easily observable above the $C\ell_2$ injector and surrounding region of the reaction chamber. Under these conditions the pressure in the reaction chamber was about 10^{-4} Torr. Fig. 4 shows a comparison between the chemiluminescence we observe and that reported by Gole et al.[1] The chemiluminescence profiles are identical for both sets of measurements, except that the present data are shifted 25 Å toward the blue with respect to the previous data. As reported by Gole et al.,[1] there appear to be no other emissions in the visible spectral region.

The smooth symmetrical shape of the narrow featureless band system of Fig. 4 is remarkable. Such a profile cannot be simulated from any known band systems of $YC\ell$. Since it seemed likely, contrary to the assertions of Gole et al.,[1] that this chemiluminescence does not arise from electronically excited $YC\ell$, a series of experiments was performed to identify the chemiluminescent emitter.

The intensity of the chemiluminescence of Fig. 4 was strongly dependent on $C\ell_2$ flow rate. This dependence is shown by the data of Fig. 5 obtained by recording the chemiluminescence intensity as the flow rate of a 1:30 mixture of $C\ell_2$ and helium was progressively increased. The data of Fig. 5 exhibit an initially supralinear growth in chemiluminescence intensity with $C\ell_2$ pressure. This feature suggests that processes that are of higher than first order in $C\ell_2$ concentration are important in the chemiluminescence mechanism. One such possibility would be the reactions:

$$Y + Cl_2 \xrightarrow{k_1} YCl + Cl \quad (3)$$

$$YCl + Cl_2 \xrightarrow{k_2} YCl_2 + Cl \quad (4)$$

$$YCl_2 + Cl_2 \xrightarrow{k_3} YCl_3 + Cl \quad (5)$$

$$YCl + Cl_2 \xrightarrow{k_4} YCl_2^* + Cl \quad (6)$$

$$YCl_2^* \xrightarrow{k_5} YCl_2 + h\nu \quad (7)$$

The chemiluminescent emission of step (7) arises from electronically excited YCl_2 formed in reaction (6).

Gole et al. have proposed that a second order dependence on Cl_2 concentration could be caused by collisionally-induced emission from a long lived metastable state.[1a] Such a mechanism would imply a pressure dependence for the apparent radiative lifetime associated with the chemiluminescence. We have found, however, in experiments described further in the following, that the radiative lifetime is pressure independent and too short to support the "collision-induced emission" hypothesis.

The radiative lifetime of the emitter responsible for the chemiluminescence of Fig. 4 was measurable with the laser induced fluorescence apparatus of Fig. 2. In preparation for those measurements the Cl_2 flow rate (with no admixed helium) was adjusted to give a maximum chemiluminescence intensity (cf. Fig. 5). The dye laser was then scanned through the region from 3700 Å to 4100 Å and the laser induced fluorescence superimposed on the background chemiluminescence was averaged and recorded. Fig. 6 shows the

intensity variation with wavelength of the laser induced fluorescence; also shown in Fig. 6 is the distribution of background chemiluminescence of Fig. 4. The wavelength interval spanned by the laser induced fluorescence corresponds approximately to that of the chemiluminescence. The good agreement between intensity distributions shown in Fig. 6 suggests that the same molecular bands are likely to be responsible for both the fluorescence and the chemiluminescence.

A series of measurements of the decay of the laser induced fluorescence was made with the dye laser tuned to wavelengths in the region from 3820 Å to 3930 Å where the chemiluminescence is strongest. No dependence of the fluorescence decay rate on either the wavelength or the Cl_2 pressure was observable. Pressures for the Cl_2 covered the range of values (cf. Fig. 5) which produced an observable chemiluminescence. The temporal decay of this laser induced fluorescence near 3900 Å is shown in Fig. 7. A simple exponential decay with a time constant of 450 ± 10 nsec was observed.

A simple experiment was performed to identify the chemiluminescent emitter of Fig. 4.[9] Fig. 8 shows the spectral profile of the chemiluminescence from the Y/Br_2 reaction system. The chemiluminescence for this system is somewhat narrower and shifted to the red of the Y/Cl_2 chemiluminescence. The spectral profiles of the Y/Br_2 and Y/Cl_2 reaction systems do not overlap strongly; it seemed feasible to look for chemiluminescence from the mixed halide YClBr which should exhibit a peak at a wavelength between the peaks for the Y/Br_2 and Y/Cl_2 systems. For these experiments separate flows of Br_2 and of a helium + Cl_2 mixture were introduced to the reaction chamber. Since the flows were introduced separately, there was no opportunity for the formation of ClBr molecules before the reaction of Y with Cl_2 or Br_2.

Figs. 9a, 9b and 9c show chemiluminescence profiles for the reaction of Y atoms with mixtures of Br_2 and $C\ell_2$ which do indeed show a well defined third chemiluminescent band system located between the Y/Br_2 and $Y/C\ell_2$ chemiluminescence features. The only possible explanation for the existence of the three separate chemiluminescent band systems of Figs. 9a, 9b and 9c is that the three emitters are $YC\ell_2$, $YC\ell Br$ and YBr_2.

Radiative lifetime data analogous to those of Fig. 7 were obtained from LIF measurements on the $YC\ell Br$ and YBr_2 band systems. The radiative lifetimes were 240 ± 24 nsec and 160 ± 16 nsec for the $YC\ell Br$ and YBr_2 band systems, respectively.

Additional experiments were performed on the $Y/C\ell_2$ reaction system which lend support to the kinetic mechanism constituted by reactions (3) to (7).

In addition to the relatively weak LIF associated with $YC\ell_2$, strong LIF signals were observable from yttrium atomic lines and from $YC\ell$ band systems. Thus it was possible to use the LIF signals to determine the dependences of the concentrations of Y, $YC\ell$, and $YC\ell_2$ on the concentration of $C\ell_2$. These dependences are qualitatively described with the kinetic mechanism of reactions (3) to (7). Figs. 10, 11 and 12 show the variations in the concentrations of Y, $YC\ell$, and $YC\ell_2$, respectively, on $C\ell_2$ partial pressure. These data were obtained by monitoring the LIF signals as the pressure of a 1:30 mixture of $C\ell_2$ with helium was systematically increased. Relationships are given in the Appendix which permit the calculation of the solid curves shown with the experimental data of Figs. 5 and 10-12. These curves are calculated with assumed values for the relative magnitudes of the rate constants k_1, k_2, k_3, and k_4. The assumed ratios of rate constants

were $k_1:k_2:k_3 = 1:2.3:1.4$. The value of k_4 was taken to be negligibly small compared with k_2. Our measured value for the radiative lifetime of the YCl_2 chemiluminescence (450 nsec) provides a determination of k_5.

The decline in yttrium atom concentration with Cl_2 pressure is determined by the magnitude of k_1. The ratio of k_2 to k_1 is determined by the rise and fall of YCl concentration with increasing Cl_2 pressure. The relative magnitude of k_3 is fixed by the dependence of YCl_2 concentration on Cl_2 pressure. Fig. 13 shows the dependence of the concentration of YCl_3 on Cl_2 pressure predicted with the rate constants used for the computed curves of Figs. 5 and 10-12. No LIF signals were observed which could have originated from YCl_3. The computed curves of Figs. 5 and 10-12 would not be expected to give a good quantitative fit to the experimental data because of the necessarily oversimplified model adopted in the absence of complete knowledge of the flow and mixing characteristics of the reaction chamber. Nevertheless, the simple kinetic scheme of reactions (3) to (7) apparently gives a good qualitative explanation for the behavior exhibited by the data of Figs. 5 and 10-12.

Figs. 14 and 15 show the chemiluminescence spectra observed from the Y/F_2 and Y/I_2 reaction systems. The chemiluminescent emitters in these systems are presumably YF_2 and YI_2 in analogy with the Y/Cl_2 and Y/Br_2 systems. Attempts to measure a radiative lifetime for the YF_2 chemiluminescence bands were unsuccessful because the LIF signal was very weak for these bands. The radiative lifetime measured for the Y/I_2 chemiluminescence band system was 260 nsec. The chemiluminescence of Fig. 14 for the Y/F_2 system is identical to that previously reported by Gole and coworkers;[1] no previous data exist for the Y/I_2 system.

B. Chemiluminescence for scandium-halogen reaction systems

Observations of chemiluminescence were made for the Sc/F_2, Sc/Cl_2, Sc/Br_2, and Sc/I_2 systems in the same manner that data were taken for the yttrium-halogen reaction systems. Fig. 16 gives chemiluminescence spectra for the Sc/F_2 reaction. A strong 400 Å FWHM peak appears at 3500 Å, but very little emission was seen throughout the remainder of the visible spectrum. Very similar data were previously reported by Gole et al.[1] The chemiluminescence profile obtained for the Sc/Cl_2 reaction system of Fig. 17 differs from profiles observed for the other yttrium and scandium halides because small contributions are clearly present from identifiable band systems associated with the monohalide. Use of the spectroscopic data of Shenyavskaya[10] permitted identification of the $\Delta v = 5,4,\ldots,-3,-4,-5$ sequences of the C→X system and $\Delta v = 4,3,2$, and 1 sequences of the B→X system in ScCl. The majority of the chemiluminescence for the Sc/Cl_2 reaction system, however, appears to originate from polyatomic emission bands. A strong 400 Å FWHM peak was observed, centered near 3500 Å. Previous chemiluminescence data for the Sc/Cl_2 reaction system have been reported.[1a]

Chemiluminescence profiles for the Sc/Br_2 and Sc/I_2 systems are given in Figs. 18 and 19. These profiles are characterized by two broad emission features which together encompass the visible spectral region. It must be noted that since the chemiluminescence data are uncorrected for photomultiplier response, the decline in intensity of the Sc/I_2 chemiluminescence beyond 6000 Å may be primarily caused by the reduced PMT response. The Sc/I_2 chemiluminescence is unique in that the blue spectral feature near 4000 Å is a minor component of the total chemiluminescence in contrast to

the other yttrium and scandium halides.

Attempts were made without success to excite enough LIF from the chemiluminescent band systems of the scandium halides to measure radiative lifetimes for the chemiluminescent emitters.

IV. DISCUSSION

The studies reported here have established that the chemiluminescences of the $Y/C\ell_2$ and Y/Br_2 reaction systems originate from electronically excited $YC\ell_2^*$ and YBr_2^* molecules instead of electronically excited $YC\ell^*$ and YBr^* monohalide molecules as was previously thought. This conclusion is based on several observations:

(1) Chemiluminescence from mixtures of $C\ell_2$ and Br_2 gases reacting with Y atoms exhibits a prominent third feature near 3975 Å in addition to the features found at 3920 Å and 4025 Å, respectively, in the $Y/C\ell_2$ and Y/Br_2 reaction systems. If the chemiluminescence had originated from the monohalides via reaction (1) as asserted by Gole et al.,[1] then the third chemiluminescent feature would not have appeared in the $(C\ell_2+Br_2)/Y$ reaction system. If the chemiluminescence had originated from the trihalides, YX_3, there would have been spectral features present from $YC\ell Br_2^*$ and $YBrC\ell_2^*$ in addition to those from $YC\ell_3^*$ and YBr_3^*.

(2) Qualitative studies of the dependence of LIF from Y, $YC\ell$ and from the chemiluminescent emitter ($YC\ell_2$) on $C\ell_2$ pressure for the $Y/C\ell_2$ reaction system show that the chemiluminescent emitter cannot be either $YC\ell_3$ or $YC\ell$. The observed and predicted dependence of the LIF from $YC\ell$ on $C\ell_2$ pressure is measurably different from the dependence observed and predicted for the chemiluminescent emitter. Moreover, the predicted

dependence of the concentration of YCl_3 pressure is drastically different from that observed for the chemiluminescent emitter (i.e., the concentration of YCl_3 approaches a constant maximum value at high Cl_2 pressures).

(3) The measured radiative lifetime for the Y/Cl_2 chemiluminescent emitter is 450 nsec compared with measured radiative lifetimes for YCl bands of 21-36 nsec.

(4) The narrow featureless peak of the chemiluminescence spectral profile cannot be plausibly simulated from relatively simple YCl diatomic emission bands.

Although comparable studies to those described for the Y/Cl_2 and Y/Br_2 systems were not made for the other yttrium and scandium halide reaction systems, it seems quite likely that the singular spectral features noted in each of these reaction systems in the 3500-4300 Å spectral region originate from the electronically excited dihalides, YX_2^* or ScX_2^*. Measured radiative lifetime values for the YCl_2, YBr_2, YClBr, and YI_2 chemiluminescent bands were 450, 160, 240, and 260 nsec, respectively.

Thermochemical considerations show that the kinetic model of Eqs. (3)-(7) can account for the observed chemiluminescence from YCl_2^* only if some of the molecules formed in the first step are highly vibrationally excited. Unfortunately, no direct measurements of bond energies for the yttrium halides are available. It is possible, however, to make estimates of bond energies for yttrium chlorides with methods that have given good results when applied to the scandium fluorides, for which direct measurements are available. Bond energy estimates and experimental values are summarized in Table I. Two types of bond energy estimates are given in Table I. The first of these is a Birge-Sponer extrapolation based on the

spectroscopic data of Janney[11] with an empirical correction to account for the ionic character of the molecules following the method of Hildebrand.[12] This type of estimate is expected to lead to underestimation of bond energies. A second type of estimate has been given by Krasnov and Timoshinin[13] who used a potential function model with polarizable ions for calculation of bond energies. The estimates of Krasnov and Timoshinin are in good agreement with experimental data for the yttrium and scandium halides as is shown in Table I. Use of the estimated dissociation energies of Krasnov and Timoshinin and the known dissociation energy of Cl_2 (58 kcal/mole)[14] leads to exoergicities of 53 kcal for reaction (3) and 61 kcal/mole for reaction (4). These values would be increased by about 6 kcal/mole if it is assumed that all of the yttrium flow translational energy appears as energy release in the reaction products. The blue chemiluminescence from Y/Cl_2 has a short wavelength cutoff of 3825 Å which corresponds to an energy release of at least 75 kcal/mole. There is therefore an energy discrepancy of at least 75-67 = 8 kcal/mole for reaction (5) which would require vibrational excitation of the YCl formed in reaction (3) to vibrational levels of at least v=8. Moreover, a maximum energy release of reaction (3) of 59 kcal/mole is 16 kcal/mole too low to permit the direct formation of electronically excited YCl at wavelengths as short as 3825 Å.

The foregoing thermochemical estimates require that a substantial fraction of the energy release of reaction (3) resides in vibrational excitation of the YCl bond. Black body radiation from the oven effectively prevents the direct observation of infrared emission from such vibrationally excited YCl molecules.

In summary, the results of this study suggest that the chemiluminescence

observed from the Y/Cl_2 reaction system originates from electronically excited YCl_2^* formed in the reaction

$$YCl^\dagger + Cl_2 \rightarrow YCl_2^* + Cl \qquad (8)$$

where $YCl^\dagger$ denotes YCl vibrationally excited to levels of at least v=8. Moreover, there is no present evidence that electronically excited YCl^* molecules are formed in reaction (3). It appears likely that an analogous situation exists for reactions of the other yttrium- and scandium-halogen reaction systems. Only in the Sc/F_2 and Y/F_2 cases is there enough energy release available that no vibrational excitation of the monohalide is required in formation of the dihalide.

It should be noted that a reaction mechanism proposed for the formation of electronically excited $BaCl_2^*$, $NaCl_2^*$, NaF_2^*, CaF_2^*, $CaCl_2^*$, and $CaBr_2^*$[15-18] would not require vibrationally excited monohalides as precursors to the formation of the electronically excited dihalide. This mechanism requires the stabilization of a long-lived complex denoted by $(MX_2^*)^\dagger$ formed by the direct reaction of a metal atom M with the halogen molecule, X_2:

$$M + X_2 \rightarrow (MX_2^*)^\dagger \text{ formation} \qquad (9)$$

$$(MX_2^*)^\dagger + Q \rightarrow MX_2^* + Q \text{ stabilization} \qquad (10)$$

$$MX_2^* \rightarrow MX_2 + h\nu \text{ radiation} \qquad (11)$$

This mechanism would not, however, lead to the formation of mixed halides such as the YClBr molecules observed to contribute to the chemiluminescence of Figs. 9a, 9b, and 9c. It should also be noted that in further study[19] of the Ba/Cl_2 reaction system Wren has rejected the

mechanism of reactions (9), (10) and (11) in favor of the two-step process involving formation of vibrationally excited monohalide molecules:

$$Ba + C\ell_2 \rightarrow BaC\ell^{\dagger} + C\ell \qquad (12)$$

$$BaC\ell^{\dagger} + C\ell_2 \rightarrow BaC\ell_2^{*} + C\ell. \qquad (13)$$

ACKNOWLEDGEMENTS

One of us (T.A.C.) would like to thank the Joint Institute for Laboratory Astrophysics, National Bureau of Standards, Boulder, Colorado, for fellowship support and assistance in the preparation of this paper.

REFERENCES

1. (a) J. L. Gole, D. R. Preuss, and C. L. Chalek, J. Chem. Phys. 66, 548 (1977); (b) J. L. Gole, "Development of Visible Chemical Lasers from Reactions Yielding Visible Chemiluminescence," Electronic Transition Chemical Lasers, Vol. III, ed. by L. E. Wilson, S. N. Suchard, and J. I. Steinfeld (MIT Press, Cambridge, Mass., 1977), p. 136.

2. See, for example, (a) C. R. Dickson and R. N. Zare, Chem. Phys. 7, 361 (1975) and references therein; (b) D. J. Ekstrom, S. A. Edelstein, D. L. Huestis, B. E. Perry, and S. W. Benson, J. Chem. Phys. 63, 3828 (1975) and references therein.

3. D. R. Fischell, H. C. Brayman, and T. A. Cool, J. Chem. Phys. 00, 0000 (1980), following paper.

4. H. C. Brayman, Ph.D. Thesis, Cornell University, 1980.

5. D. R. Fischell, Ph.D. Thesis, Cornell University, 1980.

6. R. Hultgreen, P. D. Desai, P. T. Hawkins, M. Gleiser, K. K. Kelley, and D. D. Wagman, Selected Values of the Thermodynamic Properties of the Elements (American Society of Metals, Metals Park, Ohio, 1973).

7. S. H. Bauer and D. Jeffers, J. Phys. Chem. 69, 3317 (1965).

8. T. W. Hänsch, Appl. Opt. 11, 895 (1972).

9. We are indebted to R. N. Zare for his suggestion of this experiment.

10. E. A. Shenyavskaya, A. A. Mal'tsev, and L. U. Gurvich, Opt. Spectrosc. 21, 374 (1975); R. F. Barrow, M. W. Bastin, D. L. G. Moore, and C. J. Pott, Nature 215, 1072 (1967).

11. G. M. Janney, J. Opt. Soc. Amer. 56, 1706 (1966).

12. D. L. Hildenbrand, in Advances in High Temperature Chemistry, ed. by H. L. Eyring (Academic Press, New York, 1967), Vol. I.

13. K. S. Krasnov and V. O. Timoshinin, High Temp. 7, 333 (1969).

14. JANAF Thermochemical Tables, NSRDS-NBS 37, 1971.

15. D. Wren and M. Menzinger, Chem. Phys. Lett. 20, 471 (1973).

16. D. Wren and M. Menzinger, Chem. Phys. Lett. 27, 572 (1974).

17. D. O. Ham and H. W. Chung, Chem. Phys. Lett. 24, 579 (1974).

18. M. Menzinger, Chem. Phys. 5, 350 (1975).

19. D. Wren, Ph.D. Thesis, University of Toronto, 1979.

20. P. R. Bevington, Data Reduction and Error Analysis for the Physical Sciences (McGraw Hill, New York, 1969), p. 237.

APPENDIX

Kinetic Model for the Y+$C\ell_2$ Reaction System

Differential rate equations for the processes defined in Eqs. (3) to (7) are:

$$d[Y]/dt = -k_1[Y][C\ell_2] \tag{A-1}$$

$$d[YC\ell]/dt = -k_{2+4}[YC\ell][C\ell_2] + k_1[Y][C\ell_2] \tag{A-2}$$

$$d[YC\ell_2]/dt = -k_3[YC\ell_2][C\ell_2] + k_5[YC\ell_2^*] \tag{A-3}$$

$$d[YC\ell_2^*]/dt = k_4[YC\ell][C\ell_2] - k_5[YC\ell_2^*] \tag{A-4}$$

$$d[YC\ell_3]/dt = k_3[YC\ell_2][C\ell_2] \tag{A-5}$$

where $k_{2+4} = k_2+k_4$ and the backward rates can be neglected under the present experimental conditions. The equations are integrated with the assumptions that at time $t = 0$ the Y atoms and $C\ell_2$ molecules are uniformly mixed and that reaction proceeds until the time $t = \tau$ at which LIF is observed. Moreover, it is assumed that since $[Y] \ll [C\ell_2]$ in the present experiments, then the concentration, $[C\ell_2]$, can be considered a constant; it is also assumed that $k_4 \ll k_2$. The initial conditions at $t = 0$ are $[Y] = [Y]_0$ and $[YC\ell] = [YC\ell_2] = [YC\ell_2^*] = [YC\ell_3] = 0$.

Solutions for the species concentrations with these approximations are:

$$[Y] = [Y]_0 \exp(-k_1[C\ell_2]\tau) \tag{A-6}$$

$$[YC\ell] = k_1[Y]_0[\exp(-k_2[C\ell_2]\tau) - \exp(-k_1[C\ell_2]\tau)]/(k_1-k_2) \tag{A-7}$$

$$[YC\ell_2] = k_1k_2[Y]_0\{[\exp(-k_3[C\ell_2]\tau) - \exp(-k_2[C\ell_2]\tau)]/(k_2-k_3) - [\exp(-k_3[C\ell_2]\tau) - \exp(-k_1[C\ell_2]\tau)]/(k_1-k_3)\}/(k_1-k_2) \tag{A-8}$$

$$[YCl_2^*] = k_1k_4[Y]_o[Cl_2]\{[\exp(-k_5\tau)-\exp(-k_2[Cl_2]\tau)]/(k_2[Cl_2]-k_5) \quad \text{(A-9)}$$
$$- [\exp(-k_5\tau)-\exp(-k_1[Cl_2]\tau)]/(k_1[Cl_2]-k_5)\}/(k_1-k_2)$$

$$[YCl_3] = [Y]_o\{1+[k_1k_2(k_2-k_1)\exp(-k_3[Cl_2]\tau) - k_1k_3(k_3-k_1)\exp(-k_2[Cl_2]\tau) \quad \text{(A-10)}$$
$$+ k_2k_3(k_2-k_1)\exp(-k_1[Cl_2]\tau)]/(k_1-k_2)(k_1-k_2)(k_2-k_3)\}$$

The experimental data were fitted to Eqs. (A-6),(A-7), (A-8) and (A-9) using a least squares routine described by Bevington.[20] The relative rate constants giving a best fit to the experimental data were:

$$k_1\tau = (3.9\pm0.3) \times 10^3 \text{ Torr}^{-1}$$
$$k_2\tau = (8.8\pm0.7) \times 10^3 \text{ Torr}^{-1}$$
$$k_3\tau = (5.5\pm2) \times 10^3 \text{ Torr}^{-1}$$
$$k_5\tau = 15\pm3$$

The fit was most sensitive to the choice of values for $k_1\tau$ and $k_2\tau$. Fig. 20 shows a composite of the concentrations calculated with these parameters.

TABLE I

Estimated Bond Energies (kcal/mole)

Top Row: Potential Function Model[a]
Bottom Row: Experimental[b]

Halide	D_{MX}	D_{XM-X}	D_{X_2M-X}	D_{MX_3}
Y+Cℓ	111(88)[c]	119	128	358
	---	---	---	---
Y+F	154(152)[c]	155	155	464
	143.6±5	143.4±7	166±10	453
Sc+F	134(136)[c]	142	151	427
	140.8±3	140.3±5	157±7	438

[a]K. S. Krasnov and V. S. Timoshinin, High Temp. 7, 333 (1969).

[b]K. F. Zmbov and J. L. Margrave, J. Chem. Phys. 47, 3122 (1967).

[c]Corrected Birge-Sponer extrapolation, D. L. Hildenbrand, in Advances in High Temperature Chemistry, edited by H. L. Eyring (Academic Press, New York, 1967), Vol. I.

FIGURE CAPTIONS

Fig. 1. Schematic diagram of oven and reaction chamber.

Fig. 2. Experimental arrangement employed for recording LIF excitation spectra.

Fig. 3. Experimental arrangement employed for observations of chemiluminescence.

Fig. 4. Chemiluminescence from the $Y/C\ell_2$ reaction system. The open circles are data previously reported by Gole et al. in ref. 1.

Fig. 5. Variation in chemiluminescence intensity from the $Y/C\ell_2$ reaction system with $C\ell_2$ pressure. The open circles are the experimental data; the solid curve is the variation predicted with the kinetic model discussed in the Appendix. The ordinate scale gives the $C\ell_2$ pressure in millitorr multiplied by the factor 30.

Fig. 6. Laser-induced fluorescence from the $Y/C\ell_2$ reaction system in the 3900 A region. The solid triangles show the spectral distribution of chemiluminescence presented in Fig. 4.

Fig. 7. Semilogarithmic plot of the decay of LIF from the chemiluminescent emitter ($YC\ell_2^*$) of the $Y/C\ell_2$ reaction system.

Fig. 8. Chemiluminescence from the Y/Br_2 reaction system.

Fig. 9a. Chemiluminescence from the reaction of Y atoms with $C\ell_2+Br_2$ mixtures.
Fig. 9b. Progressively greater amounts of Br_2 were added in the sequence from
Fig. 9c. Fig. 9a to 9c.

Fig. 10. Variation in the concentration of Y atoms with $C\ell_2$ pressure. The open circles are the experimental data; the solid curve is the variation predicted with the kinetic model discussed in the Appendix. The ordinate scale gives the $C\ell_2$ pressure in millitorr multiplied by the factor 30.

Fig. 11. Variation in the concentration of $YC\ell$ molecules with $C\ell_2$ pressure. The open circles are the experimental data; the solid curve is the variation predicted with the kinetic model discussed in the Appendix. The ordinate scale gives the $C\ell_2$ pressure in millitorr multiplied by the factor 30.

Fig. 12. Variation in the concentration of $YC\ell_2$ molecules with $C\ell_2$ pressure. The open circles are the experimental data; the solid curve is the variation predicted with the kinetic model discussed in the Appendix. The ordinate scale gives the $C\ell_2$ pressure in millitorr multiplied by the factor 30.

FIGURE CAPTIONS (cont.)

Fig. 13. Predicted variation in YCl_3 concentration with Cl_2 pressure based on the kinetic model discussed in the Appendix. The ordinate scale gives the Cl_2 pressure in millitorr multiplied by the factor 30.

Fig. 14. Chemiluminescence from the Y/F_2 reaction system.

Fig. 15. Chemiluminescence from the Y/I_2 reaction system.

Fig. 16. Chemiluminescence from the Sc/F_2 reaction system.

Fig. 17. Chemiluminescence from the Sc/Cl_2 reaction system.

Fig. 18. Chemiluminescence from the Sc/Br_2 reaction system.

Fig. 19. Chemiluminescence from the Sc/I_2 reaction system.

Fig. 20. Variation in the concentrations of components of the Y/Cl_2 reaction system with Cl_2 pressure predicted with the kinetic model discussed in the Appendix. The ordinate scale gives the Cl_2 pressure in millitorr multiplied by the factor 30.

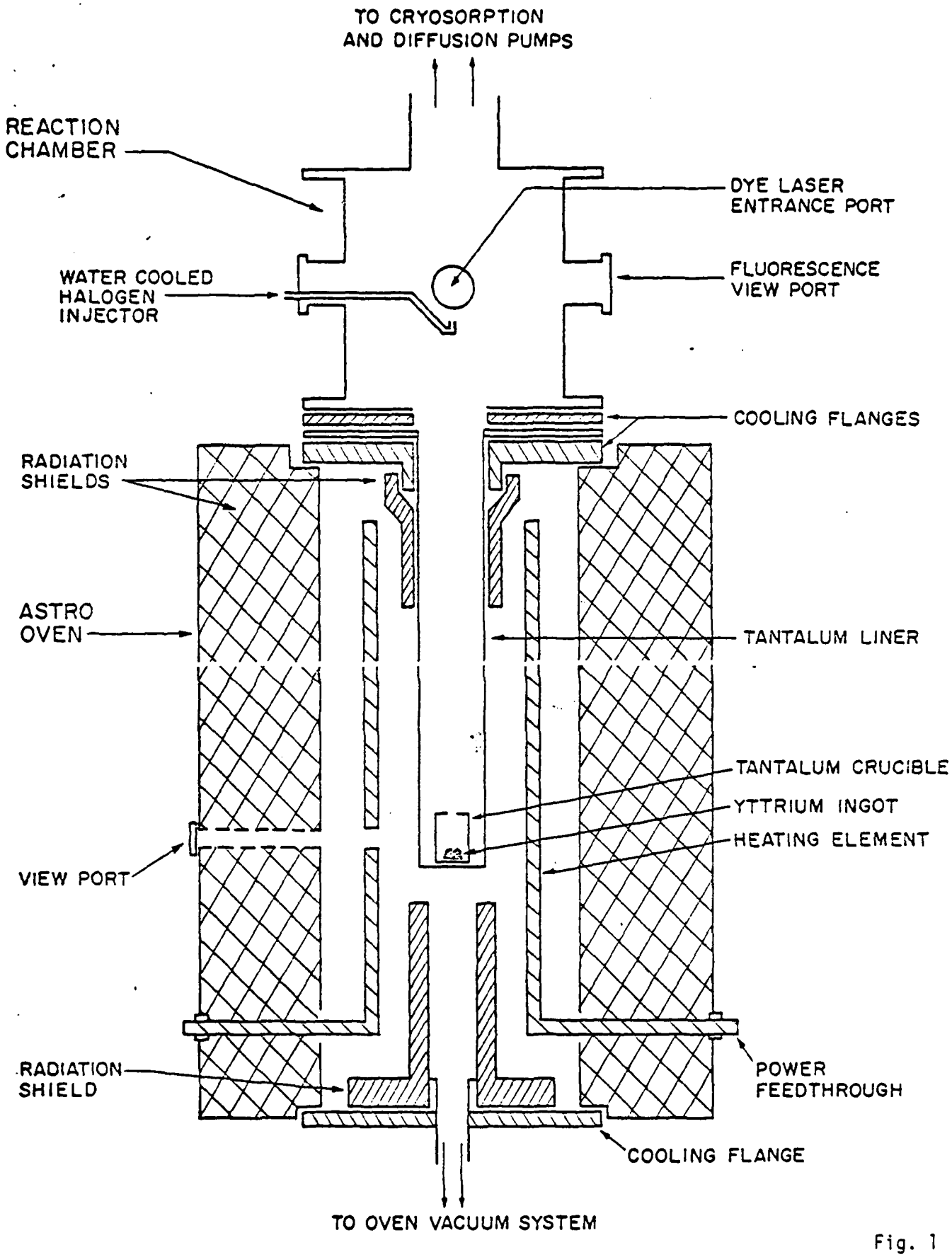
TO CRYOSORPTION
AND DIFFUSION PUMPS
REACTION
CHAMBER
DYE LASER
ENTRANCE PORT
WATER COOLED
HALOGEN
INJECTOR
FLUORESCENCE
VIEW PORT
COOLING FLANGES
RADIATION
SHIELDS
ASTRO
OVEN
TANTALUM LINER
TANTALUM CRUCIBLE
YTTRIUM INGOT
HEATING ELEMENT
VIEW PORT
RADIATION
SHIELD
POWER
FEEDTHROUGH
COOLING FLANGE
TO OVEN VACUUM SYSTEM

Fig. 1

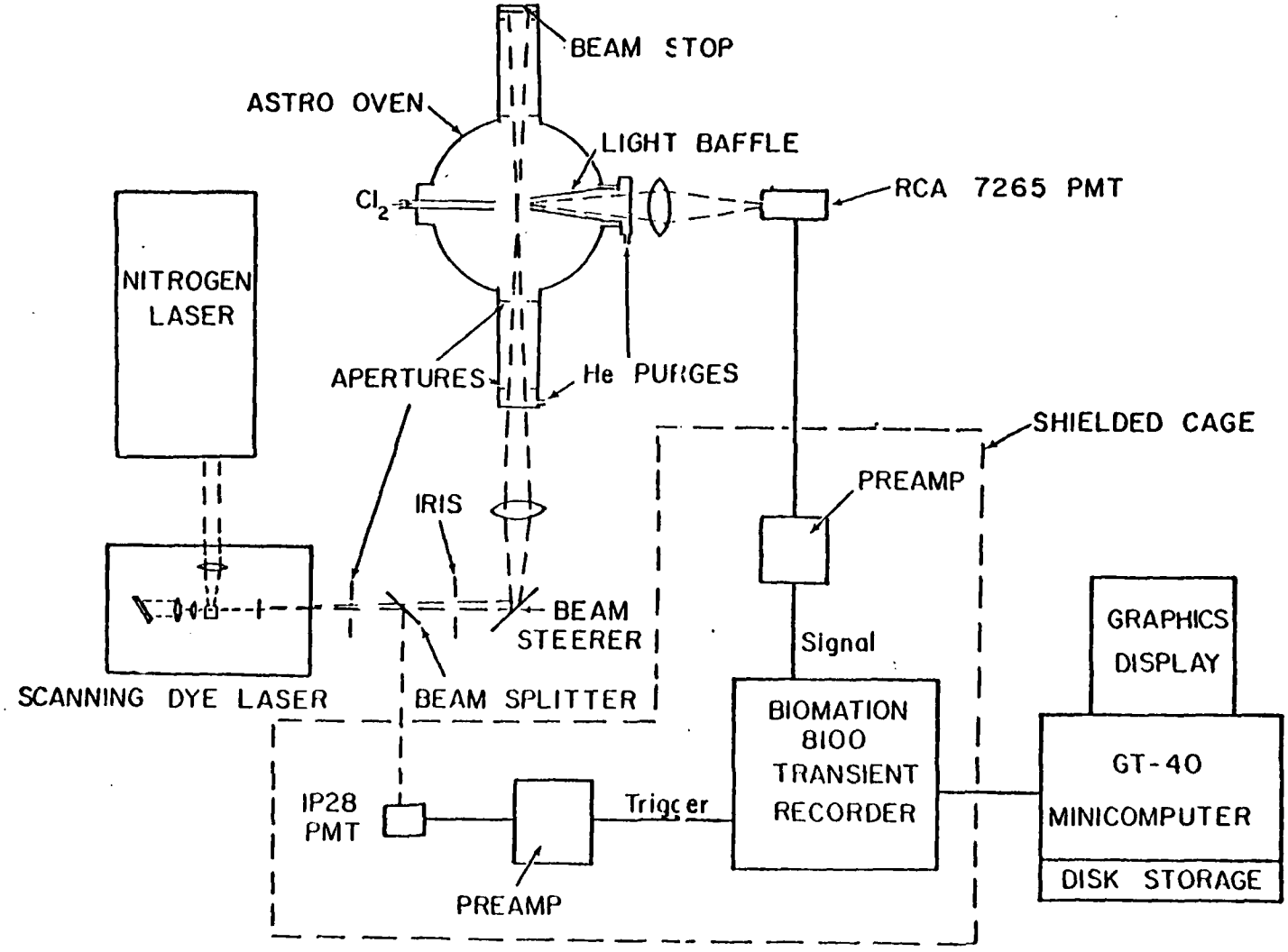
BEAM STOP
ASTRO OVEN
LIGHT BAFFLE
Cl_2
RCA 7265 PMT
NITROGEN LASER
APERTURES
He PURGES
SHIELDED CAGE
PREAMP
IRIS
BEAM STEERER
Signal
GRAPHICS DISPLAY
SCANNING DYE LASER
BEAM SPLITTER
BIOMATION 8100 TRANSIENT RECORDER
GT-40 MINICOMPUTER
IP28 PMT
Trigger
DISK STORAGE
PREAMP

Fig. 2

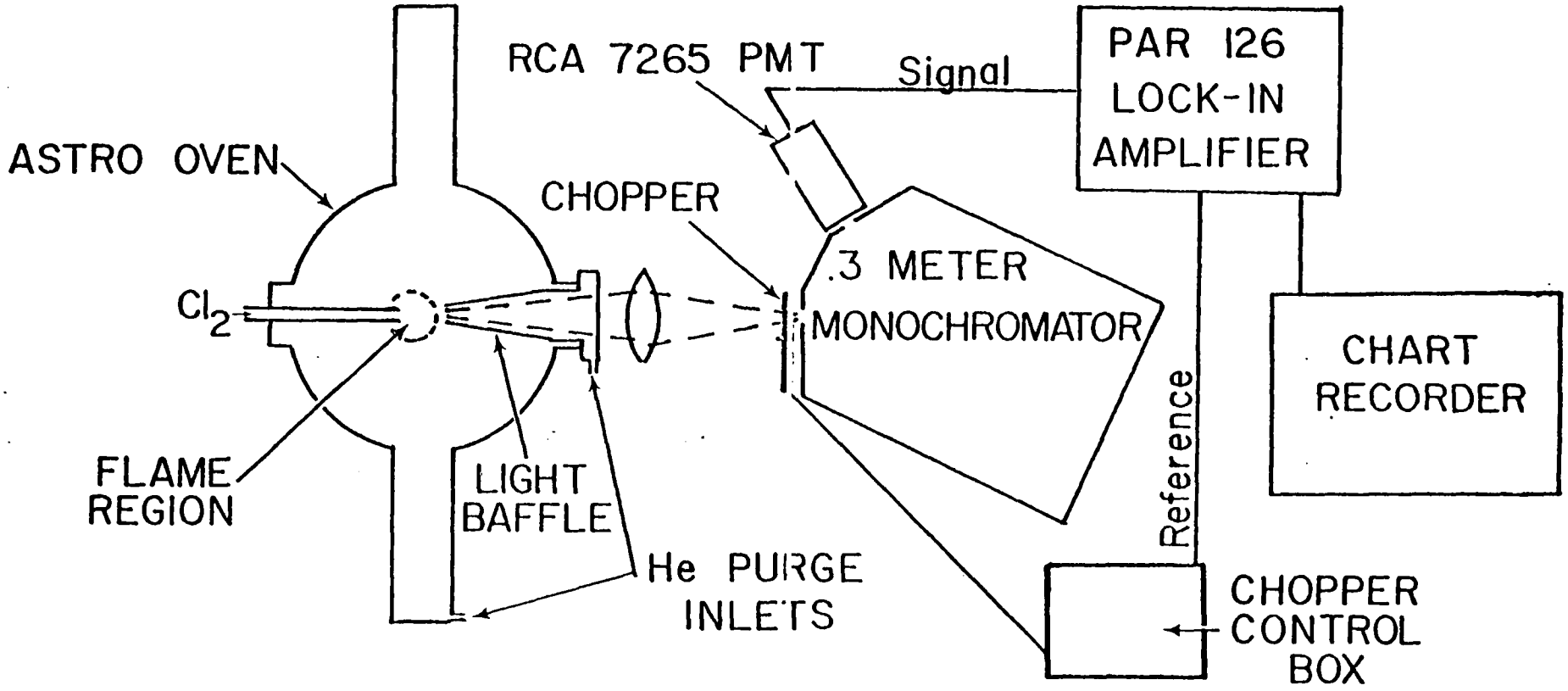
RCA 7265 PMT
Signal
PAR 126
LOCK-IN
AMPLIFIER
ASTRO OVEN
CHOPPER
.3 METER
MONOCHROMATOR
Cl_2
CHART
RECORDER
FLAME
REGION
LIGHT
BAFFLE
Reference
He PURGE
INLETS
CHOPPER
CONTROL
BOX

Fig. 3

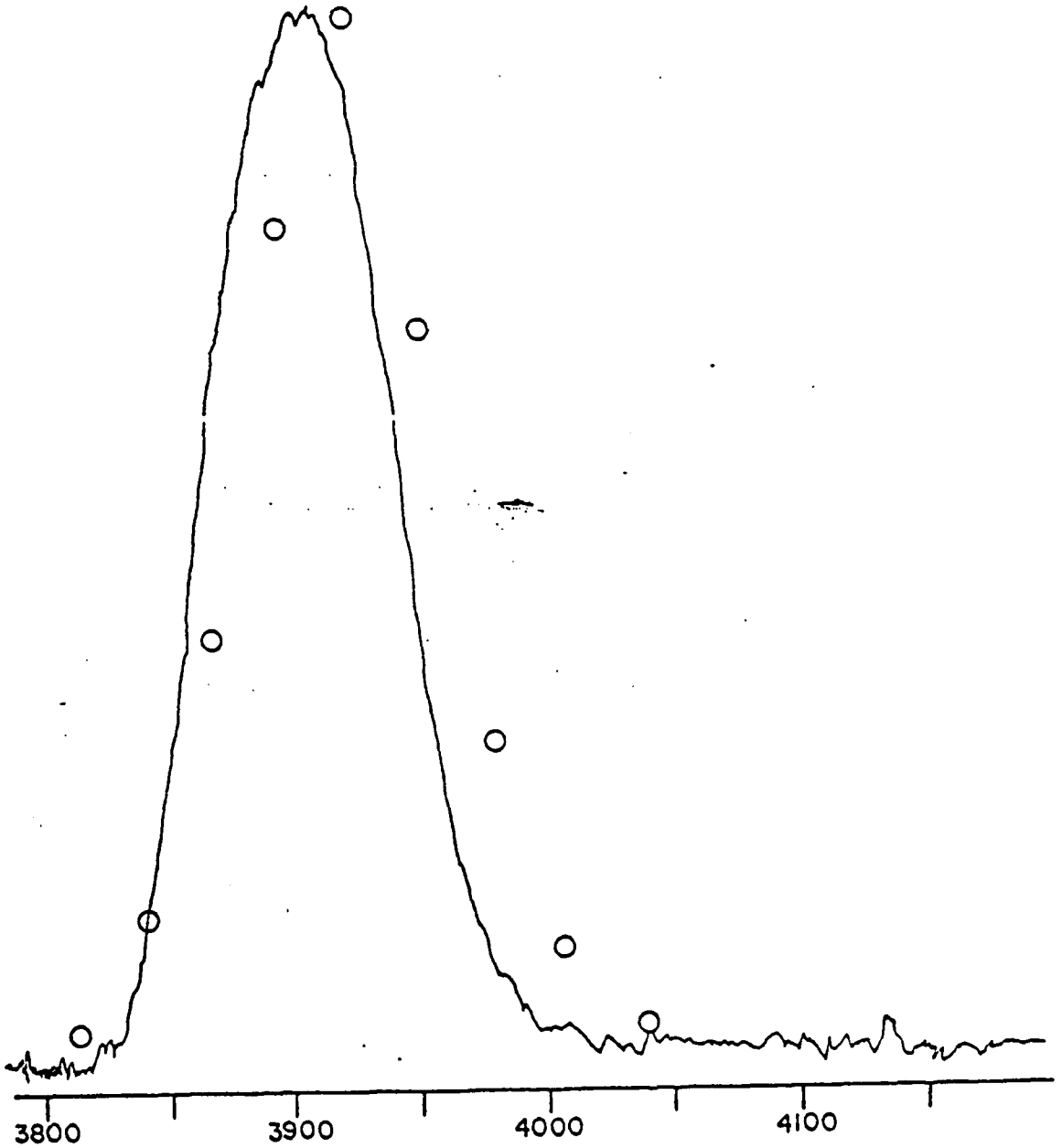

Fig. 4

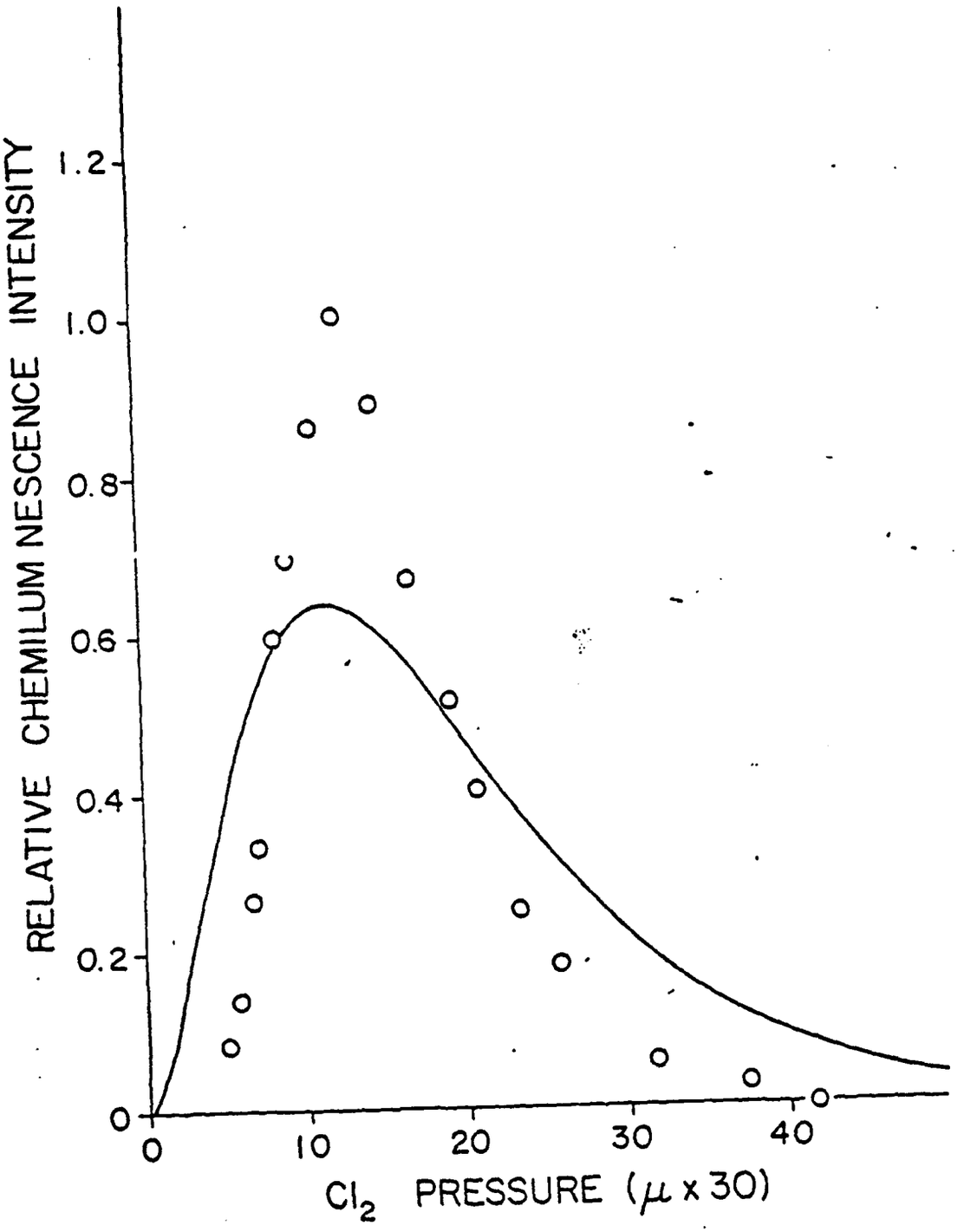
RELATIVE CHEMILUM NESCENCE INTENSITY
1.2
1.0
0.8
0.6
0.4
0.2
0
0
10
20
30
40
Cl_2 PRESSURE (μ x 30)

Fig. 5

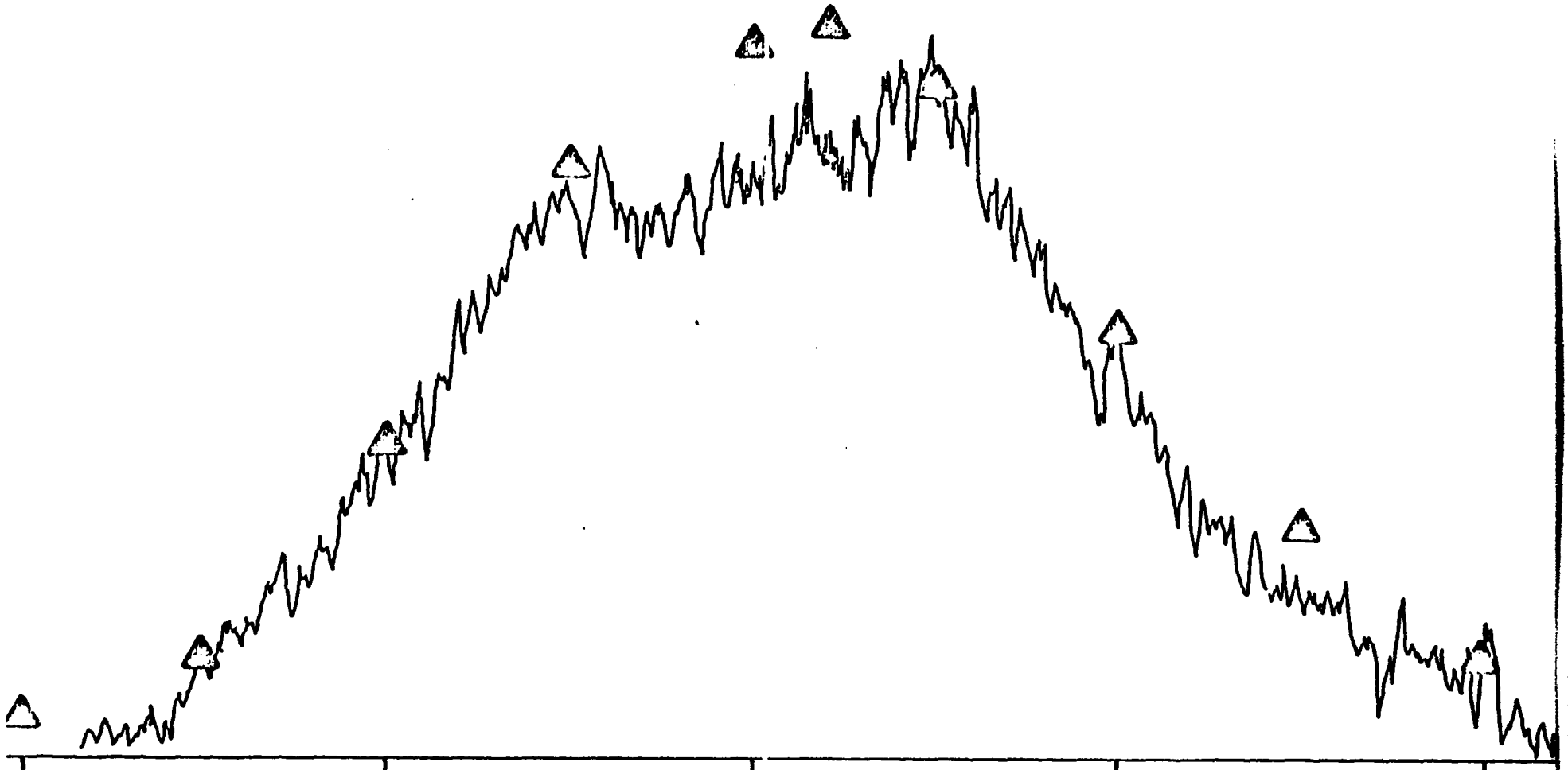

Fig. 6

Fig. 6

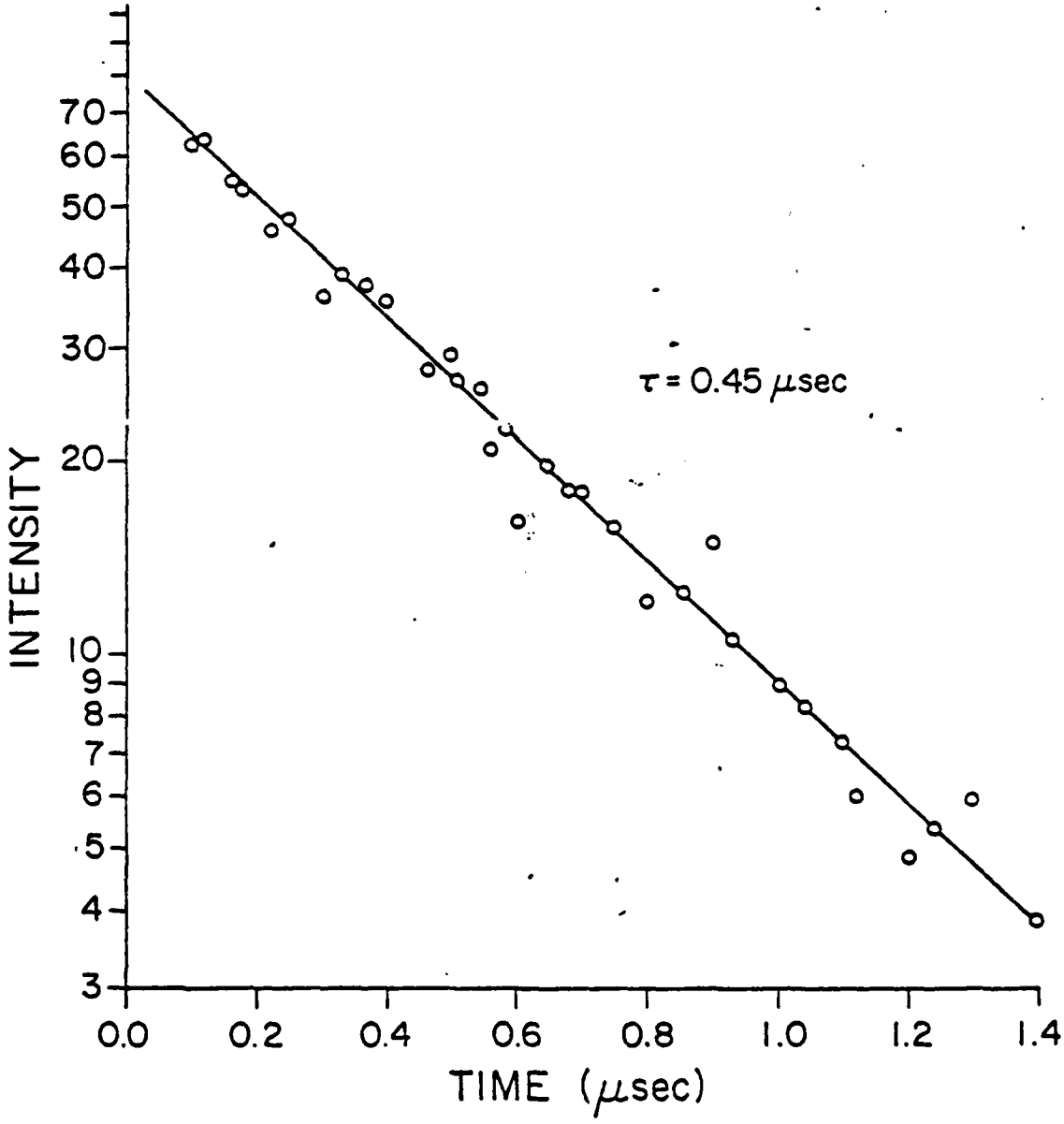
INTENSITY
70
60
50
40
30
20
10
9
8
7
6
5
4
3
0.0
0.2
0.4
0.6
0.8
1.0
1.2
1.4
TIME (μsec)
τ = 0.45 μsec

Fig. 7

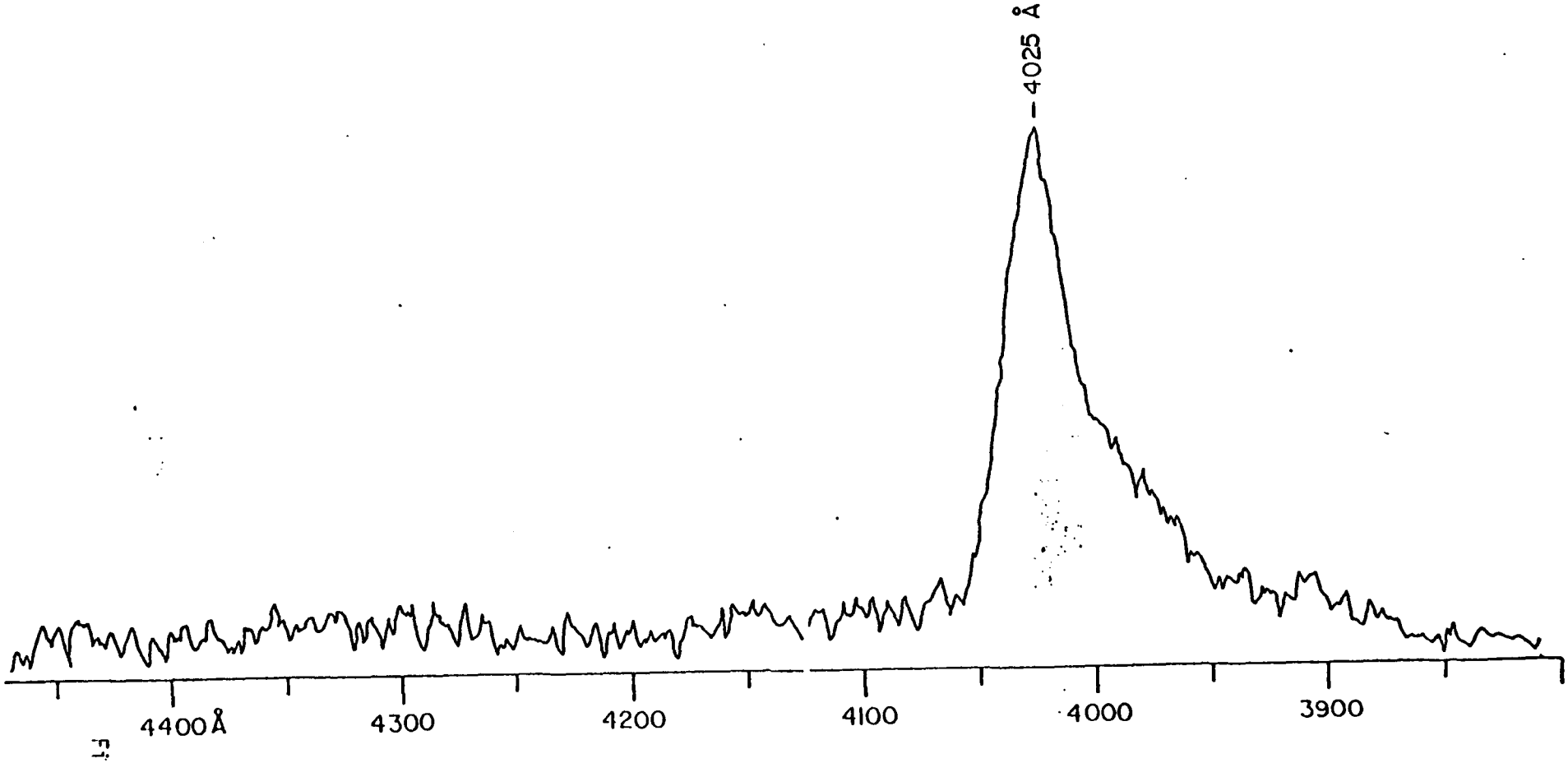

Fig. 8

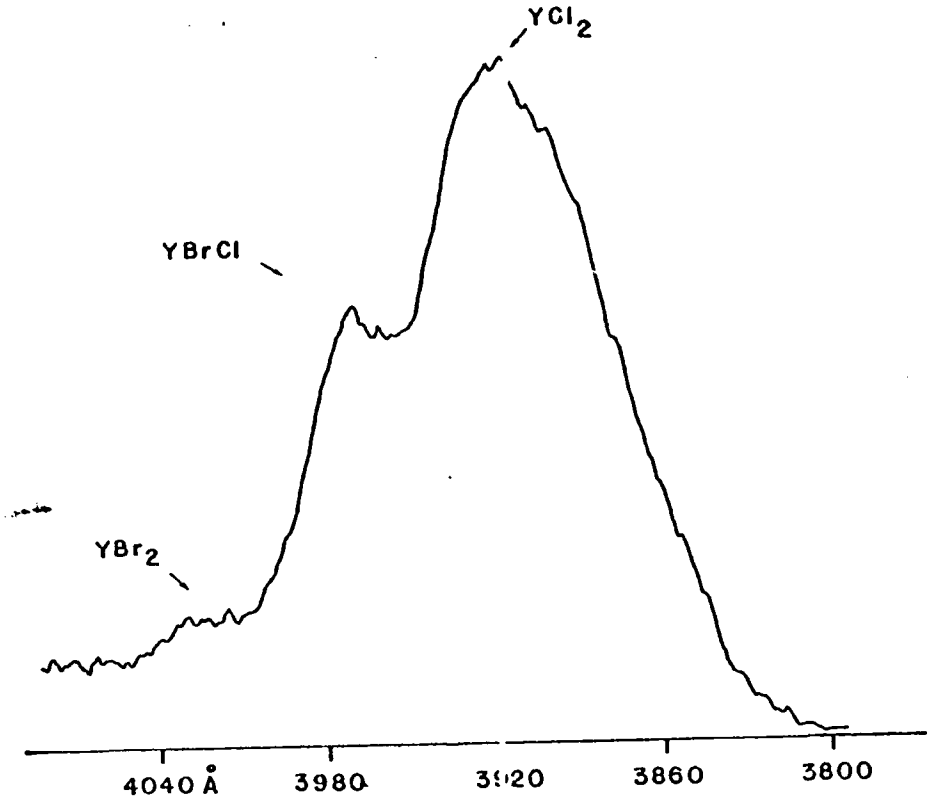

Fig. 9a

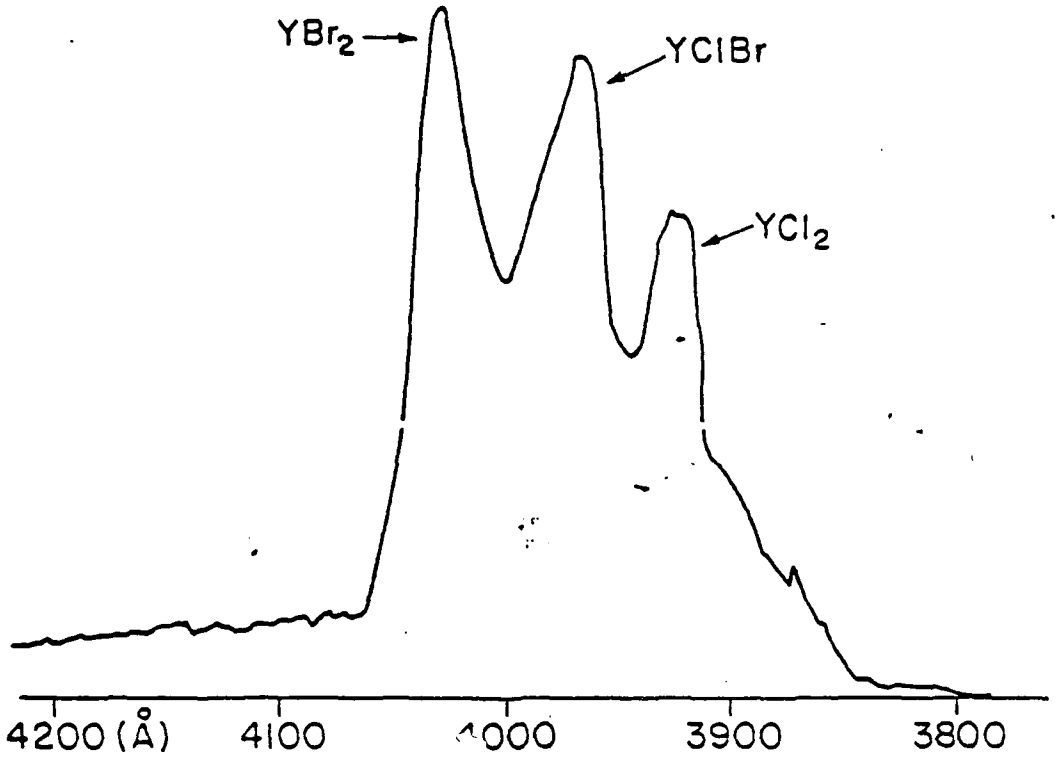

Fig. 9b

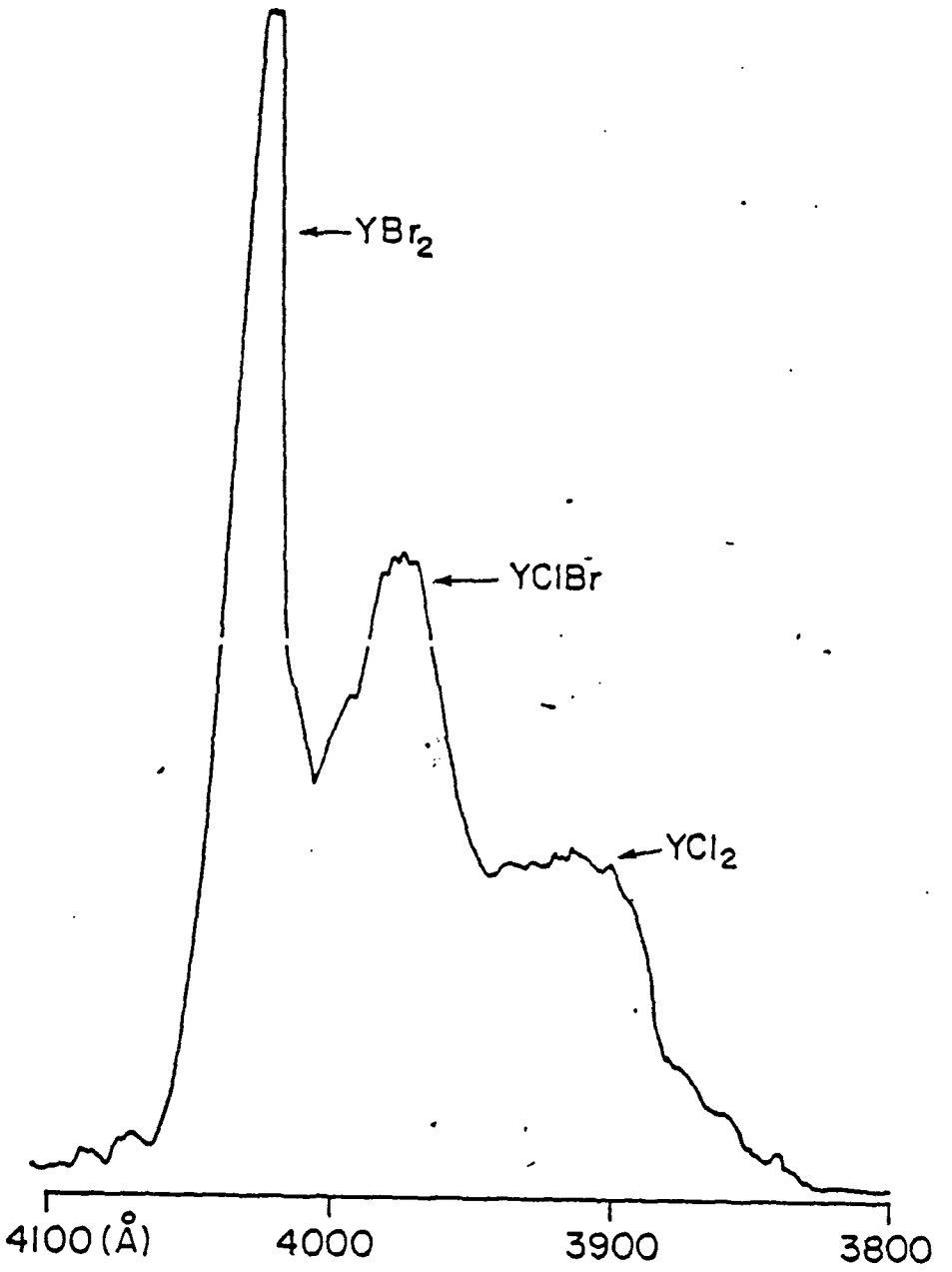

Fig. 9c

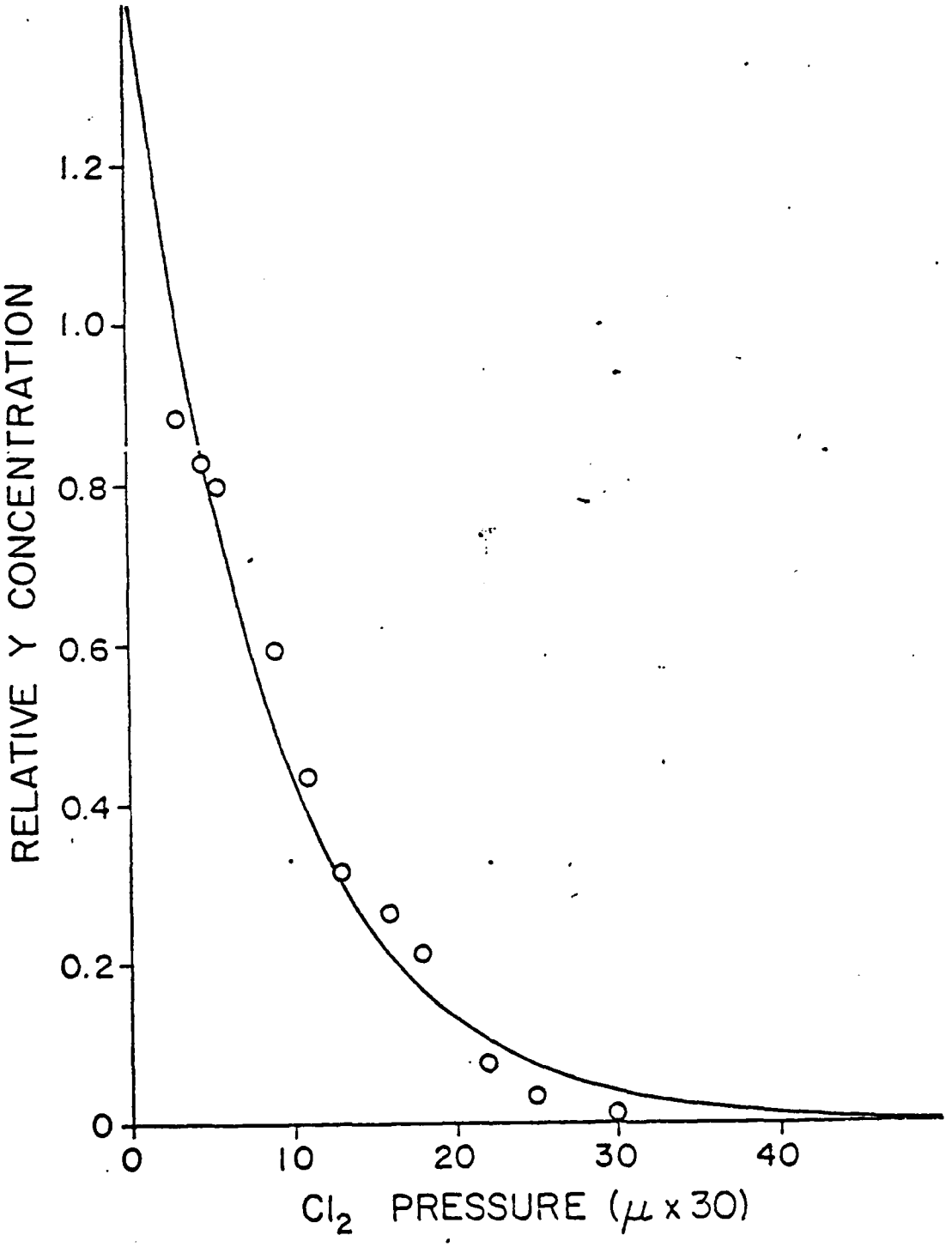
RELATIVE Y CONCENTRATION
1.2
1.0
0.8
0.6
0.4
0.2
0
0
10
20
30
40
Cl_2 PRESSURE (μ x 30)

Fig. 10

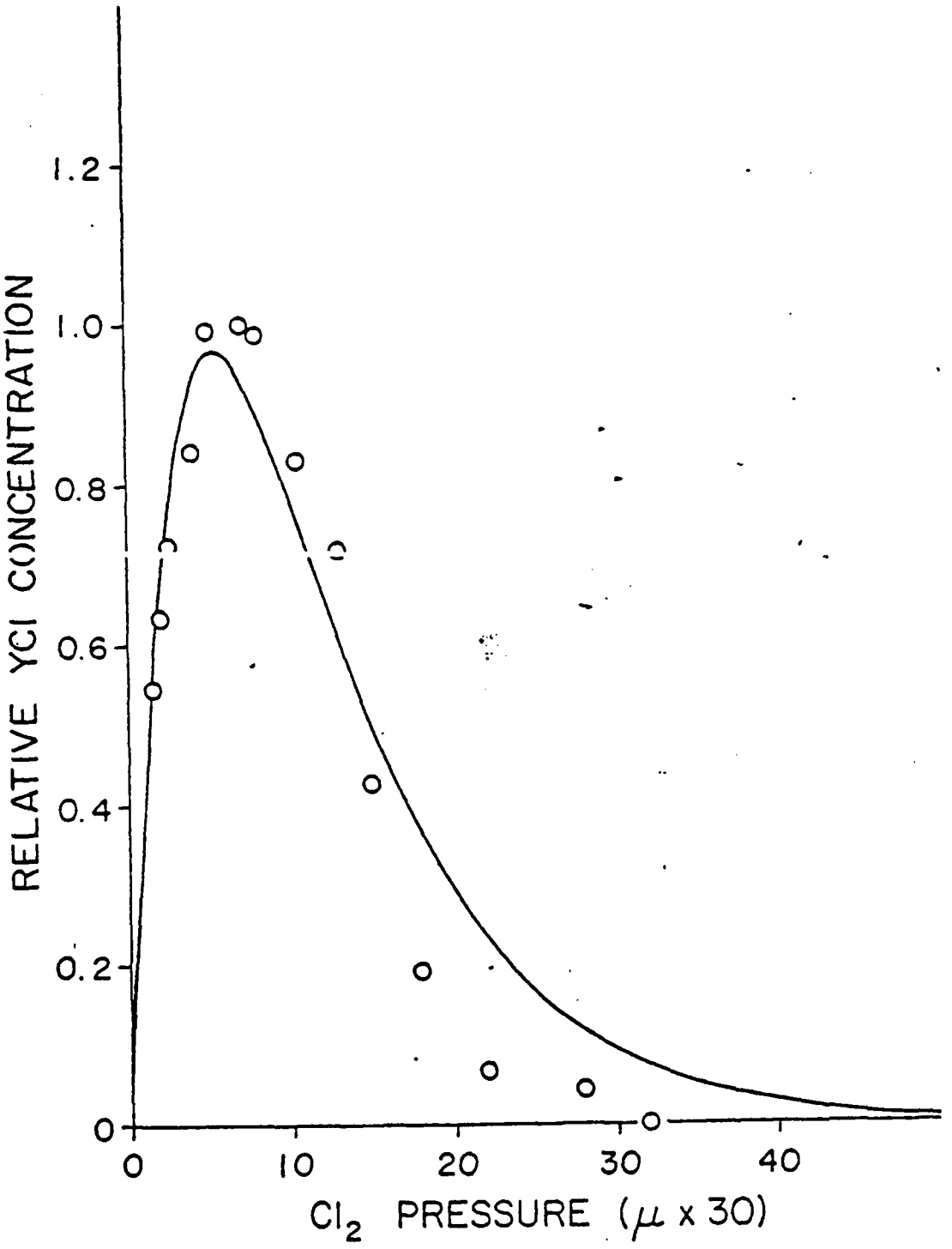
RELATIVE YCl CONCENTRATION
1.2
1.0
0.8
0.6
0.4
0.2
0
0
10
20
30
40
Cl_2 PRESSURE (μ x 30)

Fig. 11

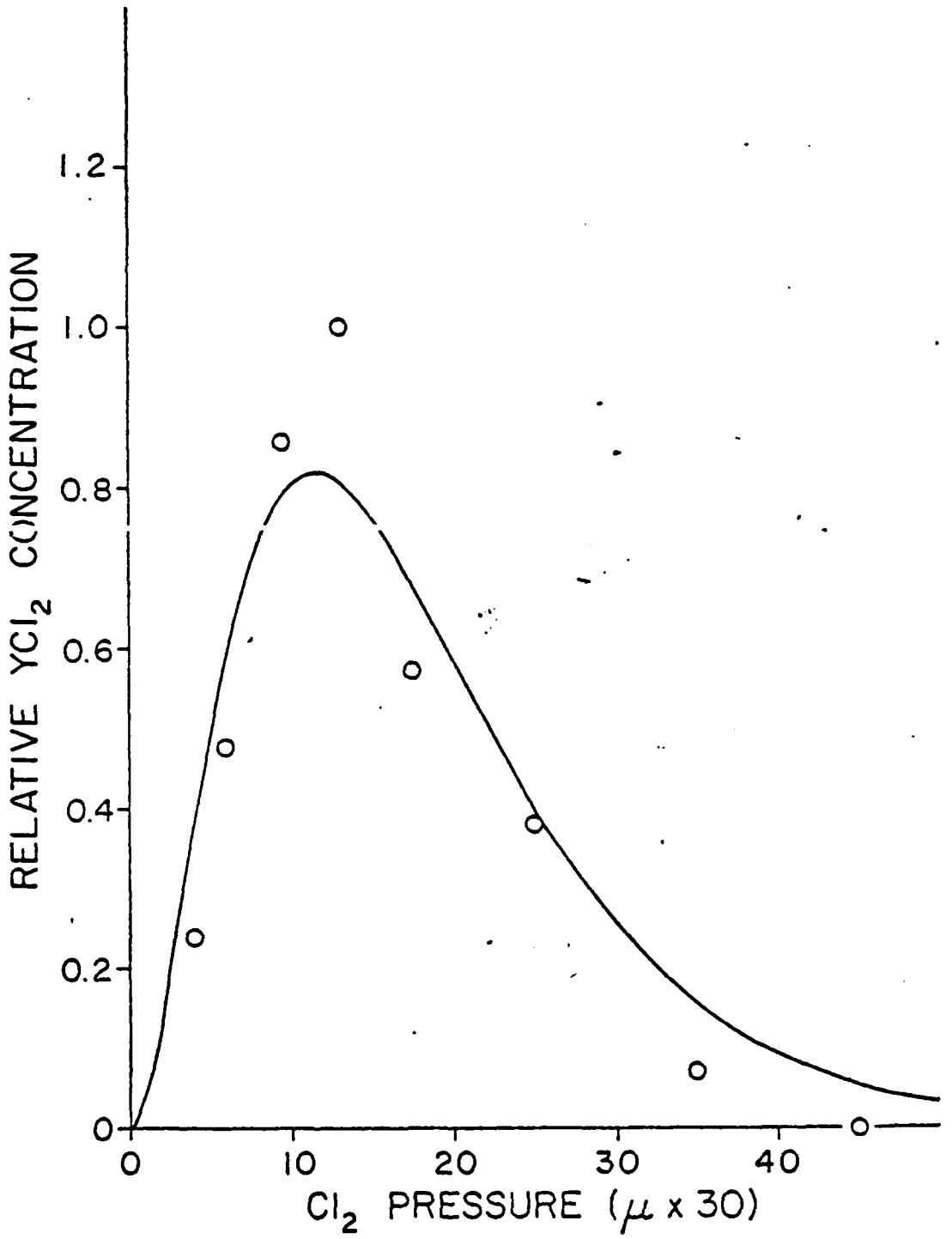
RELATIVE YCl_2 CONCENTRATION
1.2
1.0
0.8
0.6
0.4
0.2
0
0
10
20
30
40
Cl_2 PRESSURE (μ x 30)

Fig. 12

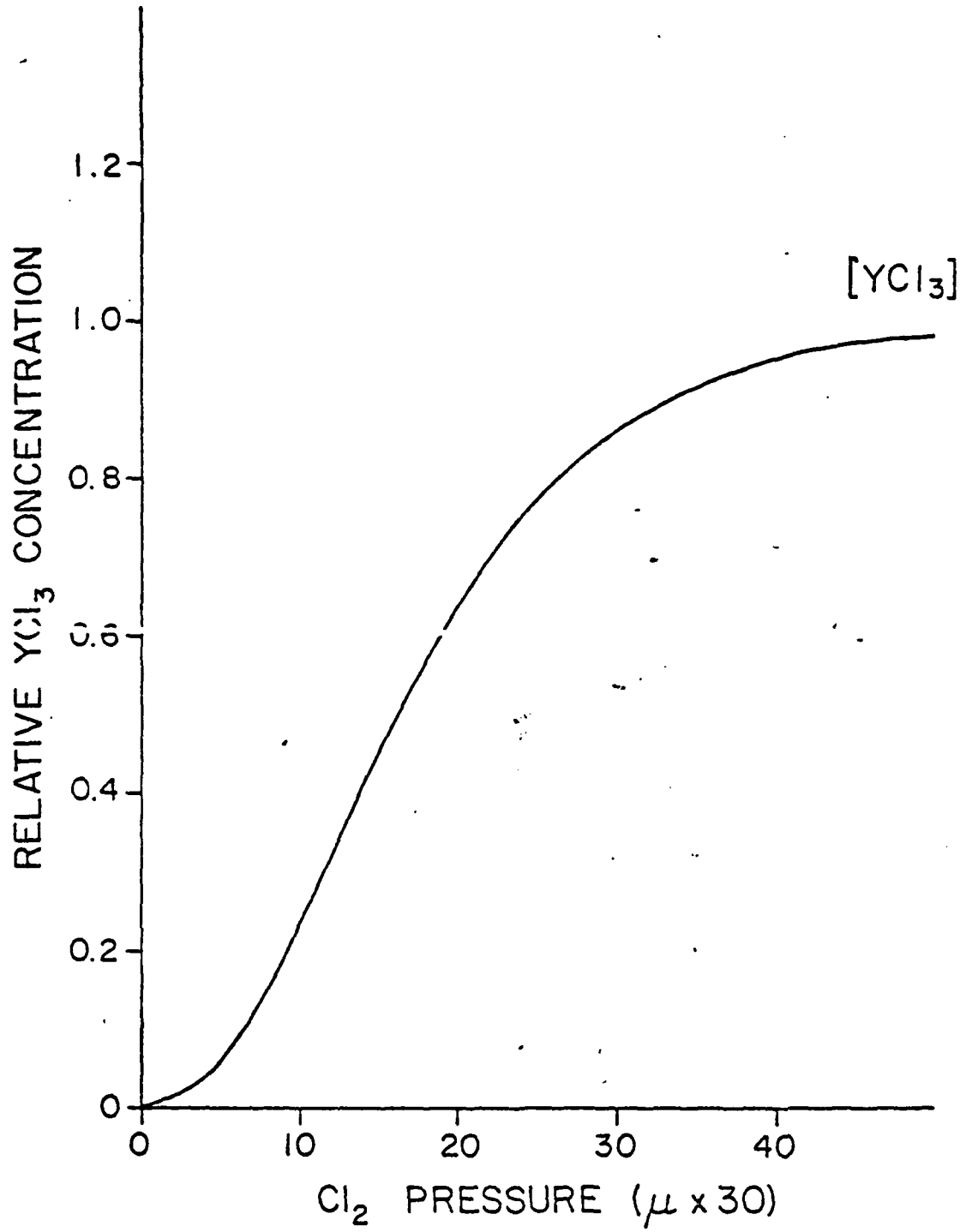
RELATIVE YCl_3 CONCENTRATION
1.2
1.0
0.8
0.6
0.4
0.2
0
0
10
20
30
40
Cl_2 PRESSURE (μ x 30)
$[YCl_3]$

Fig. 13

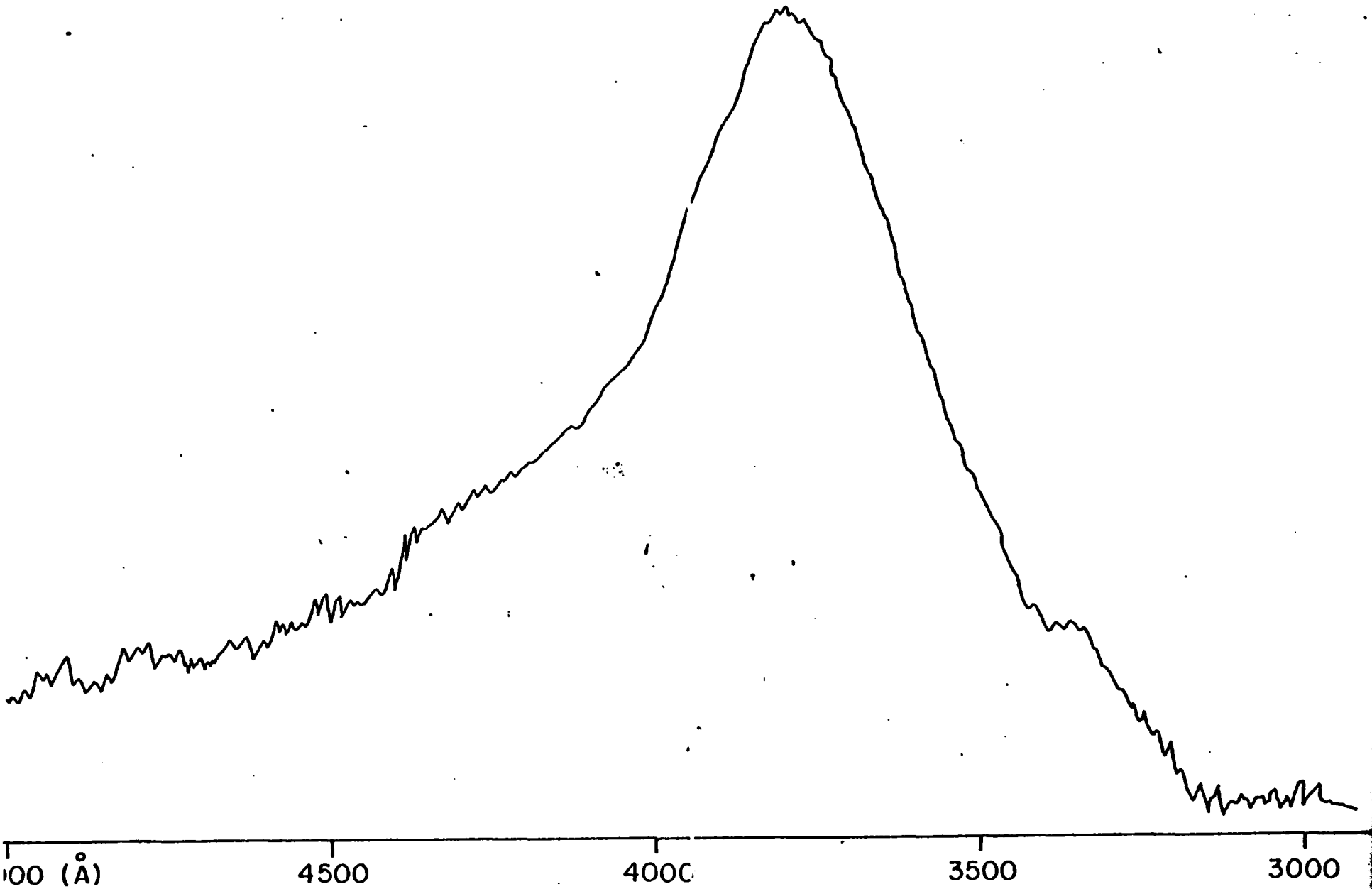

Fig.

Fig

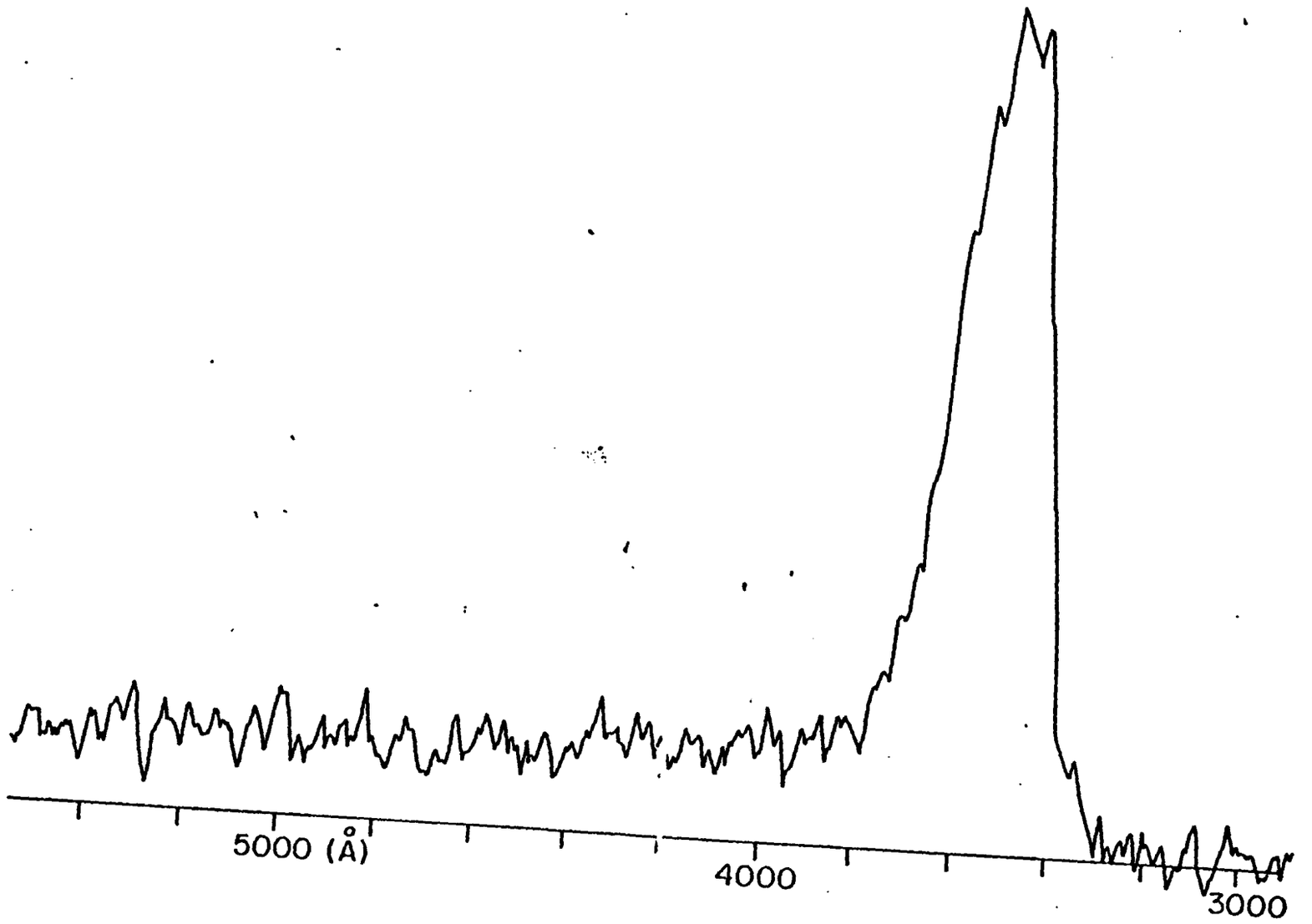

Fig. 16

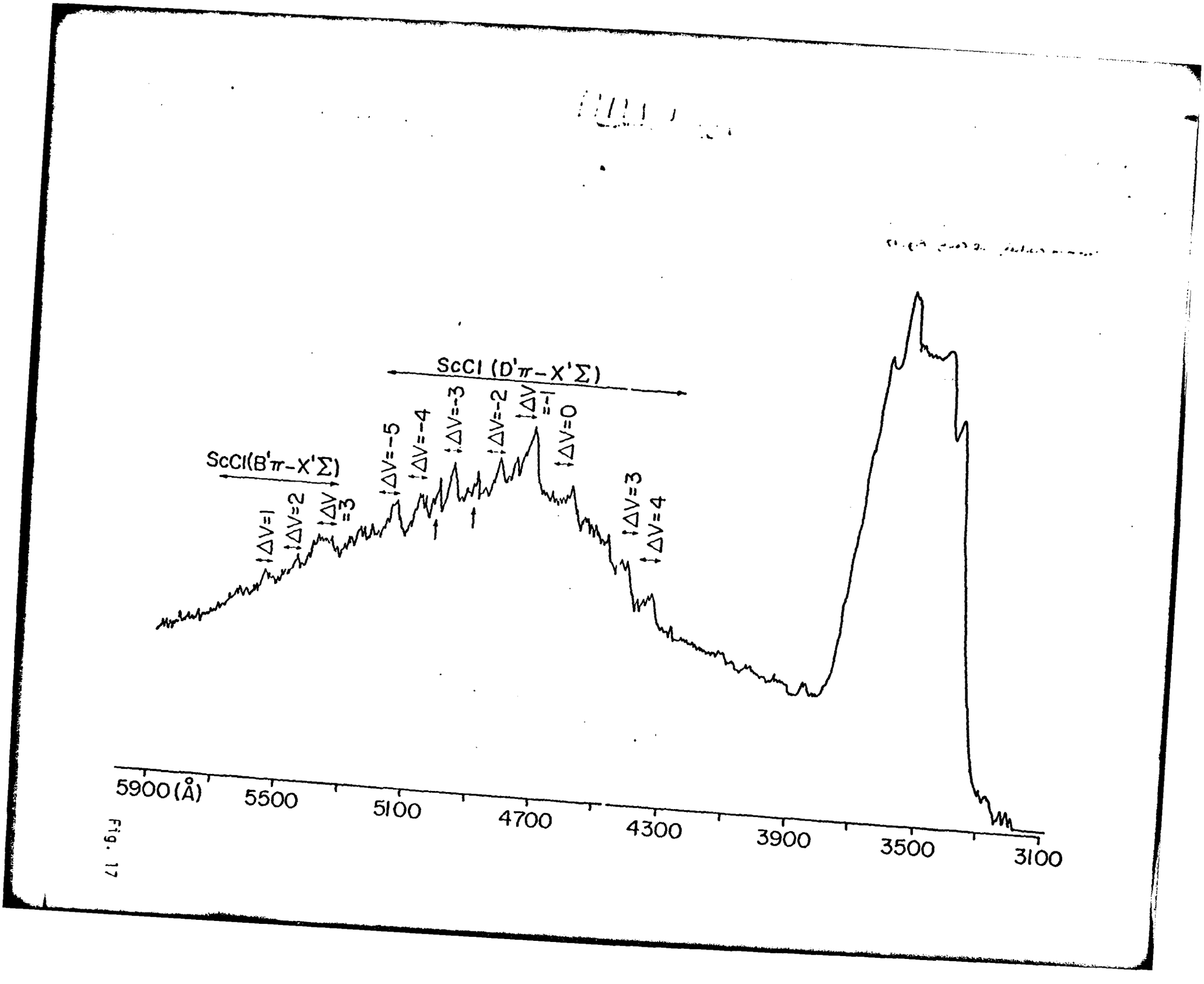
ScCl (D'π−X'Σ)
ScCl(B'π−X'Σ)
ΔV=1
ΔV=2
ΔV=3
ΔV=-5
ΔV=-4
ΔV=-3
ΔV=-2
ΔV=-1
ΔV=0
ΔV=3
ΔV=4
5900 (Å)
5500
5100
4700
4300
3900
3500
3100

Fig. 17

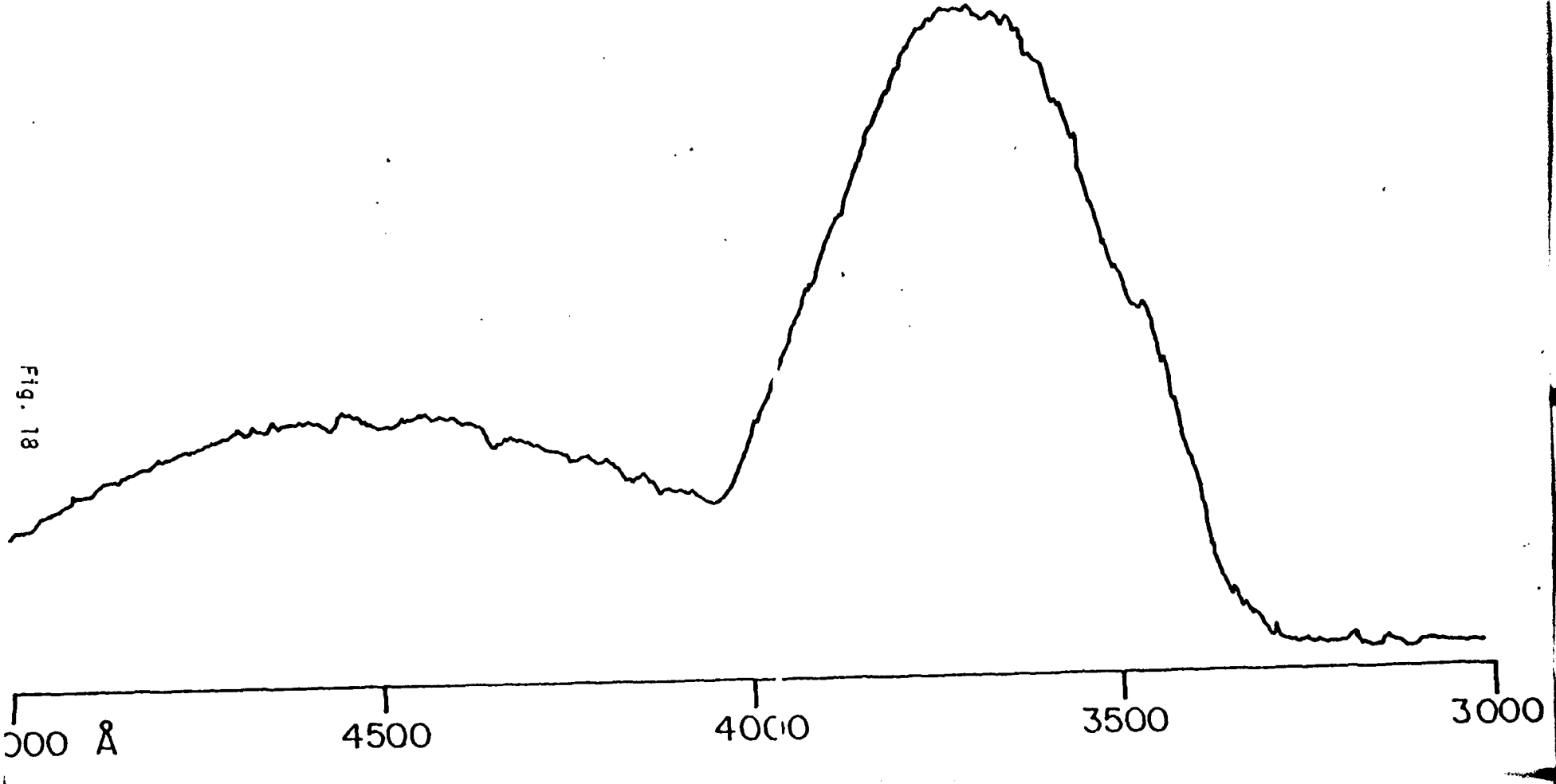

Fig. 18

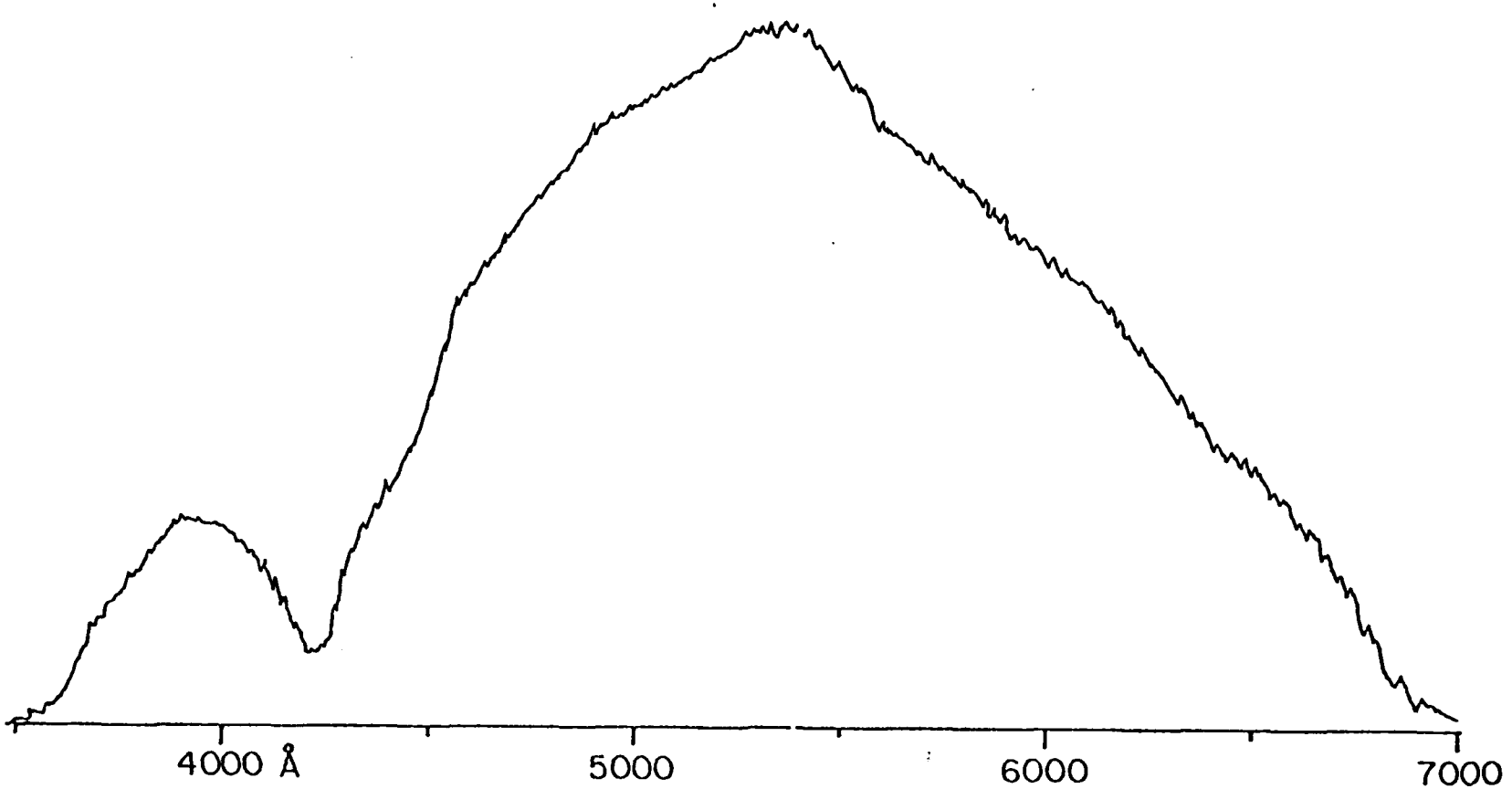

Fig. 19

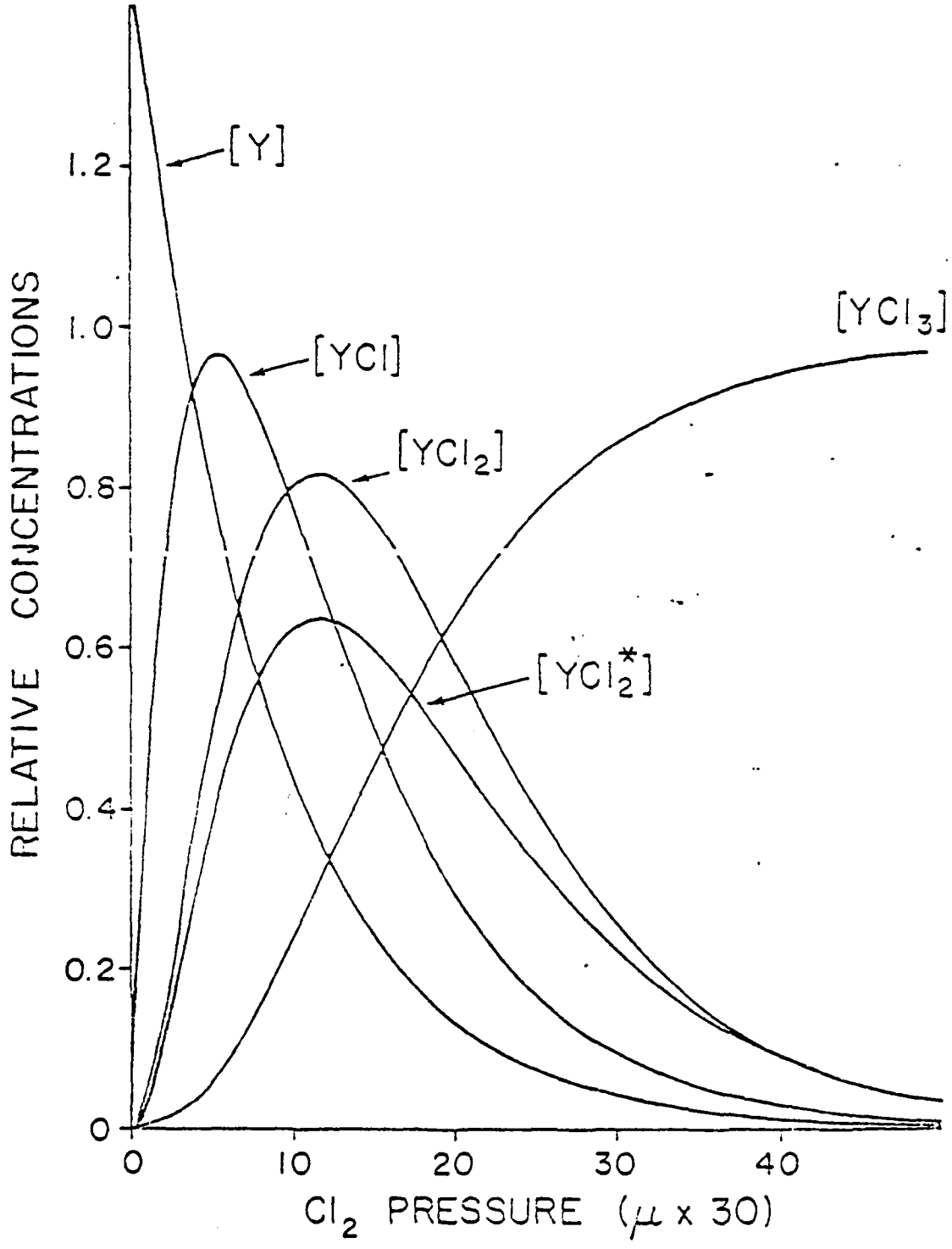
RELATIVE CONCENTRATIONS
1.2
1.0
0.8
0.6
0.4
0.2
0
[Y]
[YCl]
[YCl2]
[YCl2*]
[YCl3]
0
10
20
30
40
Cl2 PRESSURE (μ x 30)

Fig. 20

III.*

SPECTROSCOPIC STUDIES OF THE PRODUCTS OF REACTIONS OF YTTRIUM AND SCANDIUM ATOMS WITH HALOGEN MOLECULES. II. LASER INDUCED FLUORESCENCE FROM YTTRIUM AND SCANDIUM MONOHALIDES

David R. Fischell, Howard C. Brayman and Terrill A. Cool

School of Applied and Engineering Physics
Cornell University
Ithaca, New York 14853

*This section constitutes a paper submitted to the Journal of Chemical Physics.

SPECTROSCOPIC STUDIES OF THE PRODUCTS OF REACTIONS OF YTTRIUM AND SCANDIUM ATOMS WITH HALOGEN MOLECULES. II. LASER INDUCED FLUORESCENCE FROM YTTRIUM AND SCANDIUM MONOHALIDES*

David R. Fischell, Howard C. Brayman and Terrill A. Cool

School of Applied and Engineering Physics
Cornell University
Ithaca, New York 14853

ABSTRACT

Excitation spectra from the monohalides of yttrium and scandium were recorded with the laser induced fluorescence method. Spectroscopic constants and radiative lifetimes were determined for several previously unobserved electronic states. Computer generated spectral simulations were used for the determination of spectroscopic constants and Franck-Condon factors ssociated with the fluorescence band systems.

*Supported by the Air Force Office of Scientific Research under Grant AFOSR 77-3258.

I. INTRODUCTION

Present spectroscopic information on the low-lying electronic states and dissociation energies of the rare earth monohalides is quite incomplete. Of the yttrium and scandium monohalides, spectroscopic data exist only for the fluorides and chlorides.[1] The studies reported here make use of the laser induced fluorescence (LIF) technique for the measurement of radiative lifetimes and the determination of spectroscopic constants for several previously unobserved electronic states in the yttrium and scandium monohalides. Spectroscopic constants are determined by the iterative comparison of computer generated spectral simulations with observed excitation spectra. Franck-Condon factors are calculated for the observed band systems.

A description of the experimental apparatus and techniques is given in the preceding paper,[2] hereafter referred to as I.

II. EXCITATION SPECTRA AND RADIATIVE LIFETIMES FOR YF, YCℓ, YBr, AND YI

Previous spectroscopic studies of the yttrium monohalides have been limited to the YF and YCℓ molecules.[1] Spectroscopic constants for YF are known for four $^1\Pi$ excited states, two $^1\Sigma^+$ excited states, the $^1\Sigma^+$ ground state and $^3\Phi$ and $^3\Delta$ excited states.[1] For YCℓ spectroscopic constants are only known for a single $^1\Sigma^+$ excited state and the $^1\Sigma^+$ ground state.[1]

Excitation spectra with the LIF technique were readily obtainable for the YF, YCℓ, YBr, and YI molecules which permitted the determination of spectroscopic constants for several previously unobserved singlet band systems. No triplet band systems were observed; the ground states for the yttrium monohalides must therefore be $^1\Sigma^+$ states. It was found by trial

and error that the strongest LIF signals were obtainable when the halogen pressure was adjusted to a value somewhat smaller than that required to give a maximum YX_2 chemiluminescence intensity (cf. paper I). Typically the optimum halogen pressure for observation of LIF from the monohalide gave a chemiluminescence intensity only about 25-30% of the maximum. This effect is illustrated by comparison of the data of Figs. 5 and 11 of paper I; the maximum YCl concentration occurs for a Cl_2 pressure about 60% of that required for a maximum chemiluminescence intensity from YCl_2.

The determination of spectroscopic constants for the LIF band systems was accomplished with the use of computer generated simulated spectra which were compared with observed spectra. The spectral resolution of the fluorescence excitation spectra was about 1 Å; this resolution was adequate for approximate determination of values of ω_e and $\omega_e x_e$ for the electronic states of interest and was quite adequate to distinguish between singlet and triplet band systems, but was insufficient for the resolution of rotational features of the observed band systems. It was therefore not possible to directly determine whether an observed singlet band system was a $^1\Sigma^+$-$X^1\Sigma^+$ or $^1\Pi$-$X^1\Sigma^+$ system. The Franck-Condon factors used in the spectral simulations depend on assignments of values of r_e, ω_e, and $\omega_e x_e$ for the upper and lower states. More specifically the Franck-Condon factors are very sensitive to the choice of values for the <u>difference</u> in r_e values between upper and lower states; moreover, this sensitivity is largely independent of other factors such as the nature of the assumed vibrational and rotational distributions. Indeed the differences in r_e values between the upper and lower states can be specified to less than about 0.01 Å by this method for these band systems. In those cases where values of r_e'' are accurately known for the ground state, it was

therefore possible to specify the r_e' value for the upoer state to an accuracy comparable to that of the lower state even in the absence of a rotational analysis of the observed bands. This is a most useful feature of the computer simulation technique.

Figs. 1a and 1b and 2a and 2b illustrate the use of simulated spectra for the determination of spectroscopic constants for two new band systems of YCl. Figs. 1a and 2a show the experimental LIF intensity distributions; Figs. 1b and 2b are computer simulated spectra generated with the spectroscopic constants and vibrational and rotational distributions specified in Table I. Yttrium atomic lines appear in the LIF excitation spectra; these are discussed in Section V.

The simulated spectral distributions were obtained by comparison with the observed spectra with an iterative method. The separate contributions of different isotopes were not distinguished; the isotopic splittings were not important at the resolution of the present experiments. Details of the calculation of the spectral simulations are given in Appendix A. The procedure for analysis of excitation spectra is described in Appendix B. The steps followed in the iterative procedure were:

(1) Approximate values of ω_e', $\omega_e'x_e'$, T_e', B_e', and α_e' were determined from the observed spectra by standard methods.[1]

(2) A preliminary choice of a rotational temperature, T_{rot}, was selected for computation of the rotational structure associated with vibronic transitions for a given $^1\Pi$-$X^1\Sigma^+$ or $^1\Sigma^+$-$X^1\Sigma^+$ band system of interest.

(3) The relative intensities of the $(v',v'') = (n,v'')$; $n = 0,1,2,\ldots,$ vibronic progressions are independent of the vibrational distribution of molecules in the lower electronic state and are determined by the Franck-

Condon factors. Morse potential curves for the upper and lower states were estimated with use of approximate values for the dissociation energies, approximate values of r_e' and r_e'', and values of ω_e', $\omega_e'x_e'$, T_e', ω_e'', and $\omega_e''x_e''$. The relative displacement in equilibrium internuclear separation, $\Delta r_e = r_e' - r_e''$, was varied by trial and error changes in r_e' until a good initial fit for the observed intensities of the (n,v") progression was obtained. The choice of r_e'' value was not critical in the calculation of Franck-Condon factors.[5] For the YF and YCl band systems a value of r_e'' was available from previous work. In the other cases only a rough estimate of r_e'' was possible with the use of empirical rules.[6]

(4) The relative intensities of the (v',v") = (v',n); n = 0,1,2,..., progressions depend strongly on the vibrational distribution of molecules in the lower electronic state. The best fits were obtained with Boltzmann vibrational distributions in each case. Trial and error specifications of the vibrational temperatures, T_{vib}, of the lower electronic state were performed until a good fit was obtained for the observed intensities of the (v',n) progression.

(5) The calculations were repeated using refined estimates of values for r_e', T_{rot}, T_{vib}, and ω_e', $\omega_e'x_e'$, T_e', ω_e'', $\omega_e''x_e''$ until no further improvement in the simulations was possible.

The simulations of Figs. 1b and 2b and Table I give values of ω_e'' and $\omega_e''x_e''$ which agree with those measured by Janney[7] for a $^1\Sigma^+$ lower state. No other excitations corresponding to a different lower state were observed in the present work which indicates that the ground state of YCl is indeed the $^1\Sigma^+$ state identified by Janney.[7]

Radiative lifetime data for the (0,0) bands of the two YCl band systems of Figs. 1 and 2 are presented in Fig. 3. The lifetime of an additional (0,0) band of the previously observed $C^1\Sigma^+$-$X^1\Sigma^+$ band system with $T_e(C^1\Sigma^+)$= 14,907.6 cm^{-1} was also measured. Table I summarizes the lifetime data for the three YCl bands.

Observed and simulated excitation spectra for several additional band systems in YBr, YI, and YF are presented in Figs. 4 through 8. Spectroscopic constants and radiative lifetime data for the (0,0) bands of the YBr and YI band systems are given in Tables II and III. The best spectral simulation for the $C^1\Sigma^+$-$X^1\Sigma^+$ bands of YF (Fig. 8b) was found with spectroscopic constants which agreed within experimental accuracy with those previously measured.[1] The vibrational and rotational temperatures used in the simulation were kT_{vib} = 2000 cm^{-1} and kT_{rot} = 1200 cm^{-1}. Radiative lifetimes for the $C^1\Sigma^+$-$X^1\Sigma^+$ system and the $B^1\Pi$-$X^1\Sigma^+$ system of YF were measured to be 35±3 nsec and 37±3 nsec, respectively.

III. EXCITATION SPECTRA AND RADIATIVE LIFETIMES FOR ScF, ScCl, ScBr AND ScI

Comparatively complete spectroscopic information is available on the low-lying states of ScF and ScCl. This is fortunate because the LIF excitation spectra observed from these molecules were weak in comparison with the LIF spectra of the yttrium halides. It was possible nevertheless to obtain radiative lifetime estimates for one band system in ScF and three systems in ScCl. These data are summarized in Table IV. The lifetimes given here are somewhat shorter than those measured for band systems in the yttrium halides. The lifetimes of Table IV include small corrections for the rise time of the electronics (10 nsec) and the laser pulse width (8 nsec). The

shortest lifetime for which a useful estimate could be obtained with the present apparatus was approximately 14 nsec.

No previous spectroscopic data were available for low-lying states of ScBr and ScI. The LIF excitation spectrum of ScBr was weak, but revealed the presence of two overlapping blue-degraded band systems in the 4100-4300 Å region. Fig. 9 shows the observed and simulated LIF excitation spectra for ScBr. The match between observed and simulated spectra is not as satisfactory as the comparisons made for the yttrium halides. Two distinct singlet band systems with a common ground state are evident; approximate spectroscopic constants and radiative lifetimes for the (0,0) bands are given for each system in Table V.

Excitation spectra for two red-degraded singlet band systems observed for ScI are shown in Figs. 10 and 11. Here again the spectra are weak and of poorer signal-to-noise than was achievable for the yttrium halides. Spectroscopic constants obtained from the simulations of Figs. 10b and 11b for these ScI singlet systems are given in Table VI. The radiative lifetimes of the (0,0) bands for these systems were too short (< 14 nsec) to measure accurately with the present apparatus.

IV. FRANCK-CONDON FACTORS FOR YTTRIUM AND SCANDIUM MONOHALIDE BAND SYSTEMS

Tables VII-XVII contain partial arrays of Franck-Condon factors calculated for the yttrium and scandium monohalide band systems discussed here. More extensive tabulations are given in ref. 8. Rotational constants for the ground state of YCℓ were available from previous work;[7] for YCℓ the value of r_e'' is accurately known and therefore it was possible to tabulate accurate values of r-centroids along with the Franck-Condon factors for the

three band systems of Tables VII, VIII, and IX. For the other monohalides, only rough estimates of r_e'' could be made in the absence of experimental data. For these molecules the Franck-Condon factors could still be accurately determined since they depend primarily on the difference $\Delta r_e = r_e' - r_e''$, rather than on the separate magnitudes of the internuclear separations.

V. RADIATIVE LIFETIMES FOR YTTRIUM AND SCANDIUM ATOMIC STATES

Radiative lifetime data were also obtained for several electronic transitions between atomic states in yttrium and scandium. These values are given in Tables XVIII and XIX along with lifetimes estimated from emission intensity measurements.[9] Many of the lifetimes were shorter than the 14 nsec limitation of the present experiments. Reasonable agreement was obtained between the measured lifetimes and the estimates based on intensity data for scandium; the measured lifetimes for yttrium transitions tended to be somewhat shorter than the estimated values. The signal-to-noise ratios for the atomic fluorescences were considerably higher than from the molecular bands; a maximum of 200 pulses were averaged for the lifetime measurements.

VI. DISCUSSION

The laser induced fluorescence studies described here have led to the observation of several new band systems in the yttrium and scandium monohalides and to measurements of the radiative lifetimes for several of these bands. The absence of triplet band systems in the excitation spectra suggests that the ground states for all of the yttrium and scandium monohalides are $X^1\Sigma^+$ states.

The resolution of the present experiments was insufficient to provide

direct determinations of rotational constants. Nevertheless, the computer simulation procedure enabled the difference in equilibrium internuclear separations between upper and lower electronic states to be specified with high accuracy. This technique is useful in the determination of accurate spectroscopic constants for both electronic states of a given band system when rotational constants are only available for one of the states.

ACKNOWLEDGEMENTS

One of us (T.A.C.) would like to thank the Joint Institute for Laboratory Astrophysics, National Bureau of Standards, Boulder, Colorado, for fellowship support and assistance in the preparation of this paper.

REFERENCES

1. K. P. Huber and G. Herzberg, Molecular Spectra and Molecular Structure IV. Constants of Diatomic Molecules (Van Nostrand Reinhold, New York, 1979).

2. H. C. Brayman, D. R. Fischell, and T. A. Cool, J. Chem. Phys. 00, 0000 (1980), preceding paper.

3. C. J. Cheetham and R. F. Barrow, Adv. High Temp. Chem. 1, 7 (1967).

4. G. Herzberg, Molecular Spectra and Molecular Structure I. Spectra of Diatomic Molecules (Van Nostrand Reinhold, New York, 1950), 2nd ed., Ch. IV.

5. A variation of 0.1 Å in r_e'' value typically results in a variation of less than 0.1% in calculated Franck-Condon factors, provided the difference, $\Delta r_e = r_e'' - r_e'$, remains constant.

6. J. Stals, Rev. Pure Appl. Chem. 20, 1 (1970).

7. G. M. Janney, J. Opt. Soc. Am. 56, 1706 (1966).

8. D. R. Fischell, Ph.D. Thesis, Cornell University, 1980.

9. C. H. Corliss and W. R. Bozman, Experimental Transition Probabilities for Spectral Lines of Seventy Elements, NBS Monograph 53, 1962.

10. K. Liu and J. M. Parson, J. Chem. Phys. 67, 1814 (1977).

11. W. R. Jarmain, J. Quant. Spectrosc. Radiat. Transfer 21, 397 (1979).

APPENDIX A

COMPUTER SIMULATION OF LIF

The LIF intensity detected for the (v",J") → (v',J') induced transition may be written as[10]

$$I_{v'J'v"J"} = k\left[N_{v"J"}\,\rho(\lambda_{v"J"}^{v'J'})q_{v'v"}\,\frac{S_{J'J"}}{(2J"+1)}\right]$$

$$\times\sum_{v,J}\,(\nu_{vJ}^{v'J'})^{4}q_{v'v}\,P(\lambda_{vJ}^{v'J'})\,\frac{S_{J'J}}{(2J'+1)} \qquad \text{(A-1)}$$

where k is a constant of proportionality, $N_{v"J"}$ is the density of absorber molecules in the state (v",J"), $\rho(\lambda_{v"J"}^{v'J'})$ is the laser energy density at the wavelength $\lambda_{v"J"}^{v'J'}$ corresponding to the transition (v",J") → (v',J'), $q_{v'v"}$ is the Franck-Condon factor for this transition, $S_{J'J"}$ is the rotational line strength, $P(\lambda_{vJ}^{v'J'})$ is the detector response function at the wavelength $\lambda_{vJ}^{v'J'}$ corresponding to the fluorescence transition (v',J') → (v,J), $\nu_{vJ}^{v'J'}$, $q_{v'v}$ and $S_{J'J}$ are the frequency, Franck-Condon factor, and rotational line strength, respectively, for the (v'J') → (v,J) fluorescence transitions. The sum is over all states in the lower electronic energy level. The assumption of a Boltzmann rotational distribution and the approximation $B_{v"} \approx B_{e"}$ enabled the rotational intensity distribution to be evaluated independently of the specification of vibrational levels. That is, Eq. (A-1) can be written

$$I_{v'J'v"J"} \approx I_{v'v"}\,I_{J'J"}\,\rho(\lambda_{v"}^{v'}) \qquad \text{(A-2)}$$

where $$I_{v'v''} = k \left[N_{v''} q_{v'v''}\right] \sum_{v} (\nu_v^{v'}) q_{v'v} P(\lambda_v^{v'}) \qquad (A\text{-}3)$$

and $$I_{J'J''} = S_{J'J''} \exp\left[-hcB_e''J'' \frac{(J''+1)}{kT_{rot}}\right] \sum_{J} \frac{S_{J'J}}{(2J'+1)} \qquad (A\text{-}4)$$

where $I_{J'J''}$ refers to the intensity contribution associated with the $J'' \rightarrow J'$ transition of the rotational envelope associated with the vibronic transition $v'' \rightarrow v'$. The wavelengths and frequencies have been replaced by the values at band center; i.e., $\lambda_{v''J''}^{v'J'} = \lambda_{v''}^{v'}$ and $\nu_{vJ}^{v'J'} = \nu_v^{v'}$. In the present experiments, separate rotational transitions were not resolvable, but the envelope of rotational transitions associated with each vibronic transition was of importance in the simulation. Thus $I_{J'J''}$ was calculated as a function of frequency for each rotational transition associated with the vibronic transition of a given $^1\Sigma^+$-$X^1\Sigma^+$ or $^1\Pi$-$X^1\Sigma^+$ band system. The contributions of each branch (P, R or P, Q, R, respectively) were added to produce a rotational spectral profile which was then convoluted with the vibrational intensities according to Eq. (A-2). This convolution procedure is shown schematically in Figs. 12a, 12b and 12c. Fig. 12a shows a hypothetical distribution of vibrational line intensities expressed by

$$I(\lambda) = \sum_{v'v''} I_{v'v''} \delta(\lambda - \lambda_{v''}^{v'}) \qquad (A\text{-}5)$$

where $I_{v'v''}$ is given by Eq. (A-3). Fig. 12b shows the rotational intensity distribution obtained by calculation of the envelope of the intensities described in Eq. (A-4). Trial calculations showed that in each case at the resolution of the present experiments the assumption of either a P, R, or

a P, R, Q branch structure gave similar rotational envelopes which would not have been distinguishable. Fig. 12c shows the convoluted LIF intensity distribution described by Eq. (A-2).

Franck-Condon factors and r-centroids were calculated with the TRAPRB program developed by Jarmain and McCallum.[11] Morse potential energy curves were constructed from the spectroscopic constants. The Schrödinger equation was then solved numerically to provide the vibronic wavefunctions used to calculate the Franck-Condon factors and r-centroids. The wavelengths tabulated with the Franck-Condon factors are those computed with the Morse potentials and are not of high accuracy and are listed for reference only.

APPENDIX B

DATA ANALYSIS

The LIF data as originally recorded contain, in most cases, a small percentage of scattered laser light superimposed upon the laser excitation spectra. That is, the experimentally observed LIF intensity consists of two parts:

$$I(\lambda) = I_f(\lambda) + I_s(\lambda) \tag{B-1}$$

where both the fluorescence intensity $I_f(\lambda)$ and the scattered laser intensity are directly proportional to the wavelength dependent laser energy density, $b(\lambda)$. The normalized intensity may be written

$$I_n(\lambda) = \frac{I_f(\lambda)}{b(\lambda)} + C_s \tag{B-2}$$

where C_s is a constant.

The computer simulations are constructions of the $I_f(\lambda)/b(\lambda)$ term; comparison of experimental spectra with the simulated spectra will differ by the constant C_s and this must be properly accounted for in data analysis. In practice, this was possible with simple methods.

As an example, consider the excitation spectra recorded for the $^{12}C_2$ band system shown in Fig. 13 which is assumed for the purposes of calculation to be a $^1\Pi$-$X^1\Sigma^+$ system. The intensity of Fig. 13 has been normalized by the laser energy density [cf. Eq. (B-2)]. Comparisons of the intensities of the members of the (0,0), (1,0) and (2,0) progression are desired to obtain relative values of the $q_{0,0}$, $q_{1,1}$ and $q_{2,2}$ Franck-Condon factors. The band systems are degraded to the red and therefore portions of the $\Delta v=2$ sequence overlap the (1,0) band, and portions of the $\Delta v=1$ sequence overlap the (0,0) band. The wavelengths λ_3 and λ_1 correspond to the observed peaks of the

(1,0) and (0,0) vibronic bands. The wavelengths λ_4 and λ_2 are located in the troughs just to the left of λ_1 and λ_3, respectively; intensities at these wavelengths contain no contributions from the (1,0) and (0,0) band systems, respectively. The intensities at λ_4 and λ_2 are approximately the same as the intensities of the $\Delta v=2$ and $\Delta v=1$ sequences which overlap the (1,0) and (0,0) bands, respectively. The difference in intensities at λ_1 and λ_2 gives the contribution of only the (0,0) band; the difference in intensities at λ_3 and λ_4 gives the contribution of only the (1,0) band. The effects of the overlapping sequences and the scattered laser light both cancel out in the difference. The ratio of Franck-Condon factors is given by

$$R = \frac{I_n(\lambda_1)-I_n(\lambda_2)}{I_n(\lambda_3)-I_n(\lambda_4)} = \frac{I_f(\lambda_1)/\sigma(\lambda_1)-I_f(\lambda_2)/\sigma(\lambda_2)}{I_f(\lambda_3)/\sigma(\lambda_3)-I_f(\lambda_4)/\sigma(\lambda_4)} \qquad (B\text{-}3)$$

but $\sigma(\lambda_1) \approx \sigma(\lambda_2)$ and $\sigma(\lambda_3) \approx \sigma(\lambda_4)$ so that

$$R = I_{00}/I_{10} = (q_{00}/q_{10})\left\{\left[\sum_v (\nu_v^0)^4 q_{0v} P(\lambda_v^0)\right] / \left[\sum_v (\nu_v^1)^4 q_{1v} P(\lambda_v^1)\right]\right\}$$

[cf. Eq. (A-3)].

The quantities in curly brackets can be calculated iteratively on the basis of assigned values for the Franck-Condon factors. As it turned out, for the band systems to present interest the ratio in curly brackets was always very close to unity. This is illustrated in Table XX for the band system of YCl shown in Fig. 13. Thus, $R \approx q_{00}/q_{10}$.

A similar procedure employed for the (0,0), (0,1) and (0,2) progression members can be used to obtain values for the ratios

$$R' = I_{00}/I_{01} \simeq (N_0/N_1)\ (q_{00}/q_{01})$$

and

$$R'' = I_{01}/I_{02} \simeq (N_1/N_2)\ (q_{01}/q_{02})$$

which depend on the ratios of vibrational populations in addition to the ratios of Franck-Condon factors.

This procedure was extended to other progressions to provide many experimental ratios of Franck-Condon factors and many ratios of vibrational populations for use in the iterative simulation techniques described in Section II and Appendix A.

Once a good fit was obtained between the observed and calculated values for Franck-Condon factors and vibrational populations, it was possible to determine the constant C_s in Eq. (B-2) by a simple displacement of the observed excitation spectra (normalized by laser energy density) along the ordinate until a good match between observed and simulated profiles was obtained. All of the comparisons of Sections II and III show the final result after this correction for C_s has been made.

TABLE I

Spectroscopic constants for electronic states of YCl

State	1^a	2^a	$C^1\Sigma^+$	$X^1\Sigma^+$	
T_e	22,787±2cm^{-1}	27,116±2cm^{-1}	14,907.6cm^{-1}	0 cm^{-1}	
ω_e	345±2cm^{-1}	335±2cm^{-1}	324.5cm^{-1}	381±2cm^{-1}	(380.7cm^{-1})[b]
$\omega_e x_e$	1.0±0.3cm^{-1}	1.0±0.3cm^{-1}	1.14cm^{-1}	1.3±0.3cm^{-1}	(1.30cm^{-1})[b]
r_e	2.463±.005Å	2.470±.005Å	2.484Å	- - -	(2.406 Å)[b]
B_e	0.1108cm^{-1}	0.1101cm^{-1}	0.1089cm^{-1}	0.1160cm^{-1}[b]	
kT_{vib}	- - -	- - -	- - -	2000±300cm^{-1}	
kT_{rot}	- - -	- - -	- - -	1200±200cm^{-1}	
$\tau_r(0,0)$[c]	(28±2)x10^{-9}S	(21±2)x10^{-9}S	(36±3)x10^{-9}S	- - -	

[a]Singlet state of presently unknown designation.

[b]K. P. Huber and G. Herzberg, Molecular Spectra and Molecular Structure IV. Constants of Diatomic Molecules (Van Nostrand Reinnold, New York, 1979).

[c]Radiative lifetime of the (0,0) band.

TABLE II

Spectroscopic constants for electronic states of YBr

State	1[a]	2[a]	$X^1\Sigma^+$
T_e	22,026±2cm^{-1}	26,006±2cm^{-1}	0 cm^{-1}
ω_e	245±2cm^{-1}	235±2cm^{-1}	268±2cm^{-1}
$\omega_e x_e$	0.6±0.2cm^{-1}	0.6±0.2cm^{-1}	0.8±0.2cm^{-1}
r_e	2.874±.005Å	2.881±.005Å	2.800Å[b]
B_e	0.0489cm^{-1}	0.0487cm^{-1}	0.0516cm^{-1}[b]
kT_{vib}	- - -	- - -	1500±300cm^{-1}
kT_{rot}	- - -	- - -	1000±200cm^{-1}
$\tau_r(0,0)$[c]	(25±2)x10^{-9}S	(22±2)x10^{-9}S	- - -

[a]Singlet state of presently unknown designation.

[b]Values of r_e and B_e are based on an assumed value of r_e = 2.800Å for the $X^1\Sigma^+$ state; see text.

[c]Radiative lifetime of the (0,0) band.

TABLE III

Spectroscopic constants for electronic states of YI

State	1[a]	2[a]	$X^1\Sigma^+$
T_e	20,690±2cm^{-1}	23,933±2cm^{-1}	0 cm^{-1}
ω_e	195±2cm^{-1}	190±2cm^{-1}	220±2cm^{-1}
$\omega_e x_e$	0.5±0.2cm^{-1}	0.5±0.2cm^{-1}	0.7±0.2cm^{-1}
r_e	3.075±.005Å	3.080±.005Å	3.000Å[b]
B_e	0.0344cm^{-1}	0.0343cm^{-1}	0.0362cm^{-1}[b]
kT_{vib}	- - -	- - -	1500±300cm^{-1}
kT_{rot}	- - -	- - -	1000±200cm^{-1}
$\tau_r(0,0)$[c]	(30±2)x10^{-9}S	(24±2)x10^{-9}S	- - -

[a]Singlet state of presently unknown designation.

[b]Values of r_e and B_e are based on an assumed value of r_e = 3.000Å for the $X^1\Sigma^+$ state; see text.

[c]Radiative lifetime of the (0,0) band.

TABLE IV

Radiative lifetimes for ScF and ScCl

Band system	Frequency, $\nu(0,0)$ (cm^{-1})	Radiative lifetime, $\tau_r(0,0)$[a] (sec)
ScF $^1\Pi$-$X^1\Sigma^+$	26891.0	$(20\pm2)\times10^{-9}$
ScCl $E^1\Sigma$-$X^1\Sigma^+$	27033.3	$(17\pm2)\times10^{-9}$
ScCl $D^1\Pi$-$X^1\Sigma^+$	21521.1	$(20\pm2)\times10^{-9}$
ScCl $B^1\Pi$-$X^1\Sigma^+$	17576.6	$(21\pm2)\times10^{-9}$

[a]Radiative lifetime of the (0,0) band.

TABLE V

Spectroscopic constants for electronic states of ScBr

State	1[a]	2[a]	$X^1\Sigma^+$
T_e	23,459±5cm^{-1}	23,602±5cm^{-1}	0 cm^{-1}
ω_e	305±5cm^{-1}	298±5cm^{-1}	275±5cm^{-1}
$\omega_e x_e$	- - -	- - -	- - -
r_e	2.70±.02Å	2.70±.02Å	2.60Å[b]
B_e	0.0811cm^{-1}	0.0811cm^{-1}	0.0875cm^{-1}[b]
kT_{vib}	- - -	- - -	1500±400cm^{-1}
kT_{rot}	- - -	- - -	1000±300cm^{-1}
$\tau_r(0,0)$[c]	(20±2)x10^{-9}S	(19±2)x10^{-9}S	- - -

[a]Singlet state of presently unknown designation.

[b]Values of r_e and B_e are based on an assumed value of r_e = 2.60Å for the $X^1\Sigma^+$ state; see text.

[c]Radiative lifetime of the (0,0) band.

TABLE VI

Spectroscopic constants for electronic states of ScI

State	1^a	2^a	$X^1\Sigma^+$
T_e	21,368±5cm^{-1}	22,284±5cm^{-1}	0 cm^{-1}
ω_e	185±5cm^{-1}	195±5cm^{-1}	210±5cm^{-1}
$\omega_e x_e$	- - -	- - -	- - -
r_e	3.065±.005Å	3.065±.005Å	3.000Å[b]
B_e	0.0545cm^{-1}	0.0545cm^{-1}	0.0569cm^{-1}[b]
kT_{vib}	- - -	- - -	1500±400cm^{-1}
kT_{rot}	- - -	- - -	1000±300cm^{-1}
$\tau_r(0,0)$[c]	<14x10^{-9}S	<14x10^{-9}S	- - -

[a]Singlet state of presently unknown designation.

[b]Values of r_e and B_e are based on an assumed value of r_e = 3.000Å for the $X^1\Sigma^+$ state; see text.

[c]Radiative lifetime of the (0,0) band.

TABLE VII

Franck-Condon factors, wavelengths (Å), and r-centroids (Å)

for the singlet system (?)-$X^1\Sigma^+$ of YCl with $T_e' = 22{,}787 cm^{-1}$

v'	v" (lower state) 0	1	2	3	4	5
0	0.5881	0.3230	0.0775	0.0104	0.0008	0.0000
	4392.0	4466.2	4542.3	4620.6	4701.0	4783.7
	2.434	2.497	2.562	2.633	2.714	2.813
1	0.3023	0.1318	0.3647	0.1649	0.0326	0.0035
	4326.8	4398.8	4472.6	4548.5	4626.4	4706.5
	2.378	2.443	2.504	2.569	2.640	2.722
2	0.0873	0.3116	0.0050	0.2914	0.2318	0.0638
	4263.9	4333.8	4405.5	4479.0	4554.6	4632.2
	2.324	2.384	2.471	2.512	2.576	2.647
3	0.0185	0.1671	0.2202	0.0177	0.1901	0.2688
	4203.1	4271.0	4340.6	4412.0	4485.3	4560.5
	2.272	2.330	2.390	2.437	2.521	2.583
4	0.0032	0.0522	0.2081	0.1201	0.0713	0.1017
	4144.4	4210.4	4278.1	4347.4	4418.5	4491.5
	2.219	2.277	2.336	2.397	2.450	2.531
5	0.0005	0.0119	0.0909	0.2097	0.0472	0.1203
	4087.7	4151.9	4217.6	4285.0	4354.1	4424.9
	2.164	2.225	2.283	2.341	2.405	2.459

TABLE VIII

Franck-Condon factors, wavelengths (Å), and r-centroids (Å)

for the singlet system (?)-$X^1\Sigma^+$ of YCl with $T_e' = 27{,}116 cm^{-1}$

v" (lower state)

v'	0	1	2	3	4	5
0	0.5232	0.3486	0.1064	0.0193	0.0023	0.0002
	3691.0	3743.2	3796.6	3851.1	3906.8	3963.7
	2.437	2.495	2.553	2.614	2.680	2.752
1	0.3298	0.0660	0.3324	0.2053	0.0566	0.0089
	3646.1	3697.1	3749.2	3802.3	3856.6	3912.1
	2.387	2.446	2.503	2.560	2.621	2.687
2	0.1130	0.2894	0.0031	0.2097	0.2579	0.1031
	3602.7	3652.4	3703.2	3755.1	3808.0	3862.1
	2.337	2.393	2.441	2.511	2.568	2.629
3	0.0276	0.1983	0.1609	0.0624	0.0944	0.2624
	3560.5	3609.0	3658.6	3709.2	3760.9	3813.6
	2.287	2.344	2.400	2.455	2.521	2.576
4	0.0053	0.0738	0.2223	0.0572	0.1259	0.0242
	3519.5	3567.0	3615.4	3664.8	3715.2	3766.7
	2.236	2.294	2.350	2.407	2.463	2.535
5	0.0009	0.0193	0.1209	0.1963	0.0070	0.1552
	3479.7	3526.1	3573.4	3621.6	3670.9	3721.1
	2.181	2.243	2.301	2.357	2.412	2.471

TABLE IX

Franck-Condon factors, wavelengths (Å), and r-centroids (Å)

for the $C^1\Sigma^+$-$X^1\Sigma^+$ system of YCℓ with $T_e(C^1\Sigma^+)$ = 14,907.6cm^{-1}

v" (lower state)

v'	0	1	2	3	4	5
0	0.4316	0.3721	0.1510	0.0379	0.0065	0.0000
	6721.5	6896.8	7080.1	7272.1	7473.4	7684.5
	2.442	2.493	2.545	2.597	2.651	2.707
1	0.3515	0.0108	0.2609	0.2476	0.1006	0.0242
	6579.0	6746.8	6922.2	7105.6	7297.6	7498.9
	2.398	2.450	2.501	2.553	2.605	2.658
2	0.1540	0.2231	0.0470	0.0956	0.2522	0.1625
	6443.4	6604.3	6772.2	6947.7	7131.1	7323.2
	2.354	2.405	2.457	2.510	2.560	2.612
3	0.0480	0.2268	0.0665	0.1354	0.0099	0.1937
	6314.1	6468.6	6629.6	6797.7	6973.2	7156.7
	2.310	2.362	2.412	2.464	2.523	2.568
4	0.0119	0.1142	0.2003	0.0021	0.1602	0.0065
	6190.9	6339.2	6493.8	6655.0	6823.1	6998.7
	2.266	2.319	2.369	2.415	2.472	2.513
5	0.0025	0.0395	0.1623	0.1250	0.0162	0.1255
	6073.1	6215.9	6364.4	6519.1	6680.4	6848.6
	2.220	2.275	2.326	2.377	2.431	2.480

Table X

Franck-Condon factors and wavelengths (Å) for the singlet system (?)-$X^1\Sigma^+$ of YBr with $T_e' = 22{,}026 cm^{-1}$

v" (lower state)

v'	0	1	2	3	4	5
0	0.4221 4542.0	0.3843 4597.6	0.1532 4654.3	0.0349 4712.0	0.0050 4770.8	0.0005 4830.7
1	0.3461 4492.3	0.0087 4546.7	0.2748 4602.1	0.2564 4658.5	0.0934 4716.0	0.0183 4774.5
2	0.1588 4443.8	0.2059 4497.1	0.0483 4551.3	0.1107 4606.4	0.2746 4662.6	0.1552 4719.8
3	0.0536 4396.7	0.2188 4448.8	0.0570 4501.8	0.1337 4555.8	0.0182 4610.7	0.2320 4666.7
4	0.0148 4350.7	0.1184 4401.7	0.1825 4453.6	0.0013 4506.5	0.1605 4560.2	0.0013 4614.9
5	0.0036 4305.9	0.0453 4355.9	0.1577 4406.7	0.1087 4458.4	0.0158 4511.1	0.1338 4564.6

TABLE XI

Franck-Condon factors and wavelengths (Å) for the singlet system (?)-$X^1\Sigma^+$ of YBr with $T_e' = 25{,}006 cm^{-1}$

v" (lower state)

v'	0	1	2	3	4	5
0	0.3624 3847.3	0.3836 3887.1	0.1867 3927.6	0.0549 3968.6	0.0108 4010.2	0.0015 4052.5
1	0.3536 3813.0	0.0000 3852.1	0.2036 3891.8	0.2665 3932.1	0.1321 3973.0	0.0368 4014.4
2	0.1863 3779.5	0.1589 3817.9	0.0928 3856.9	0.0419 3896.5	0.2318 3936.6	0.1941 3977.3
3	0.0701 3746.7	0.2254 3784.5	0.0196 3822.8	0.1608 3861.7	0.0003 3901.1	0.1462 3941.0
4	0.0210 3714.7	0.1435 3751.8	0.1552 3789.5	0.0062 3827.6	0.1406 3866.3	0.0345 3905.6
5	0.0053 3683.3	0.0613 3719.8	0.1736 3756.8	0.0664 3794.4	0.0527 3832.4	0.0796 3871.0

Table XII

Franck-Condon factors and wavelengths (Å) for the singlet system (?)-$X^1\Sigma^+$ of YI with T_e' = 20,690 cm^{-1}

v" (lower state)

v'	0	1	2	3	4	5
0	0.4085 4836.0	0.3821 4887.7	0.1616 4940.2	0.0404 4993.4	0.0066 5047.4	0.0007 5102.3
1	0.3516 4791.1	0.0050 4841.8	0.2537 4893.3	0.2582 4945.5	0.1045 4998.5	0.0235 5052.3
2	0.1650 4747.2	0.2007 4797.0	0.0578 4847.5	0.0885 4898.7	0.2610 4950.7	0.1669 5003.5
3	0.0556 4704.3	0.2251 4753.2	0.0504 4802.8	0.1416 4853.1	0.0086 4904.1	0.2046 4955.9
4	0.0150 4662.4	0.1232 4710.4	0.1849 4759.1	0.0003 4808.5	0.1587 4858.6	0.0062 4909.4
5	0.0034 4621.5	0.0463 4668.7	0.1642 4716.5	0.1075 4765.0	0.0209 4814.2	0.1231 4864.0

TABLE XIII

Franck-Condon factors and wavelengths (Å) for the singlet system (?)-$X^1\Sigma^+$ of YI with $T_e' = 23{,}933\ cm^{-1}$

v" (lower state)

v'	0	1	2	3	4	5
0	0.3652 4181.0	0.3817 4219.6	0.1855 4258.6	0.0549 4298.1	0.0109 4338.1	0.0015 4378.5
1	0.3556 4148.2	0.0000 4186.2	0.2037 4224.6	0.2642 4263.5	0.1316 4302.8	0.0371 4342.6
2	0.1853 4116.1	0.1644 4153.5	0.0902 4191.3	0.0428 4229.6	0.2298 4268.3	0.1926 4307.4
3	0.0682 4084.7	0.2287 4121.5	0.0225 4158.7	0.1594 4196.4	0.0002 4234.5	0.1451 4273.0
4	0.0198 4053.9	0.1421 4090.1	0.1623 4126.8	0.0046 4163.9	0.1418 4201.4	0.0329 4239.3
5	0.0048 4023.7	0.0587 4059.4	0.1757 4095.5	0.0736 4132.0	0.0487 4169.0	0.0825 4206.3

TABLE XIV

Franck-Condon factors and wavelengths (Å) for the singlet system (?)-$X^1\Sigma^+$ of ScBr with T_e' = 23,459 cm^{-1}

v" (lower state)

v'	0	1	2	3	4	5
0	0.2920 4260.0	0.3777 4310.5	0.2250 4362.2	0.0815 4415.2	0.0199 4469.5	0.0034 4525.1
1	0.3404 4205.4	0.0154 4254.6	0.1266 4305.0	0.2625 4356.5	0.1746 4409.4	0.0633 4463.5
2	0.2165 4152.1	0.0869 4200.1	0.1429 4249.2	0.0030 4299.4	0.1680 4350.9	0.2208 4403.5
3	0.0991 4100.2	0.1996 4147.0	0.0001 4194.8	0.1518 4243.8	0.0306 4293.9	0.0607 4345.2
4	0.0364 4049.6	0.1694 4095.2	0.0858 4141.8	0.0491 4189.5	0.0763 4238.4	0.0942 4288.3
5	0.0114 4000.2	0.0929 4044.7	0.1607 4090.1	0.0103 4136.7	0.1045 4184.3	0.0135 4233.0

TABLE XV

Franck-Condon factors and wavelengths (Å) for the singlet system (?)-$X^1\Sigma^+$ of ScBr with T_e' = 23,602 cm^{-1}

v" (lower state)

v'	0	1	2	3	4	5
0	0.2961 4235.0	0.3746 4284.9	0.2221 4336.0	0.0817 4388.3	0.0208 4441.9	0.0039 4496.8
1	0.3456 4182.2	0.0138 4230.9	0.1266 4280.7	0.2569 4331.7	0.1726 4383.9	0.0651 4437.4
2	0.2158 4130.7	0.0950 4178.2	0.1412 4226.8	0.0032 4276.5	0.1624 4327.4	0.2146 4379.5
3	0.0955 4080.5	0.2082 4126.8	0.0000 4174.2	0.1552 4222.7	0.0297 4272.3	0.0574 4323.1
4	0.0336 4031.5	0.1695 4076.7	0.0974 4122.9	0.0442 4170.2	0.0820 4218.6	0.0934 4268.1
5	0.0099 3983.6	0.0883 4027.7	0.1690 4072.9	0.0158 4119.0	0.1024 4166.2	0.0169 4214.5

TABLE XVI

Franck-Condon factors and wavelengths (Å) for the singlet system (?)-$X^1\Sigma^+$ of ScI with $T_e' = 21{,}368cm^{-1}$

v" (lower state)

v'	0	1	2	3	4	5
0	0.6626 4682.7	0.2542 4729.3	0.0662 4776.7	0.0139 4825.1	0.0026 4874.5	0.0004 4924.9
1	0.2885 4642.5	0.2301 4688.2	0.2936 4734.8	0.1345 4782.4	0.0409 4830.9	0.0099 4880.4
2	0.0459 4603.0	0.3911 4647.9	0.0459 4693.7	0.2362 4740.5	0.1773 4788.1	0.0738 4836.8
3	0.0029 4564.1	0.1136 4608.3	0.3834 4653.3	0.0001 4699.2	0.1515 4746.1	0.1883 4793.9
4	0.0000 4525.9	0.0108 4569.3	0.1853 4613.6	0.3192 4658.7	0.0201 4704.8	0.0764 4751.7
5	0.0000 4488.3	0.0002 4531.0	0.0249 4574.6	0.2489 4618.9	0.2346 4664.2	0.0613 4710.3

TABLE XVII

Franck-Condon factors and wavelengths (Å) for the singlet system (?)-$X^1\Sigma^+$ of ScI with $T_e' = 22{,}284 cm^{-1}$

v" (lower state)

v'	0	1	2	3	4	5
0	0.6559 4489.2	0.2659 4532.0	0.0642 4575.5	0.0118 4619.9	0.0018 4665.2	0.0002 4711.3
1	0.2864 4450.3	0.2196 4492.3	0.3152 4535.0	0.1345 4578.6	0.0357 4623.1	0.0072 4668.4
2	0.0524 4412.0	0.3728 4453.3	0.0397 4495.3	0.2631 4538.1	0.1839 4581.8	0.0668 4626.3
3	0.0051 4374.4	0.1231 4414.9	0.3494 4456.2	0.0001 4498.3	0.1787 4541.2	0.2044 4584.9
4	0.0003 4337.4	0.0174 4377.2	0.1908 4417.8	0.2761 4459.2	0.0259 4501.4	0.0990 4544.3
5	0.0000 4301.0	0.0012 4340.2	0.0372 4380.1	0.2437 4420.8	0.1900 4462.2	0.0722 4504.4

TABLE XVIII

Radiative lifetimes for atomic yttrium

State	Energy (cm^{-1})	Radiative Lifetimes (10^{-9}S) (arc emission spectra)[a]	(this work)
x $^2P_{1/2}$	27,824	5.4	<14
x $^2P_{3/2}$	28,140	5.7	<14
y $^2D_{3/2}$	24,131	10.0	<14
y $^2D_{5/2}$	24,747	12.4	<14
y $^2F_{5/2}$	24,519	11.1	<14
y $^2F_{7/2}$	24,900	15.6	<14
y $^2P_{1/2}$	24,699	18.2	17
y $^2P_{3/2}$	24,481	21.7	18
z $^2F_{5/2}$	21,529	132	43
z $^2F_{7/2}$	21,915	185	82
z $^2D_{3/2}$	16,146	769	180
z $^2D_{5/2}$	16,066	1111	190

[a]The radiative lifetimes in this column are estimated from emission intensity measurements (C. H. Corliss and W. R. Bozman, Experimental Transition Probabilities for Spectral Lines of Seventy Elements, NBS Monograph No. 53, 1962). The radiative lifetime of a state m is defined with the relationship $\tau_m = \sum_n A_{nm}$ where A_{nm} is the radiative transition probability to the state n lying below the state m.

TABLE XIX

Radiative lifetimes for atomic scandium

State	Energy (cm^{-1})	Radiative Lifetimes (10^{-9}S) (arc emission spectra)[a]	(this work)
y $^2F_{5/2}$	25,585	4.08	<14
y $^2F_{7/2}$	25,724	5.26	<14
y $^2D_{3/2}$	24,866	3.51	<14
y $^2D_{5/2}$	25,014	4.59	<14
y $^2P_{1/2}$	24,657	8.5	22
z $^2F_{5/2}$	21,033	923	1000
z $^2F_{7/2}$	21,086	1600	1200

[a]See Table XVIII.

TABLE XX

Relative values of the emission term of Eq. (A-3)

for the YCℓ band system of Fig. 13

v'	$\sum_v (\nu_v^{v'})^4 q_{v'v} P(\lambda_v^{v'})$
0	99.6
1	100.0
2	99.6
3	99.3
4	99.1
5	98.8
6	98.6
7	98.5
8	98.0

FIGURE CAPTIONS

Fig. 1. (a) Upper: LIF excitation spectrum for a singlet band system in YCℓ with $T_e' = 22{,}787\ cm^{-1}$.

(b) Lower: computer simulated spectrum for this band system.

Fig. 2. (a) Upper: LIF excitation spectrum for a singlet band system in YCℓ with $T_e' = 27{,}116\ cm^{-1}$.

(b) Lower: computer simulated spectrum for this band system.

Fig. 3. Semilogarithmic plots of the decay of LIF from the (0,0) bands of singlet system 1 ($\lambda = 4392$ Å, $T_e' = 22{,}787\ cm^{-1}$) and singlet system 2 ($\lambda = 3691$ Å, $T_e' = 27{,}116\ cm^{-1}$) of YCℓ.

Fig. 4. (a) Upper: LIF excitation spectrum for a singlet band system in YBr with $T_e' = 22{,}026\ cm^{-1}$.

(b) Lower: computer simulated spectrum for this band system.

Fig. 5. (a) Upper: LIF excitation spectrum for a singlet band system in YBr with $T_e' = 26{,}006\ cm^{-1}$.

(b) Lower: computer simulated spectrum for this band system.

Fig. 6. (a) Upper: LIF excitation spectrum for a singlet band system in YI with $T_e' = 20{,}690\ cm^{-1}$.

(b) Lower: computer simulated spectrum for this band system.

Fig. 7. (a) Upper: LIF excitation spectrum for a singlet band system in YI with $T_e' = 23{,}933\ cm^{-1}$.

(b) Lower: computer simulated spectrum for this band system.

Fig. 8. (a) Upper: LIF excitation spectrum for the $C^1\Sigma^+$-$X^1\Sigma^+$ band system of YF with $T_e(C^1\Sigma^+) = 19{,}242.4\ cm^{-1}$.

(b) Lower: computer simulated spectrum for this band system.

Fig. 9. (a) Upper: LIF excitation spectrum for ScBr. Two distinct singlet band systems are evident. For system 1, T_e' = 23,459 cm^{-1}; for system 2, T_e' = 23,602 cm^{-1}.

(b) Lower: computer simulated spectra for these band systems.

Fig. 10. (a) Upper: LIF excitation spectrum for a singlet band system in ScI with T_e' = 21,368 cm^{-1}.

(b) Lower: computer simulated spectrum for this band system.

Fig. 11. (a) Upper: LIF excitation spectrum for a singlet band system in ScI with T_e' = 22,284 cm^{-1}.

(b) Lower: computer simulated spectrum for this band system.

Fig. 12. (a) Hypothetical vibrational line spectrum.

(b) An example of a rotational intensity distribution at the resolution of the present experiments.

(c) Convoluted LIF intensity distribution.

Fig. 13. Normalized excitation spectrum for the YCℓ band system with T_e' = 22,787 cm^{-1}. The designated wavelengths are used to illustrate the data analysis procedure described in Appendix B.

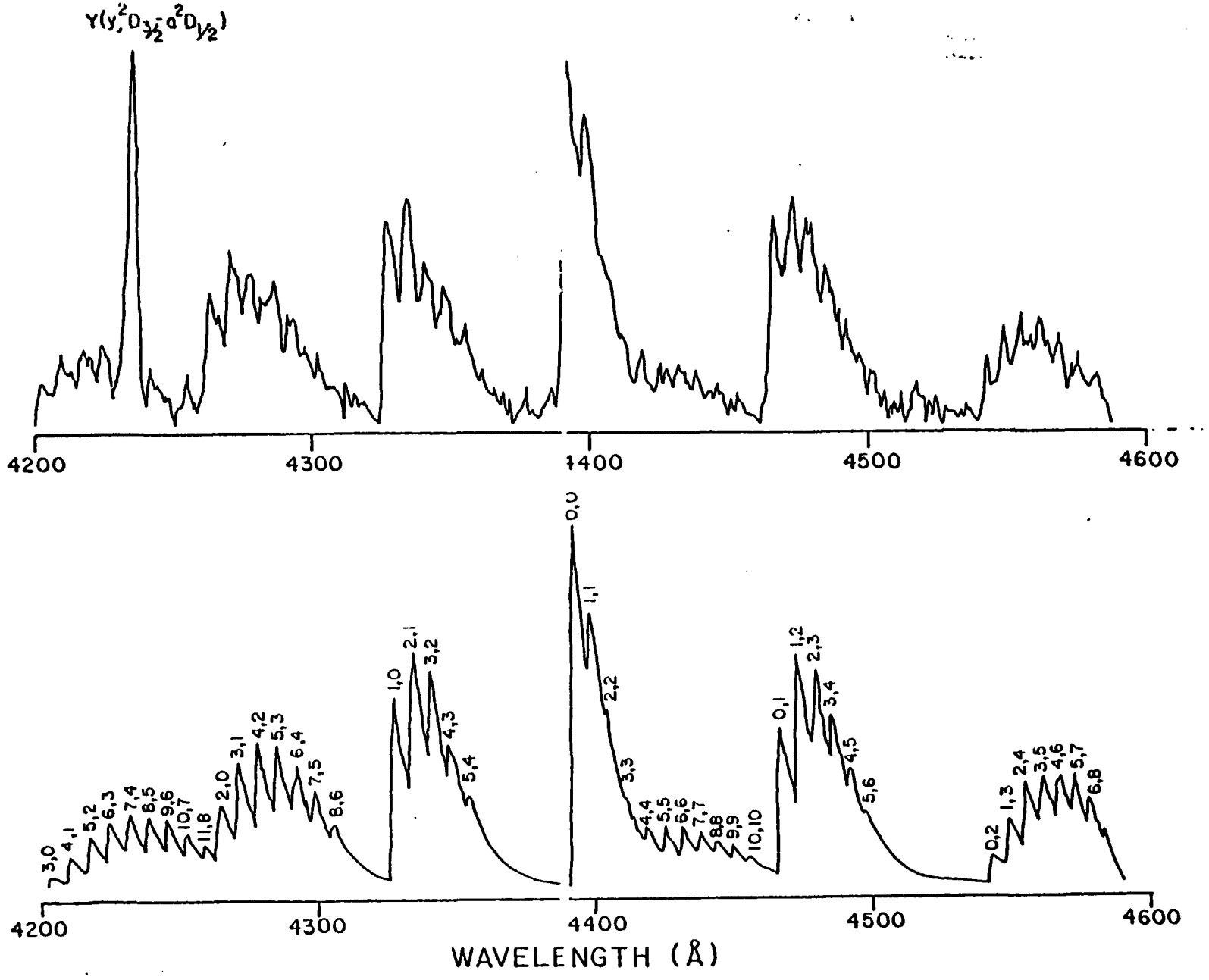
Y(y²D3/2 - a²D3/2)
4200
4300
4400
4500
4600
0,0
1,1
2,2
3,3
4,4
5,5
6,6
7,7
8,8
9,9
10,10
1,0
2,1
3,2
4,3
5,4
3,0
4,1
5,2
6,3
7,4
8,5
9,6
10,7
11,8
2,0
3,1
4,2
5,3
6,4
7,5
8,6
0,1
1,2
2,3
3,4
4,5
5,6
0,2
1,3
2,4
3,5
4,6
5,7
6,8
WAVELENGTH (Å)

Fig. 1

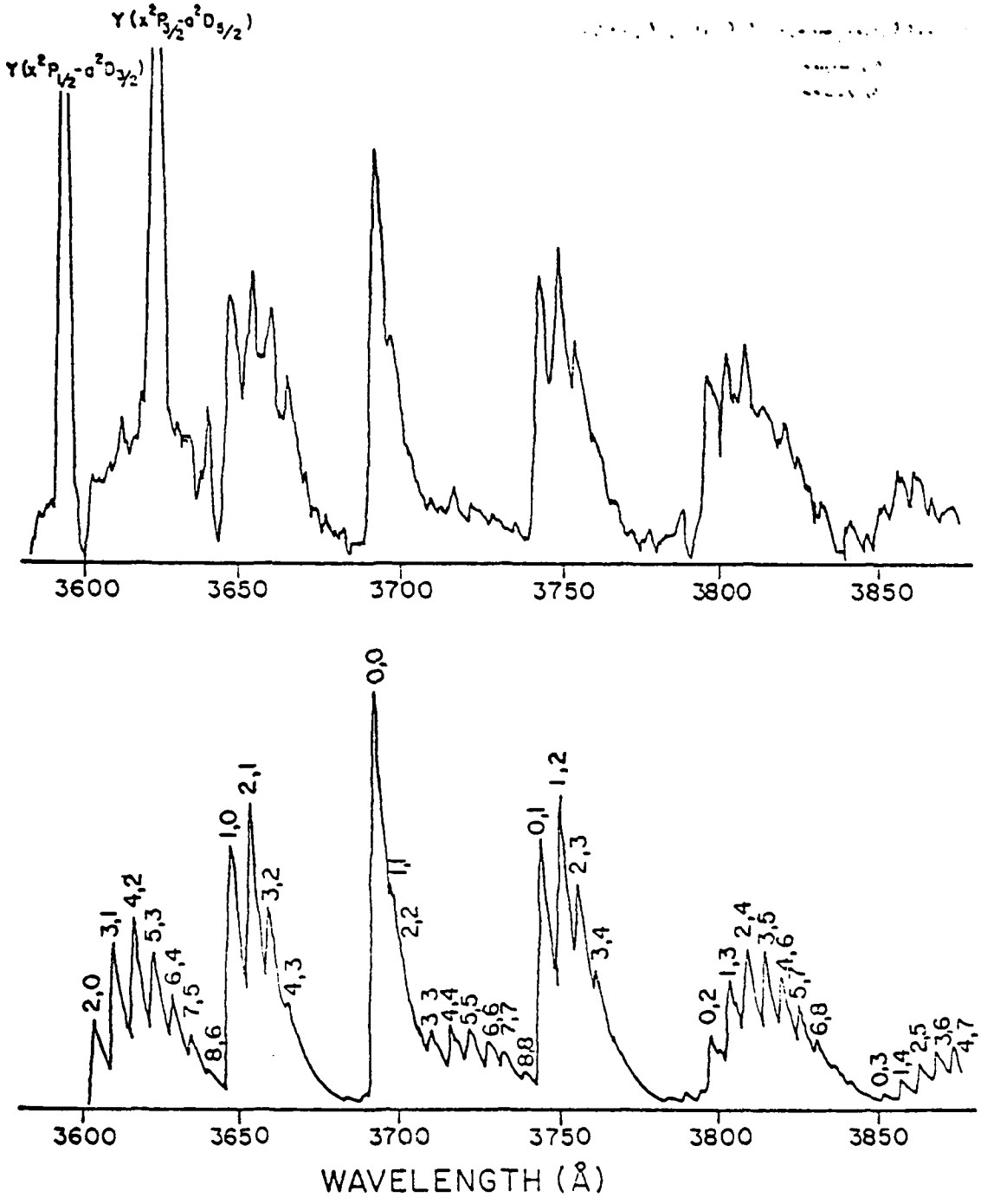
Y(x²P3/2-a²D5/2)
Y(x²P1/2-a²D3/2)
3600
3650
3700
3750
3800
3850
0,0
1,1
2,2
3,3
4,4
5,5
6,6
7,7
8,8
1,0
2,1
3,2
4,3
2,0
3,1
4,2
5,3
6,4
7,5
8,6
0,1
1,2
2,3
3,4
0,2
1,3
2,4
3,5
4,6
5,7
6,8
0,3
1,4
2,5
3,6
4,7
WAVELENGTH (Å)

Fig. 2

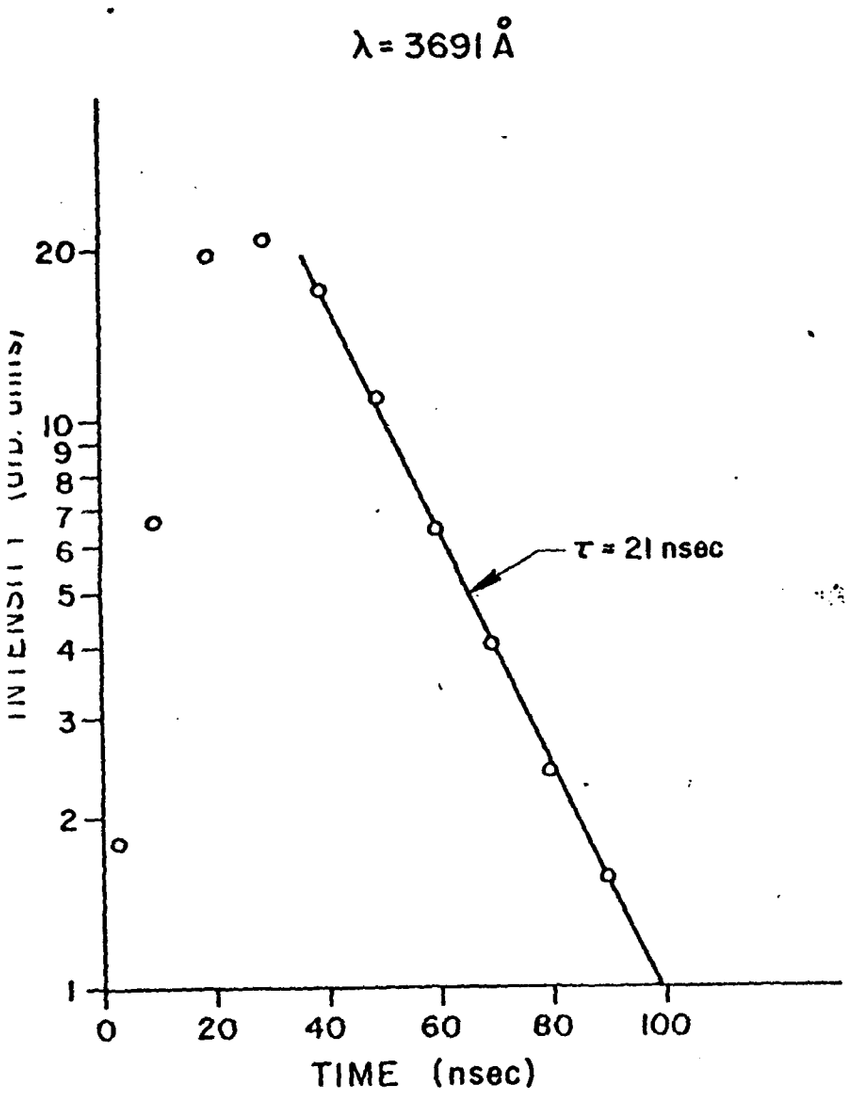
λ = 3691 Å
INTENSITY (arb. units)
20
10
9
8
7
6
5
4
3
2
1
0
20
40
60
80
100
TIME (nsec)
τ = 21 nsec

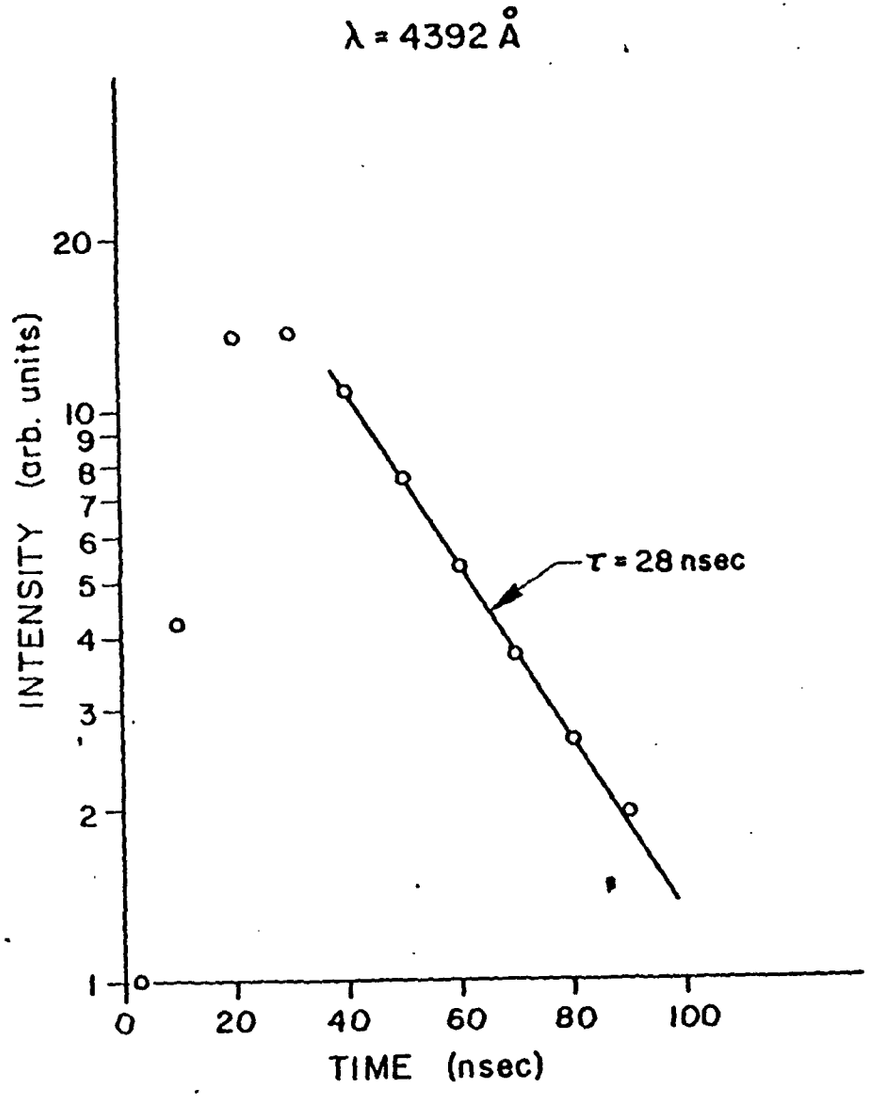
λ = 4392 Å
INTENSITY (arb. units)
20
10
9
8
7
6
5
4
3
2
1
0
20
40
60
80
100
TIME (nsec)
τ = 28 nsec

Fig. 3

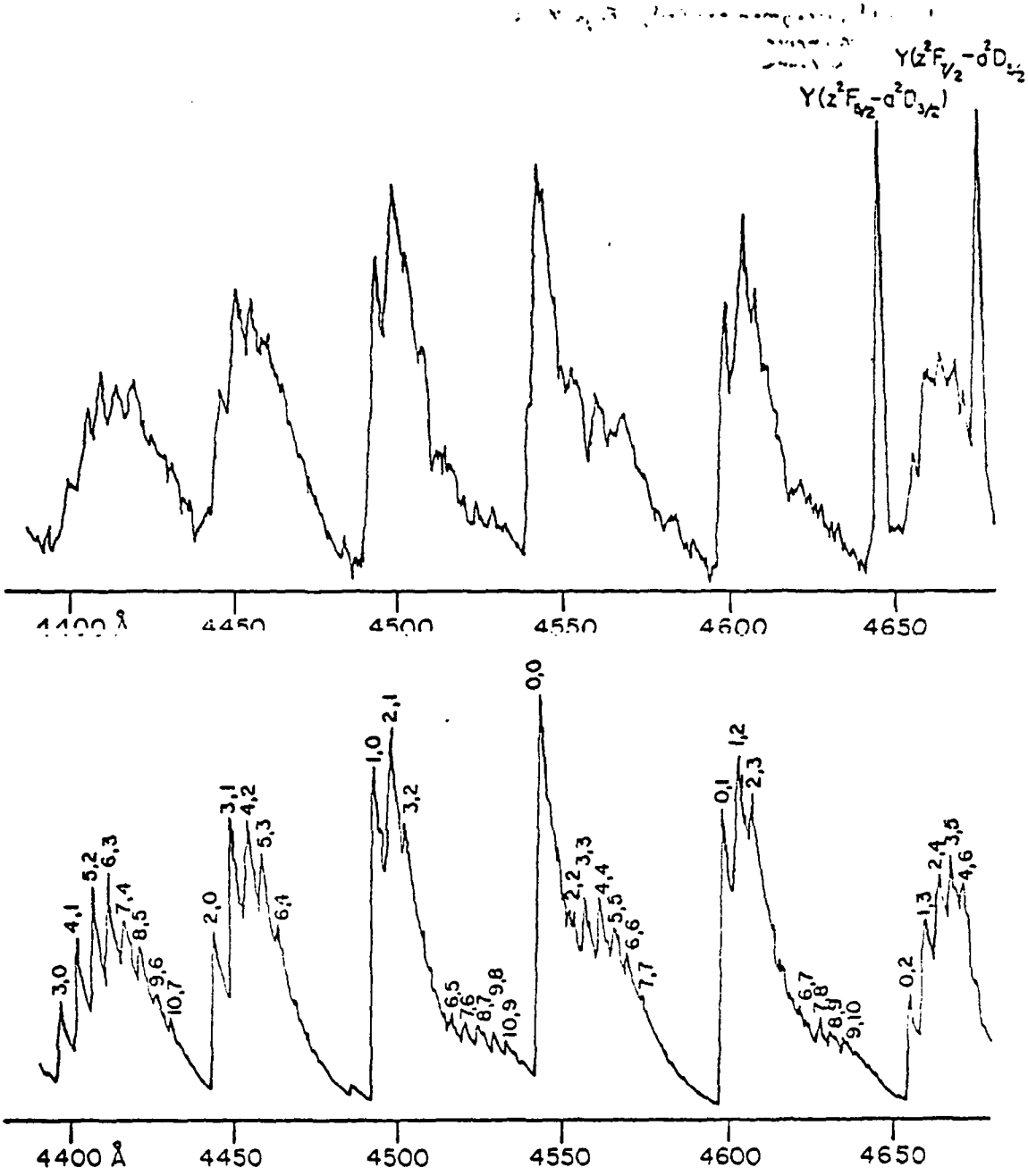
Y(z²F5/2 - a²D3/2)
4400 Å
4450
4500
4550
4600
4650
3,0
4,1
5,2
6,3
7,4
8,5
9,6
10,7
2,0
3,1
4,2
5,3
6,4
1,0
2,1
3,2
6,5
7,6
8,7
9,8
10,9
0,0
2,2
3,3
4,4
5,5
6,6
7,7
0,1
1,2
2,3
6,7
7,8
8,9
9,10
0,2
1,3
2,4
3,5
4,6

Fig. 4

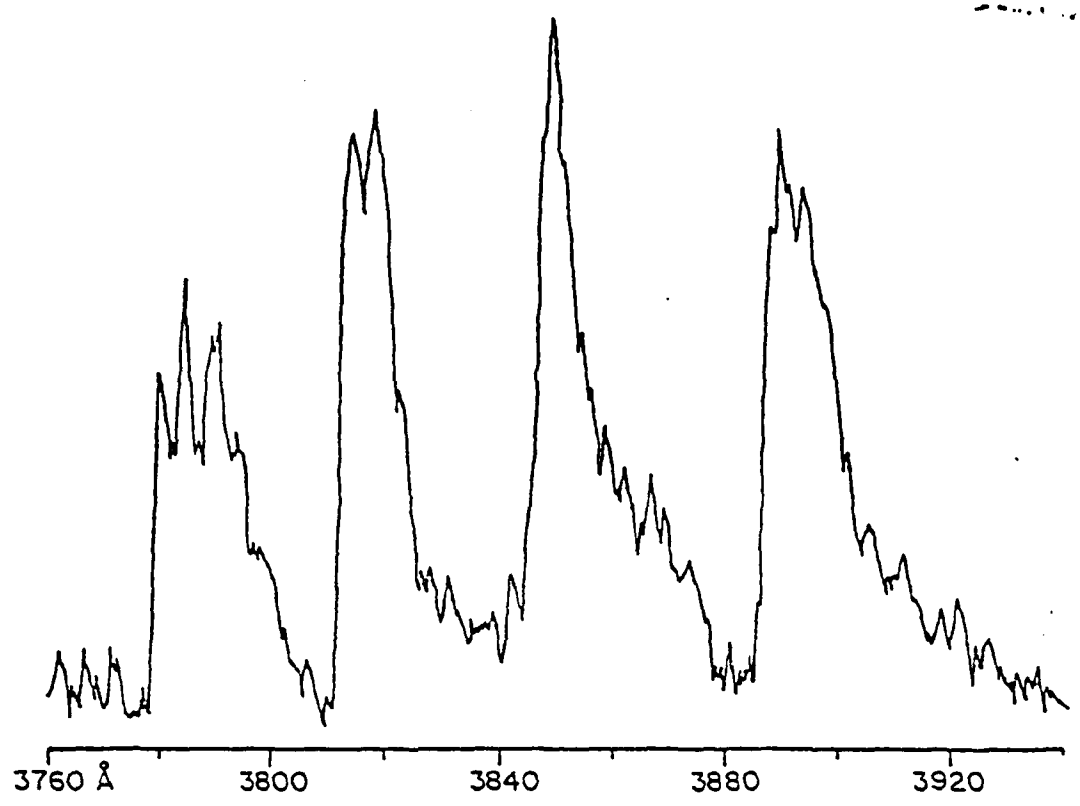
3760 Å
3800
3840
3880
3920

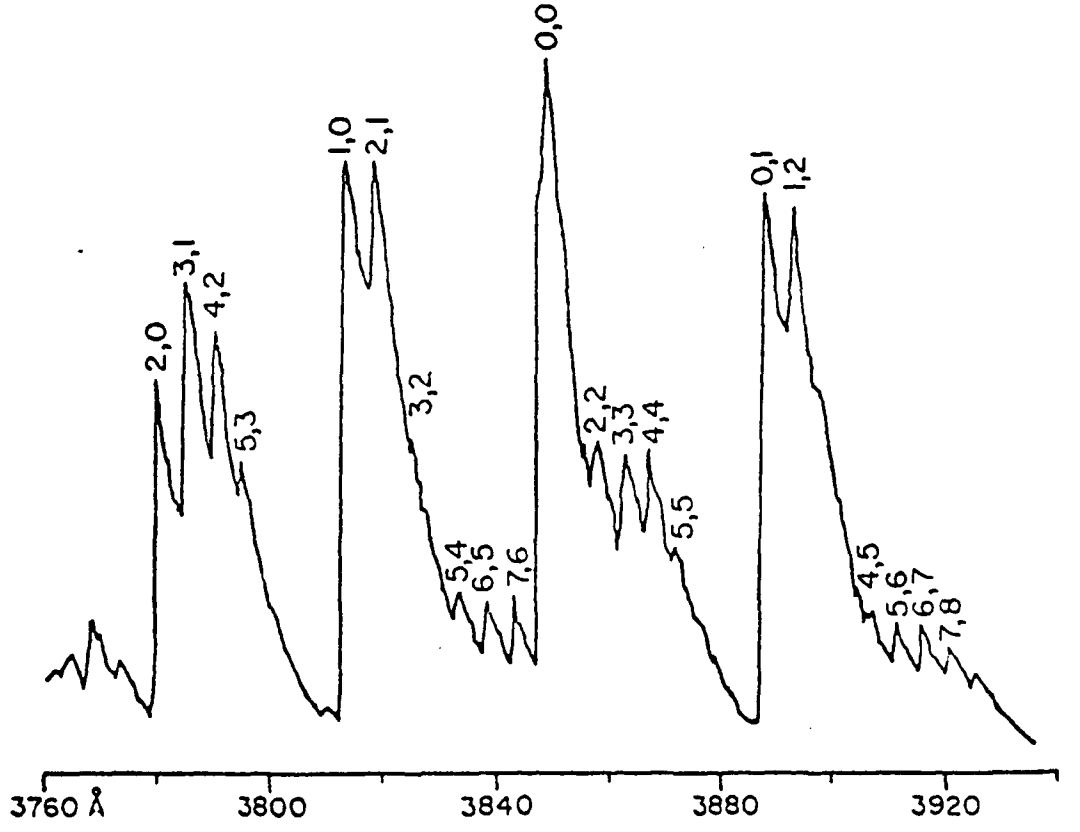
2,0
3,1
4,2
5,3
1,0
2,1
3,2
5,4
6,5
7,6
0,0
2,2
3,3
4,4
5,5
0,1
1,2
4,5
5,6
6,7
7,8
3760 Å
3800
3840
3880
3920

Fig. 5

AD-A085 264 CORNELL UNIV ITHACA NY SCHOOL OF APPLIED AND ENGINEE--ETC F/G 20/5
CHEMICAL LASER SYSTEMS.(U)
MAR 79 T A COOL
AFOSR-77-3258
UNCLASSIFIED AFOSR-TR-80-0423 NL

2 OF 2
AD
A085 264

END
DATE FILMED
6-80
DTIC

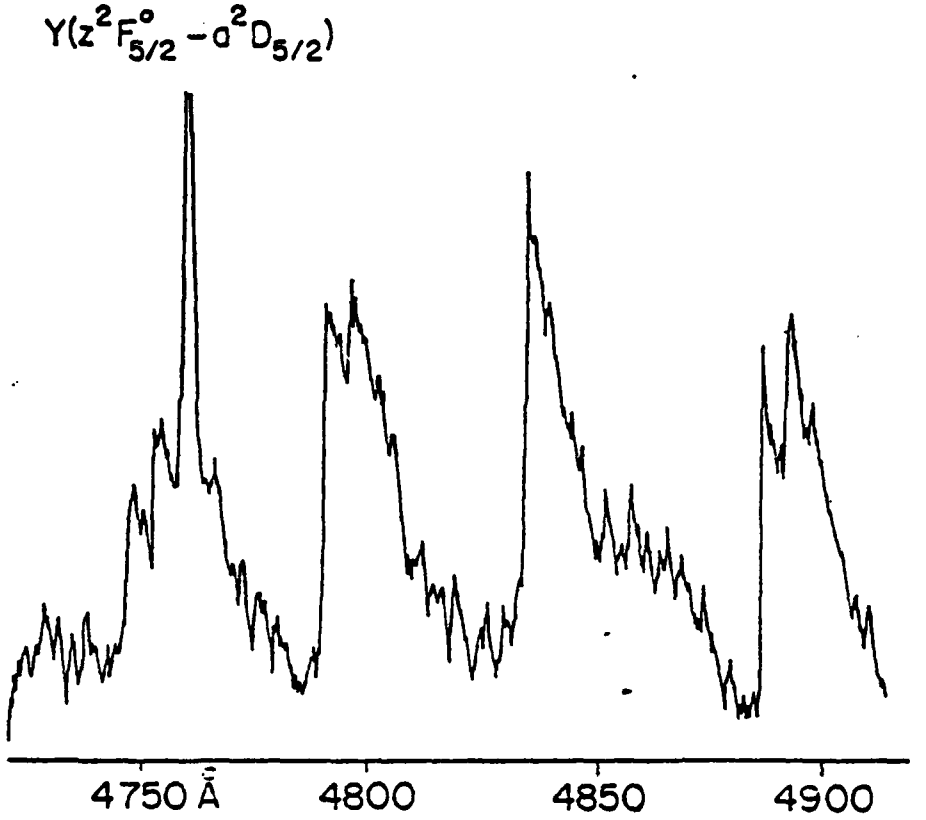
$Y(z^2F^o_{5/2} - a^2D_{5/2})$
4750 Å
4800
4850
4900

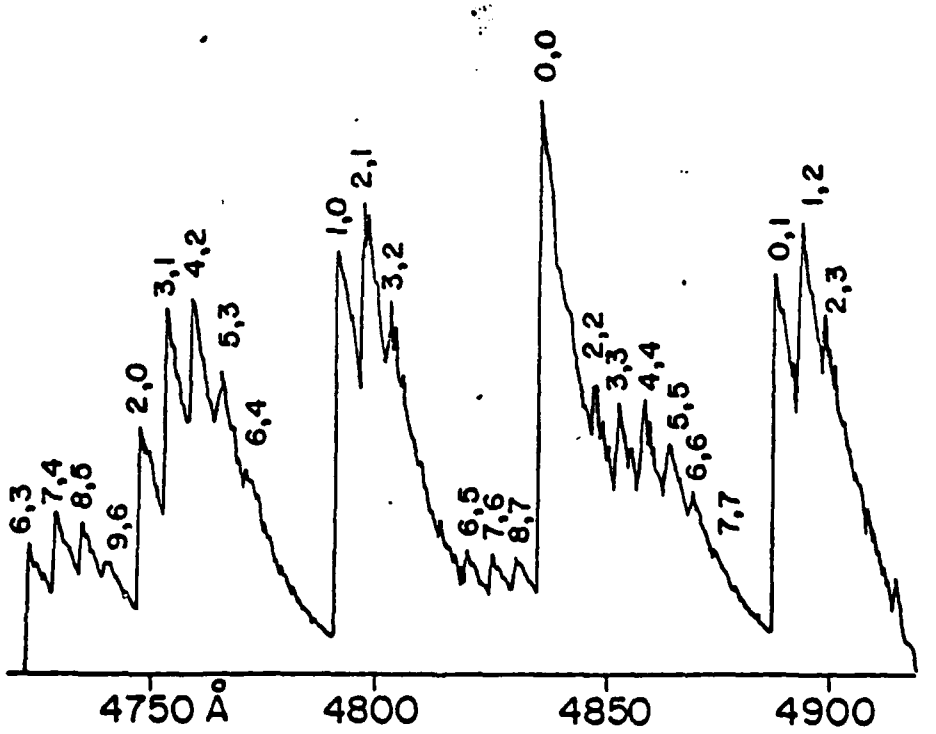
0,0
1,0
2,1
3,2
2,0
3,1
4,2
5,3
6,4
6,3
7,4
8,5
9,6
6,5
7,6
8,7
2,2
3,3
4,4
5,5
6,6
7,7
0,1
1,2
2,3
4750 Å
4800
4850
4900

Fig. 6

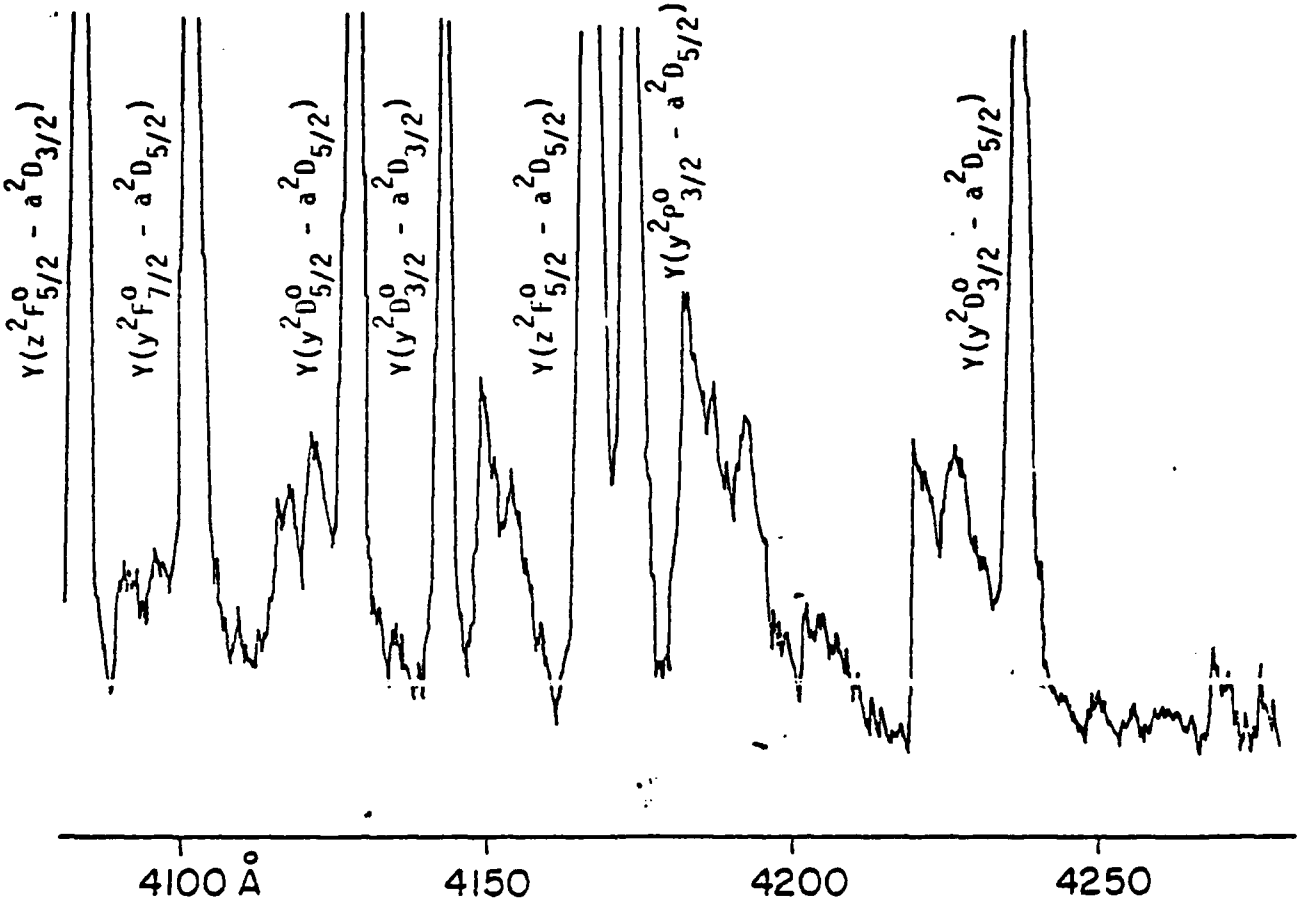
Y(z²F°5/2 - a²D3/2)
Y(y²F°7/2 - a²D5/2)
Y(y²D°5/2 - a²D5/2)
Y(y²D°3/2 - a²D3/2)
Y(z²F°5/2 - a²D5/2)
Y(y²P°3/2 - a²D5/2)
Y(y²D°3/2 - a²D5/2)
4100 Å
4150
4200
4250

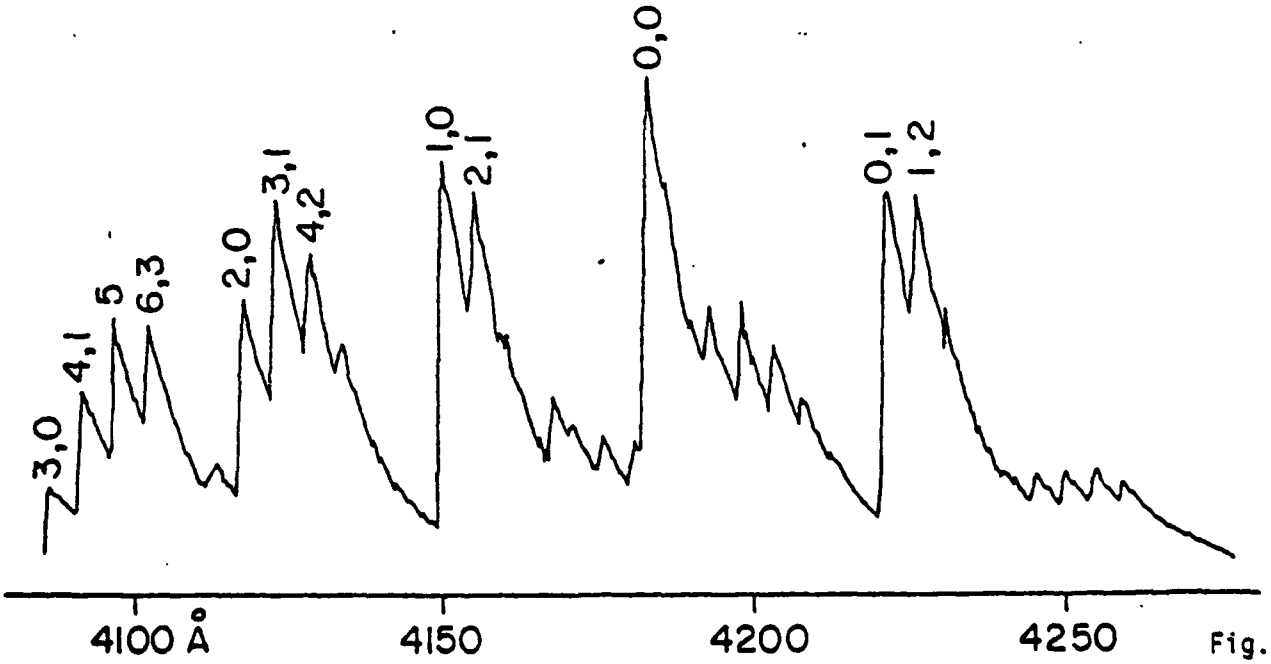
3,0
4,1
5
6,3
2,0
3,1
4,2
1,0
2,1
0,0
0,1
1,2
4100 Å
4150
4200
4250

Fig. 7

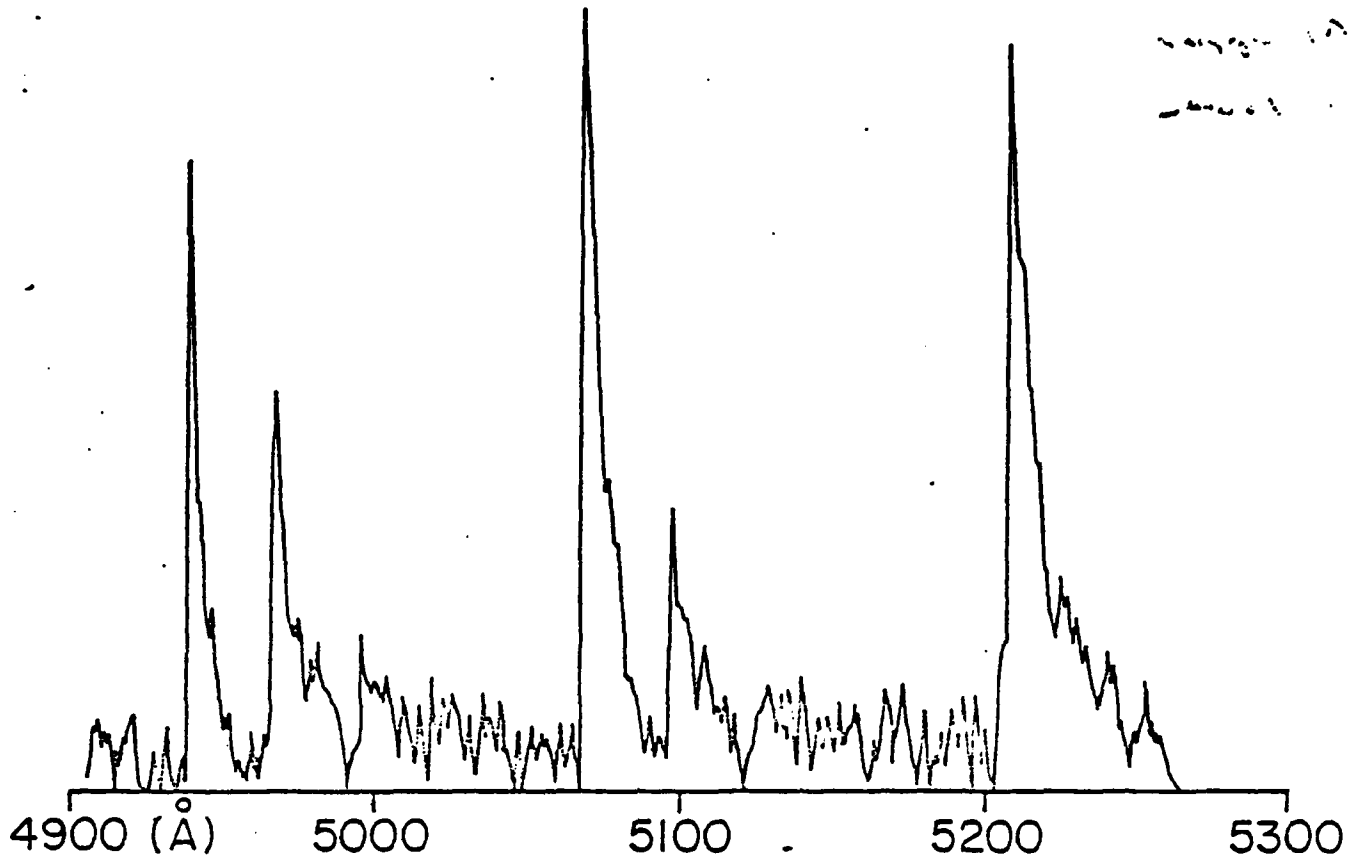
4900 (Å)
5000
5100
5200
5300

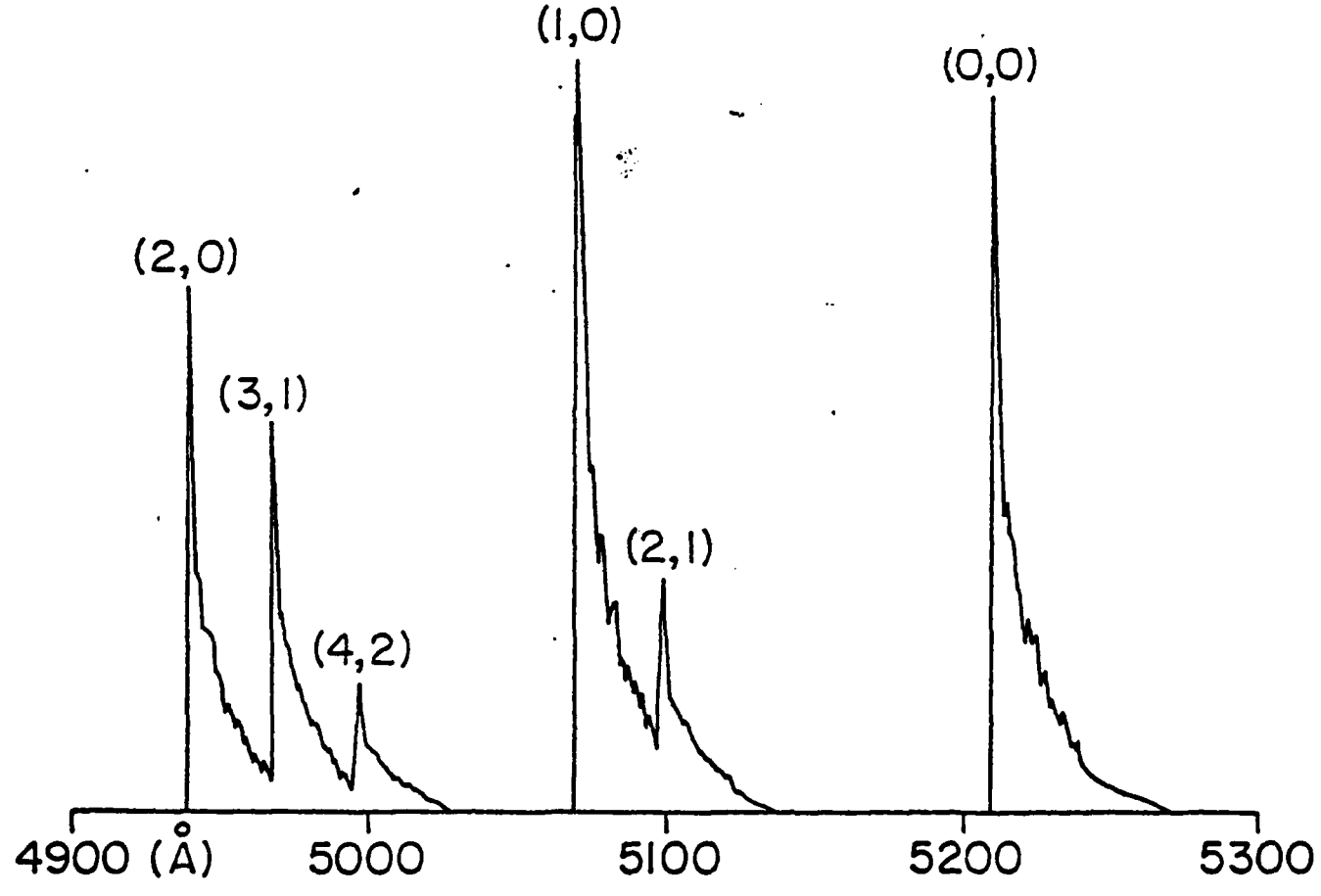
(1,0)
(0,0)
(2,0)
(3,1)
(2,1)
(4,2)
4900 (Å)
5000
5100
5200
5300

Fig. 8

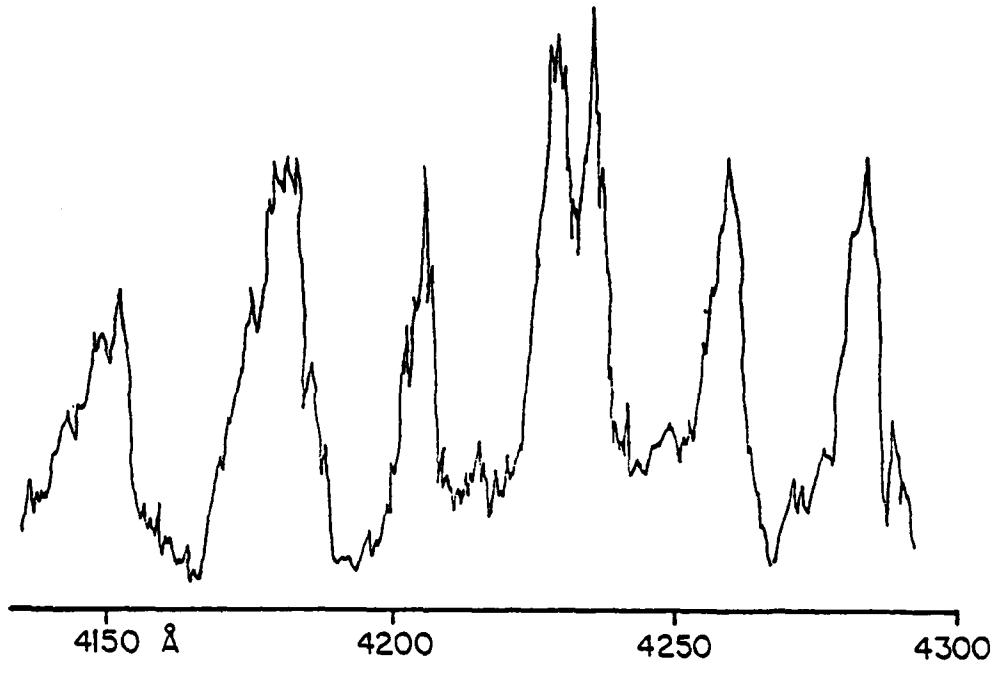
4150 Å
4200
4250
4300

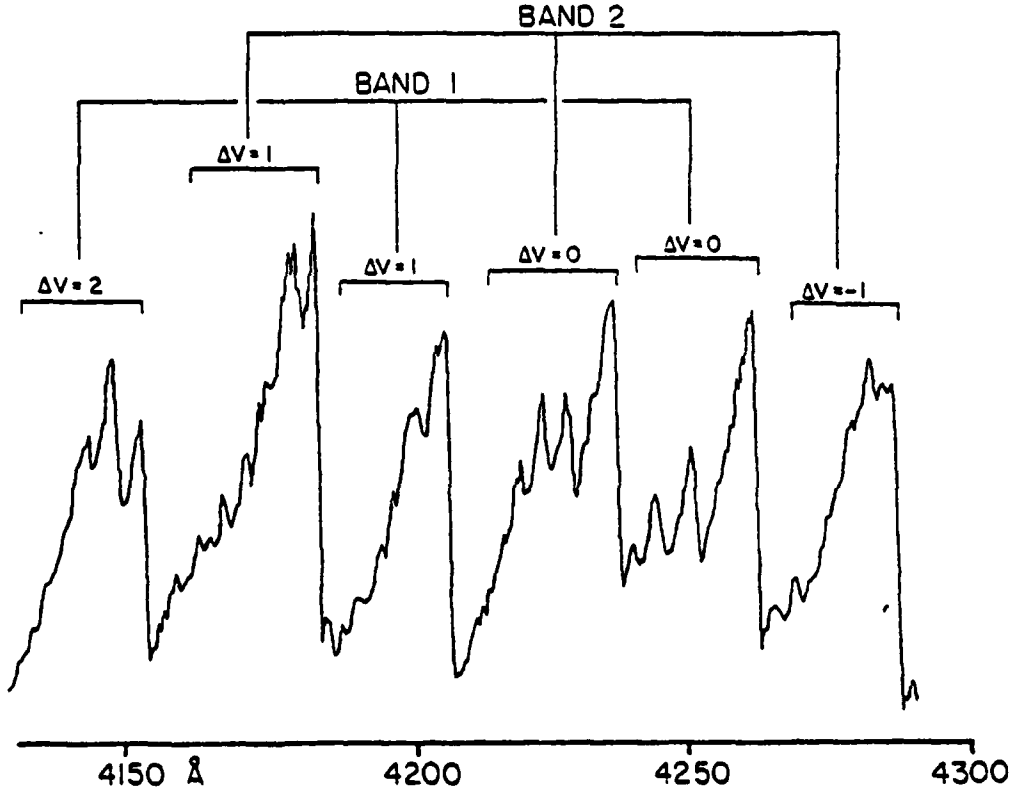
BAND 2
BAND 1
ΔV = 1
ΔV = 2
ΔV = 1
ΔV = 0
ΔV = 0
ΔV = -1
4150 Å
4200
4250
4300

Fig. 9

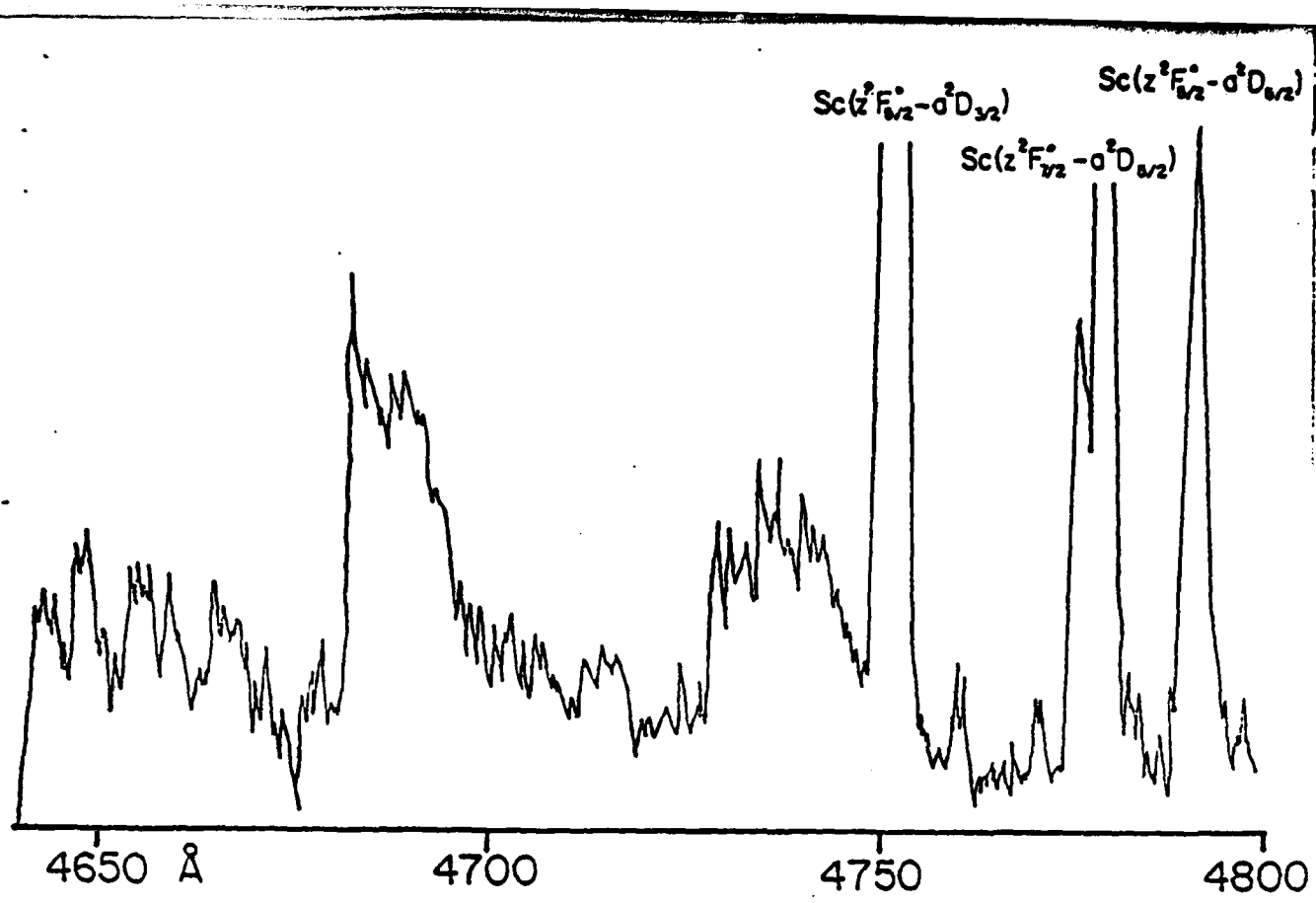
Sc(z²F°5/2-a²D3/2)
Sc(z²F°5/2-a²D5/2)
Sc(z²F°7/2-a²D5/2)
4650 Å
4700
4750
4800

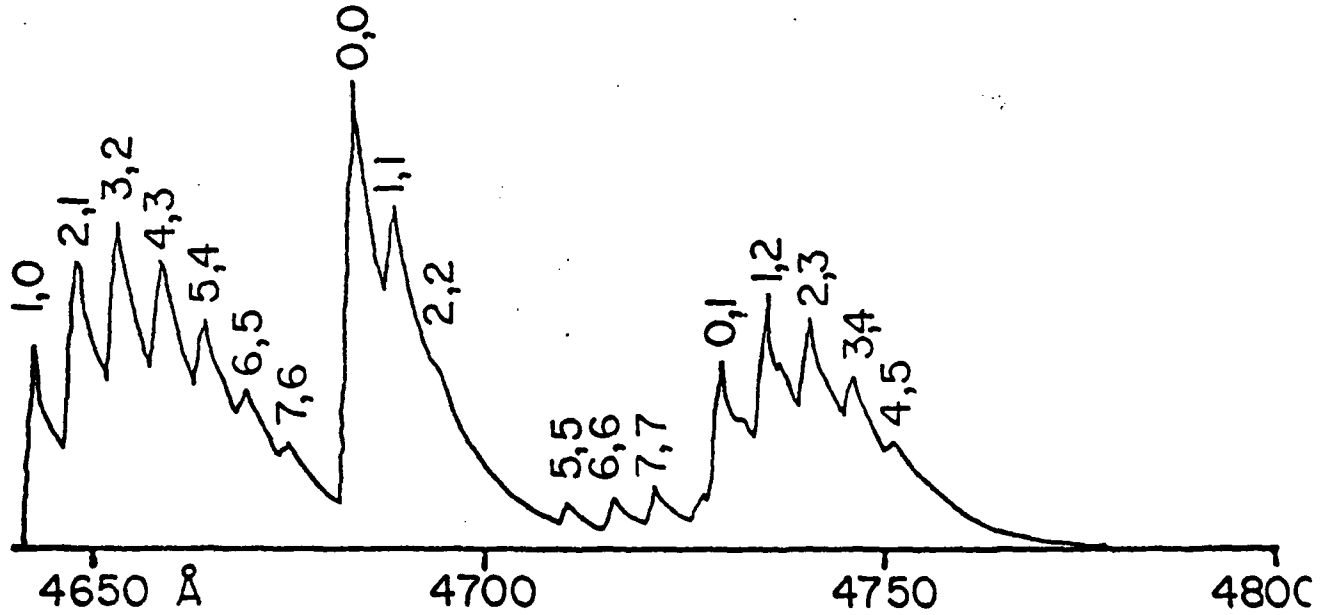
1,0
2,1
3,2
4,3
5,4
6,5
7,6
0,0
1,1
2,2
5,5
6,6
7,7
0,1
1,2
2,3
3,4
4,5
4650 Å
4700
4750
480C

Fig. 10

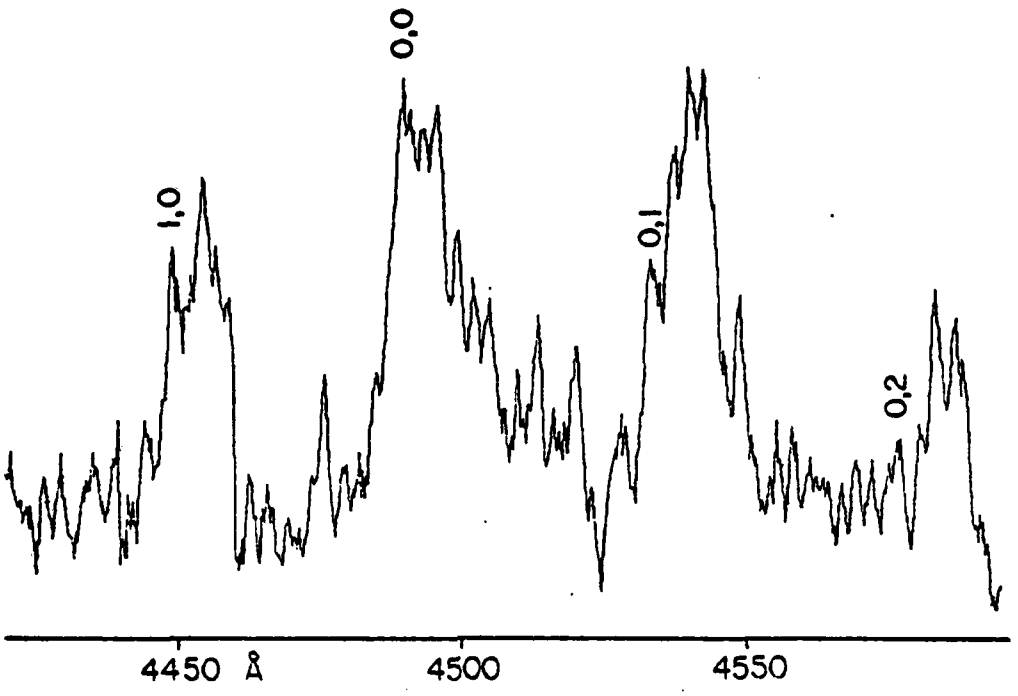
0,0
1,0
0,1
0,2
4450 Å
4500
4550

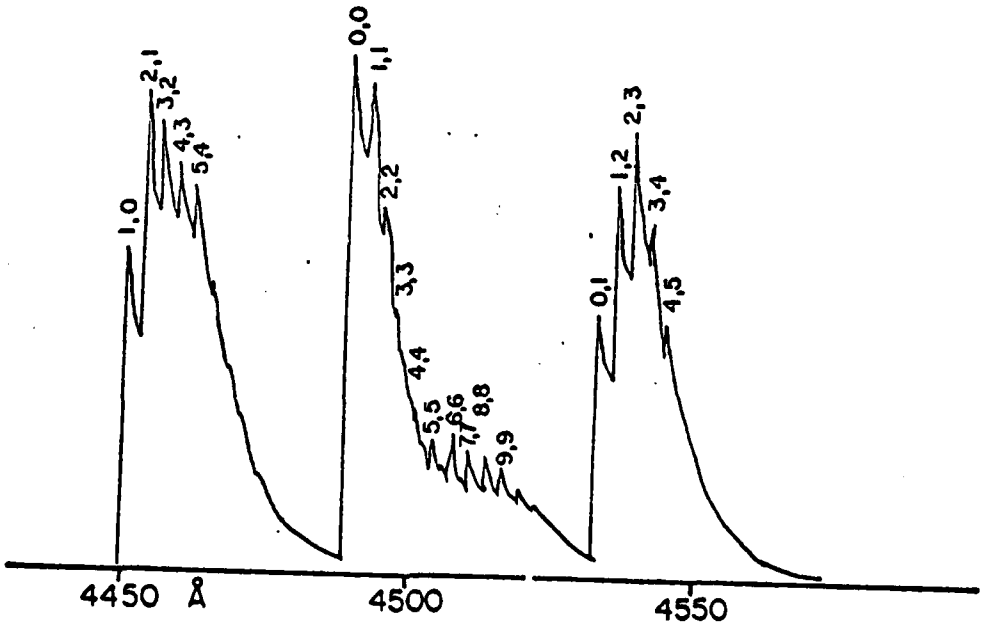
0,0
1,1
2,1
3,2
4,3
5,4
1,0
2,2
3,3
4,4
5,5
6,6
7,7
8,8
9,9
0,1
1,2
2,3
3,4
4,5
4450 Å
4500
4550

Fig. 11

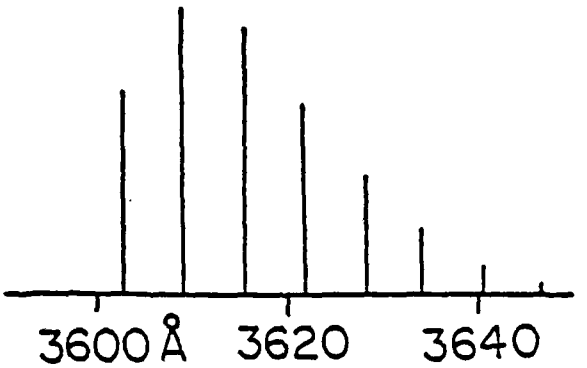

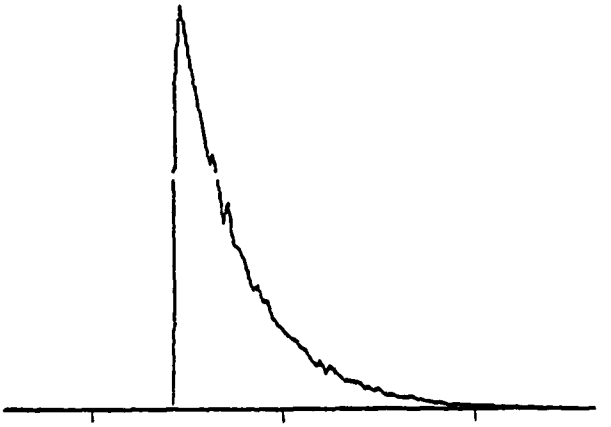

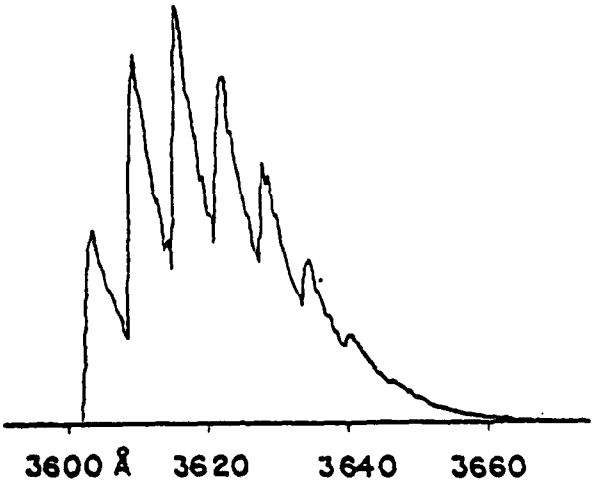

Fig. 12

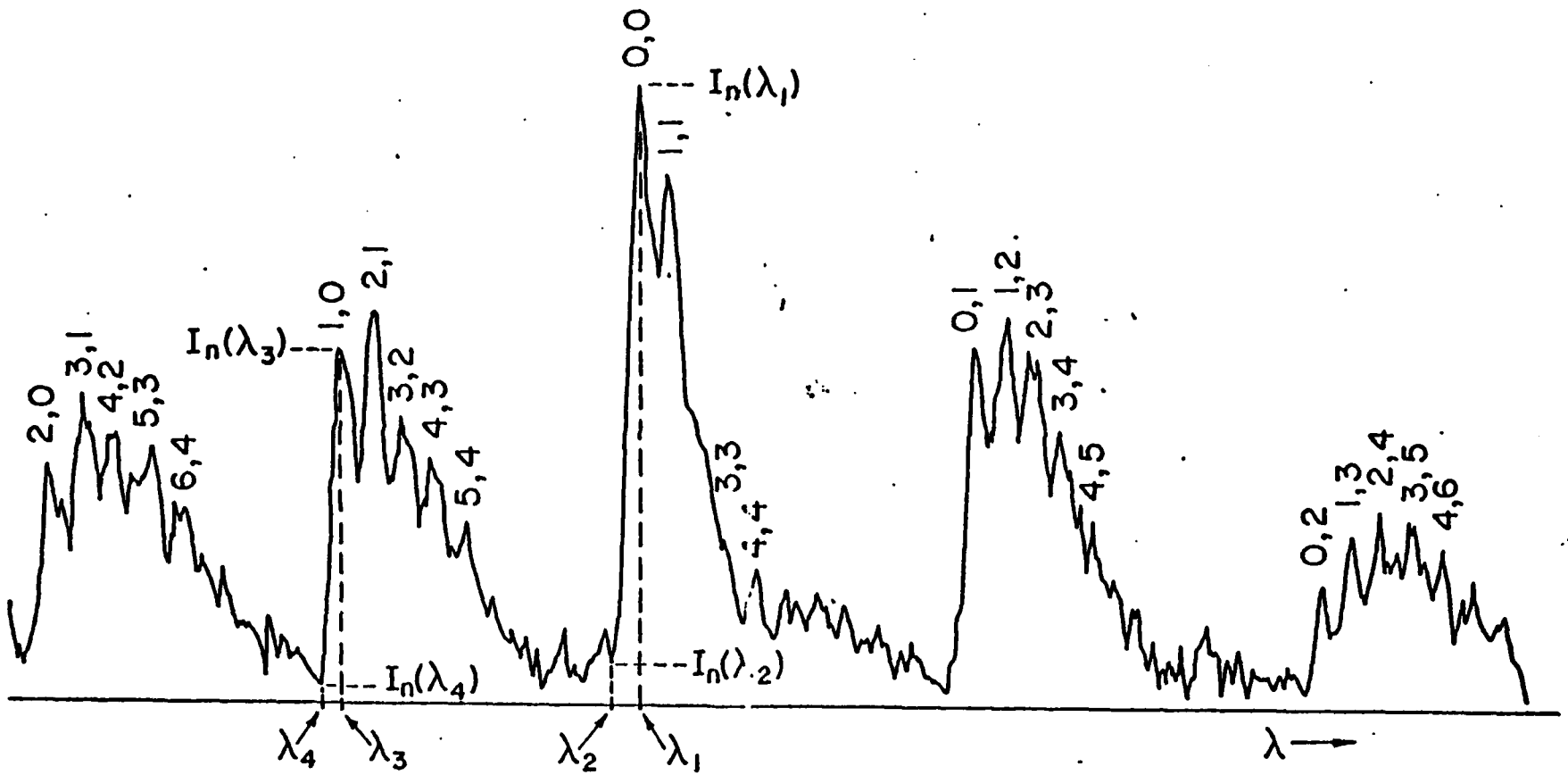
0,0
$I_n(\lambda_1)$
1,1
2,0
3,1
4,2
5,3
6,4
$I_n(\lambda_3)$
1,0
2,1
3,2
4,3
5,4
3,3
4,4
0,1
1,2
2,3
3,4
4,5
0,2
1,3
2,4
3,5
4,6
$I_n(\lambda_4)$
$I_n(\lambda_2)$
λ_4
λ_3
λ_2
λ_1
λ

Fig. 13

IV. A CHEMICALLY PUMPED EXCIMER: REACTION OF PH_3 AND N_2O*

An experimental investigation of the PH_3/N_2O reaction system was undertaken to assess its potential for development of a visible chemical laser.

Reactions of mixtures of phosphine (PH_3) and nitrous oxide (N_2O) were initiated by a fast electrical discharge. Photographic spectra were taken of the chemiluminescent emission from 2300 to 9000 Å. These high resolution spectra show a continuum emission beginning at 3250 Å and extending throughout the visible spectrum. Relatively weak molecular emission bands from MPO, PH_2, and PO are superimposed on the strong continuum emission. Temporal emission studies indicate that the chemiluminescent intensity increases as the square of the reagent pressure. The emission was found to be relatively insensitive to changes in reagent composition and to the presence of added gases. The chemiluminescent intensities at the PH_3:N_2O ratios of 20:80 and 70:30 were approximately 70% of that at the optimum ratio of 40:60.

A standard lamp allowed the high resolution spectra to be corrected for film response. It also allowed an estimate to be made of the photon yield of the reaction. The photon yield was found to increase linearly with pressure up to the highest pressure investigated, 666 Torr, where it had the value 2×10^{-4}.

Flashlamp absorption and intracavity dye laser spectroscopy measurements yielded no absorption which could be associated with an emitter of the continuum. The only absorption found was that which corresponded to the molecular emission which is superimposed on the continuum. Sodium line reversal studies indicated that the reaction emission is a true continuum by showing a reversal of the D lines. The sodium D lines first appear in emission superimposed on the continuum at low reagent pressures. As the reagent pressure is increased, the reaction chemiluminescent intensity increases as the square of the reagent pressure, while the sodium concentration remains constant. The sodium atoms begin to absorb from the continuum and finally at 560 Torr a line reversal takes place.

Cavity tests carried out on the reaction showed no lasing action. Attempts to stimulate the chemiluminescent emission with a high power short pulse ruby laser were unsuccessful. The technique of intracavity dye laser spectroscopy, which is sensitive to both loss or gain, indicates that the media is essentially transparent in the region investigated, 5300 to 6500 Å. That is, the loss or gain was determined to be less than 0.003%/cm.

The results of this study, and those of other investigators, strongly suggest that the source of the continuum emission is the $(PO)_2$* excimer formed by the association between PO molecules and PO* metastable molecules. The large bandwidth of the emission implies that the density of states involved in the transition is high. Since the emitted intensity is partitioned over a large number of states, the transition strength in any small wavelength interval is very weak; thus the gain of the medium is too low to be a useful laser. This hypothesis is consistent with the intracavity dye laser results which indicated that the medium is transparent.

*A complete discussion of completed research is presented in D. G. Harris' Ph.D. Thesis, Cornell University, 1980.

PUBLICATIONS, THESES, AND PRESENTATIONS

1. H. C. Brayman, "Origin of the Chemiluminescence in the Reactions of Yttrium and Scandium with the Halogens," Ph.D. Thesis, Cornell University, 1980.

2. D. R. Fischell, "Laser Induced Fluorescence Spectroscopy of the Group IIIB Halides," Ph.D. Thesis, Cornell University, 1980.

3. D. G. Harris, "A Spectroscopic Investigation of the Phosphine and Nitrous Oxide Reaction," Ph.D. Thesis, Cornell University, 1980.

4. H. C. Brayman, D. R. Fischell, and T. A. Cool, "Spectroscopic Studies of the Products of Reactions of Yttrium and Scandium Atoms with Halogen Molecules. I. The Origin of Chemiluminescence," submitted to J. Chem. Phys.

5. D. R. Fischell, H. C. Brayman, and T. A. Cool, "Spectroscopic Studies of the Products of Reactions of Yttrium and Scandium Atoms with Halogen Molecules. II. Laser Induced Fluorescence from Yttrium and Scandium Monohalides," submitted to J. Chem. Phys.

6. T. A. Cool, "Spectroscopic Constants and Radiative Lifetimes for Newly Observed Electronic States of the Yttrium and Scandium Monohalides," paper presented at the AFOSR/FJSRL Molecular Dynamics Research Conference, 3-5 October 1979, U.S.A.F. Academy, Colorado Springs, Colorado.